PARTIAL DISCHARGE MEASUREMENT AND MODELLING WITHIN AN ARTIFICIAL CYLINDRICAL-SHAPED INSULATION UNDER NON-UNIFORM ELECTRIC FIELD

MOHSIN ALI TUNIO

FACULTY OF ENGINEERING
UNIVERSITY OF MALAYA
KUALA LUMPUR

2016

PARTIAL DISCHARGE MEASUREMENT AND MODELLING WITHIN AN ARTIFICIAL CYLINDRICAL-SHAPED INSULATION UNDER NON-UNIFORM ELECTRIC FIELD

MOHSIN ALI TUNIO

THESIS SUBMITTED IN FULFILMENT OF THE REQUIREMENTS FOR THE DEGREE OF DOCTOR OF PHILOSOPHY

FACULTY OF ENGINEERING
UNIVERSITY OF MALAYA
KUALA LUMPUR

2016

UNIVERSITY OF MALAYA

ORIGINAL LITERARY WORK DECLARATION

Name of Candidate: **Mohsin Ali Tunio**

Registration/Matric No: **KHA120062**

Name of Degree: **Doctor of Philosophy**

Title of Thesis: **PARTIAL DISCHARGE MEASUREMENT AND MODELLING WITHIN AN ARTIFICIAL CYLINDRICAL-SHAPED INSULATION MATERIAL UNDER NON- UNIFORM ELECTRIC FIELD**

Field of Study: **High Voltage Engineering**

I do solemnly and sincerely declare that:

(1) I am the sole author/writer of this Work;
(2) This Work is original;
(3) Any use of any work in which copyright exists was done by way of fair dealing and for permitted purposes and any excerpt or extract from, or reference to or reproduction of any copyright work has been disclosed expressly and sufficiently and the title of the Work and its authorship have been acknowledged in this Work;
(4) I do not have any actual knowledge nor do I ought reasonably to know that the making of this work constitutes an infringement of any copyright work;
(5) I hereby assign all and every rights in the copyright to this Work to the University of Malaya ("UM"), who henceforth shall be owner of the copyright in this Work and that any reproduction or use in any form or by any means whatsoever is prohibited without the written consent of UM having been first had and obtained;
(6) I am fully aware that if in the course of making this Work I have infringed any copyright whether intentionally or otherwise, I may be subject to legal action or any other action as may be determined by UM.

Candidate's Signature Date:

Subscribed and solemnly declared before,

Witness's Signature Date:

Name:

Designation:

ABSTRACT

In the presence of void in cable insulation, repetition of partial discharge (PD) occurrences is one of the main sources of insulation degradation, which may lead to complete breakdown. Therefore, it is important to monitor the condition of cable insulation through PD measurement. Replicating PD measurement on a test object with a shape similar to power cable insulation geometry may help a better understanding of PD characteristics within cable insulation to be achieved. Therefore, in this work, test samples of cylindrical insulation-shaped material containing an artificial void were prepared in the laboratory for PD experiments. PD measurements on test specimens containing an artificial void within cylindrical insulation-shaped geometry for various amplitude, frequency and waveshape of the applied voltage, void sizes and temperature of the insulation material were performed.

A physical model of PD activities within an artificial void in void in cylindrical insulation-shaped geometry was also proposed using Finite Element Analysis method and MATLAB. The advantage of this model over the previously reported models is this model can be used for simulation of PDs within a non-uniform electric field distribution in a void. The model was applied for simulation of PDs within the void in cylindrical insulation-shaped geometry to increase the understanding on PD physical phenomena through comparison with the measurement results. PD model parameters related to electron generation rate were determined using an optimisation method, the particle swarm optimisation (PSO). Comparison between the simulation and measurement results has managed to reveal the important parameters affecting PD phenomena within a void having non-uniform distribution of the electric field. These include distribution of charges on the void wall, decay rate of charges by surface conduction, inception field, extinction field and electron generate rate through surface emission and volume ionisation.

ABSTRAK

Dalam kehadiran lompang di dalam penebat kabel, pengulangan kejadian pelepasan separa (PD) adalah salah satu sumber utama degradasi penebat yang boleh membawa kepada kerosakan sepenuhnya. Oleh itu, adalah penting untuk memantau keadaan penebat kabel melalui pengukuran PD. Mereplikasi pengukuran PD pada objek ujian dengan bentuk yang sama di dalam penebat kabel boleh membantu pemahaman yang lebih baik bagi ciri-ciri PD di dalam penebat kabel yang perlu dicapai. Oleh itu, dalam kerja ini, sampel ujian kabel penebat berbentuk silinder yang mengandungi lompang tiruan telah disediakan di makmal untuk eksperimen PD. Pengukuran PD telah dijalankan ke atas bahan eksperimen yang mengandungi lompang tiruan berbentuk silinder untuk pelbagai amplitud, frekuensi dan bentuk gelombang voltan, saiz lompang dan suhu penebat telah dijalankan.

Model fizikal aktiviti PD di dalam sebuah lompang tiruan di dalam penebat kabel berbentuk silinder juga direka dengan menggunakan kaedah analisis unsur dan kod pengaturcaraan MATLAB. Kelebihan model ini berbanding model yang telah diunsurkan sebelum ini ialah model ini boleh digunakan untuk simulasi PD yang mempunyai medan elektrik yang berubah-ubah di dalam lompang. Model telah disimulasi dengan lompang di dalam penebat kabel berbentuk silinder untuk meningkatkan pemahaman pada fenomena fizikal PD melalui perbandingan dengan keputusan pengukuran yang diperolehi. Model berkaitan dengan kadar generasi elektron disahkan menggunakan cara pengoptimuman kawanan zarah (PSO). Perbandingan antara simulasi dan pengukuran adalah untuk mendapatkan parameter penting yang mempengaruhi fenomena PD didalam lompang yang mempunyai medan eletrik yang tidak sekata. Ini juga termasuk pengedaran caj pada dinding lompang, kadar pereputan caj oleh pengaliran permukaan, medan penubuhannya, medan kepupusan dan kadar elektron yang terlepas melalui permukaan dan isipadu pengionan.

ACKNOWLEDGEMENTS

With the name of ALLAH (most gracious and merciful), I am really grateful to Him in blessing me with the knowledge, giving me the courage to tackle the problems and always help me in each step of my life.

In successful completion of this work, I owe an enormous debt of gratefulness to my supervisors, Dr. Hazlee Azil Illias and Dr. Ab Halim Abu Bakar. I cannot find the right words to express the admiration and sincere gratitude towards my supervisors who gave me the opportunity to be a part of this work. They helped, encouraged and motivated me in every step of research, during the time I have spent with them. Their suggestions were always valuable and their technical comments lead to the completion of this research project.

I express my sincere gratitude to the UM High Voltage Laboratory and Malaysian Ministry of Education (MOE) for the financial support of this project through the High Impact Research (HIR) grant (H-16001-D00048).

I would also like to thank all my colleagues in the UM High Voltage Laboratory for being cooperative and helping.

Lastly, I would also like to thank all my family members and friends for their encouragement and support.

TABLE OF CONTENTS

LIST OF FIGURES

LIST OF TABLES

LIST OF SYMBOLS AND ABBREVIATIONS

AC	:	Alternating current
EGR	:	Electron generation rate
FEA	:	Finite Element Analysis
LDPE	:	LDPE Low density polyethylene
PC	:	Personal computer
PD	:	Partial discharge
PE	:	Polyethylene
PRPDA	:	Phase resolved partial discharge analysis
PSO	:	Particle swarm opimisation
XLPE	:	Cross-linked polyethylene

CHAPTER 1: INTRODUCTION

1.1 Introduction

Electrical energy consumption is increasing over the years in the developed countries as more high voltage transmission and distribution systems are constructed in city areas. In the city areas high voltage underground cable system are constructed and this become the key important to operate grids efficiently. Therefore, any fault in the cable system may cause service disruption to customers and economic losses []. Different defects such as voids and contamination within polymeric insulation of power cables may arise during the manufacturing processes and could be the main source of partial discharge (PD) activity under high electric field (EF) (Lei et al., 2014; Tian Y et al., 2002). Continuous PDs degrade the insulation material, which ultimately lead to insulation breakdown that will affect the reliability of the power system (Mardiana et al., 2010; Xiaoxing et al., 2014).

PD measurement is a recognized diagnostic tool to assess the quality of power cables and can improve the reliability of power system by providing premature warning to avoid service disruption (Mohamed F. P et al., 2013a; Mohamed F. P. et al., 2014). This measurement is conventional electrical testing according to IEC60270 standard and usually performed offline with well screened laboratory to detect defects in solid insulation.

Partial discharge, defined by IEC60270, is an electrically localised discharge, which bridges the insulation partially between two conductors (Chen et al., 2014; Mohamed F. P et al., 2013b). A few pico-Coulomb of PD magnitudes may cause irreversible damage to polymeric dielectric. Therefore, it is important to observe PDs within cables and eliminate their main source in order to avoid complete failure of the system (Bojie,

Chengke, et al., 2014; Lemke, 2013). It is also important to assess the cable insulation to check if replacement and maintenance of operating cables is required to avoid unexpected failure.

1.2 Problem statement

PD is one of the major sources that reduces the life of the cable insulation (Bojie, Wenjun, et al., 2014). The main source of PD is the presence of void in the cable insulation. PD may continuously degrade the insulation and will cause unexpected insulation breakdown (Ashtiani et al., 2013). Therefore, it is important to monitor PDs in the cable insulation. Many researches have been carried out in the past using specimens with the consideration of uniform electric field (EF) distribution in the void and dielectric material. In (Bang-Wook et al., 2013), the study was conducted using flat test sample of PPLP in order to investigate the PD inception voltage and Break down voltage under Ac and DC stresses. From experiment, the inception voltage of PD and breakdown voltage found higher under DC stress. PD measurement was performed on dielectric bound cavities in polyester under different energizing methods. This presented work discussed the usage of various energizing methods for the detection of PD event. It was found from this work that the magnitude of minimum charge remains unchanged under very low frequency and damped ac voltage method (Bodega et al., 2004). Experiments of rod-to-plane electrode arrangement with the consideration of non-uniform distribution of EF to observe PDs on insulation surface under semi square voltage was performed in (Florkowska, Roehrich, et al., 2011). The study presented non-uniform distribution of EF to assess the influence of high pressure on discharge mechanisms through phase resolved partial discharge (PRPD) patterns. It was concluded that the occurrence of PD depends on the voltage polarity and gap spacing between the electrodes (Florkowska, Florkowski, et al., 2011). The distribution of charges on the void surface is one of the factors that affect PD events in the void. It

changes the distribution of EF in a void and directly affects the next discharge occurrence time.

Although many works on modelling and measurement of PDs in void in dielectric material have been done in the past, modelling and measurement of PDs in a void within test samples of cylindrical insulation-shaped geometry have never been performed in the past. This is due to most the previous works have considered only uniform electric field distribution in the void, i.e. from flat surface insulation. The main motivation of this work is to develop a model of PD within non-uniform electric field distribution in a void using Finite Element Analysis method parallel with MATLAB code and replicate PD measurements in insulation material with a shape similar to power cable insulation geometry. Hence, a better understanding of PD characteristics under non-uniform electric field distribution in a void may be achieved.

1.3 Research objectives

In this work, a model of PD within an artificial void in a cylindrical insulation-shaped geometry is developed for simulation of PD occurrences within the void using Finite Element Analysis. Measurement results on PDs within test samples which consist of a cylindrical void in a cylindrical insulation-shaped polyethylene material were obtained. The results from the measurement and simulation were compared to identify physical parameters which influence PDs within non-uniform electric field distribution. Through this work, understanding on PD characteristics under non-uniform electric field distribution within a void in a cylindrical insulation-shaped geometry may be enhanced.

The key objectives of this research work are:

1. To propose a physical model of PD within an artificial void in a cylindrical insulation-shaped geometry using Finite Element Analysis method for simulation of PD occurrences within the void
2. To investigate the impact of amplitude, frequency and waveshape of the applied voltage on PDs within the test samples of cylindrical insulation-shaped geometry through PD measurements
3. To analyse the effect of void size and temperature of the insulation material on PD activity within the test object of cylindrical insulation-shaped geometry through PD measurements
4. To replicate the measurement results using the PD modelling through an optimisation method, the particle swarm optimisation (PSO)
5. To identify the key parameters affecting PDs within non-uniform electric field distribution through comparison of the measurement and simulation results.

1.4 Research methodology

There are 6 main stages involved in this work. First, literature review related to this work and the previous studies of this research area were performed. This includes partial discharge in a void, PD measurement methods, past PD measurements and also past PD modelling. Then, simulation model of PD of a void in a cylindrical insulation-shaped geometry was developed. Subsequently, test samples consisting of a void in a cylindrical insulation-shaped geometry were developed. Measurements of PD were done on the test samples that have been developed. After that, the measurement results were replicated through the simulation results from the PD model using an optimisation method, the particle swarm optimisation (PSO). Finally, a thesis report of the overall work was written.

1.5 Thesis organisation

This thesis is divided into six chapters. Chapter 1 consists of an introduction, which introduces the background, problem statement, research objectives and research methodology of this work and outline of the report.

Chapter 2 deals with literature review while overviewing the previous related studies of this research area. This includes partial discharge in a void, PD measurement methods, past PD measurements and also past PD modelling.

Chapter 3 presents the research methodology to achieve the objectives of this study. This includes the development of cylindrical insulation-shaped geometry model using FEA software in parallel with MATLAB code, preparation of the test specimens and the PD measurements that have been performed in this work. This chapter also includes particle swarm optimisation (PSO) algorithm used to choose the simulation model parameters.

In Chapter 4, all measurement results that have been performed in this work are detailed. This includes PD measurement under different amplitude, frequency and waveshape of the applied voltage, void size and temperature of the insulation material.

Chapter 5 deals with all simulation results. This chapter also deals with the comparison of PD activities between measurement and simulation results under different amplitude, frequency and waveshape of the applied voltage, void size and temperature of the insulation material.

Finally, Chapter 6 presents the conclusions and the future work of this research work.

CHAPTER 2: PD MODELLING AND MEASUREMENT

2.1 Introduction

Insulation is important in high voltage system because its failure may cause sudden breakdown that will affect the reliability of the whole power system (Mu-kuen et al., 2014). Mostly, solid dielectric materials are used in all kinds of devices to insulate different voltage potentials. In the past, severe cracks have been observed in the insulation during normal operating condition or after long time duration and a sudden insulation breakdown occurred without any odd indications. One of the main reasons declared behind these sudden failures is partial discharge (PD), which degrades the insulation and may cause unexpected breakdown. Therefore, it is important to monitor insulation used in high voltage system to schedule maintenance actions timely. PD occurs when there are defects in the solid insulation material such as small air gap or void, which may cause electrical discharge that partially bridges the insulation between two conductors (Mohamed F. P, et al., 2013b). These defects may be formed during manufacturing process and may be undetected under factory test but will affect the insulation during operation. PD testing is one of the diagnostics tool used to detect defects in the insulation.

2.2 Significance of partial discharges in power cables

Power cables have great importance in the power system because any fault in cable insulation may cause breakdown. In past literature, it was found that majority of breakdowns in cable network are due to internal defects in the insulation system or accessories of cable system. A sudden failure of cable system or its accessories may affect the reliability of the whole power system. Figure 2.1 shows examples of defects in power cables.

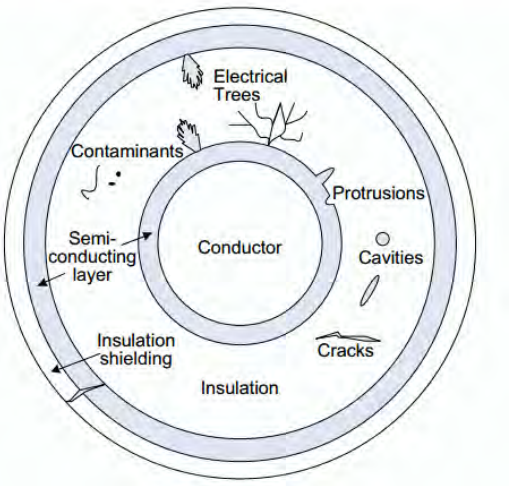

Figure 2.1: Defects in power cables (Lei, et al., 2014)

The power cable system consists of cables and their accessories, including joints and terminations. These joints and terminations are the special components used to join two cables together and to provide the end of the cables respectively. The purpose of cable joint is to join two cables while termination is used to provide the end of the cable. Many factors have to be considered during the installation of cable joints and termination to avoid any insulation deterioration in all applications. The cable accessories may be deteriorated during installation; hence, care should be taken during installation.

Breakdown in power cables are usually due to digging activities (Wester et al., 2001). However, more than half of the breakdowns in the cable network are caused by internal fault in the insulation system of the cable network as shown in Table 2.1. Visual assessment of the troubled components provides insight in the different types of breakdown related to insulation defects. Based on these visual assessments, a list of defects in different components of cable network is shown in Table 2.1. For many years, withstand test (AC and DC) was the only testing method applied in power cables network. As shown in Table 2.2, PD diagnosis are used to provide the best indications

of discharging weak spots in the high voltage insulation (Gulski et al., 2005). The tolerance level of PD for power cables is given in Table 2.3.

Table 2.1: Defects in insulation for various types of power cable component (Gulski, et al., 2005)

Cable Type	Accessories	Insulation
Paper insulated lead covered (PILC)	Low oil level Sharp edges on connectors Moisture penetration Air/Gas bubbles Bad hardened resin	Outer sheet damage Tracking Internal damage (as a result of bending)
Cross-linked polyethylene (XLPE)	Sharp edges on connectors Moisture penetration Air/Gas bubbles Field grading movement Bad hardened resin Interface problems Remaining semicon	Outer sheet damage

Table 2.2: Insulation degradation processes of cable insulation (Gulski, et al., 2005)

Accessories	interface problems → PD → tracking; bad hardening → cracking → PD; conductors problems → overheating → cracking → PD; local field concentrations → PD
Extruded Insulation	water trees → electrical trees → PD insulation voids → delamination → electrical trees → PD local field concentrations → PD
Paper oil Insulation	oil leaks → dry regions → overheating → PD water ingress → local effects → overheating → PD local field concentrations → PD

Table 2.3: Tolarence level of PD for MV cables

PILC Cables	0 pC-3000 pC	Discharge within acceptable limits
	3000 pC - 6500 pC	Some concern, monitoring recommended
	6500 pC -10,000 pC	Some concern, regular monitoring recommended
	>10,000 pC	Major concern, repair or replace
XLPE Cables	0 pC - 250 pC	Discharge within acceptable limits
	250 pC -350 pC	Some concern, monitoring recommended
	350 pC - 500 pC	Some concern, regular monitoring recommended
	>500 pC	Major concern, repair or replace

Partial discharge is one of key sources for degradation of cable insulation in practice or service. PD is an electrically localised discharge, which bridges the insulation partially between two conductors (Kai et al., 2004; Mohamed F. P, et al., 2013b). PD occurs when the insulation systems have defects such as voids within the dielectric material. These defects in the insulation may arise during installation and could be the key reason of PD under high electric field. PD occurs in power cables due to voids. Basically, the gas filled cavities are known as voids, which may be formed during manufacturing process. PD gives an indication of defect, which exists in the insulation material and does not cause complete breakdown (Ye et al., 2014). PD degrades the insulation and may cause energy loss. In (Su et al., 2013), 35 failure cases of XLPE, 6.6 kV cables were due to the insulation faults over the period of 3 years. The measurement analysis in (Noske et al., 2014) has shown that the higher percentage of cable failure cases was located at the place of concentrated PDs, recognized in the measurement prior to the failure. Figure 2.2 shows the summary of cables in percentage subjected to PD activity at the place of failure.

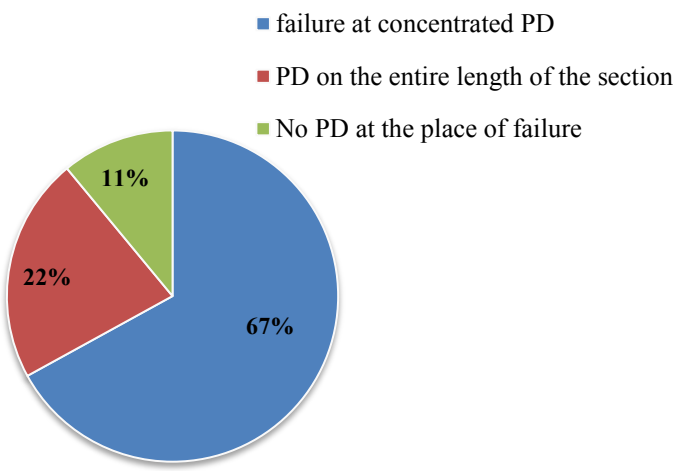

Figure 2.2 : Summary of cables subjected to PD activity at the place of failure (Noske, et al., 2014)

The propagation of PD in XLPE cable is much faster. Therefore, it is important to monitor PDs in power cables to avoid unexpected failure of whole power system. PD measurement is one of the most important diagnostics tool which can be used to detect the faults or defect in the insulation. PDs can be categorized into three types such as internal, surface and corona discharge (Kreuger, 1992).

2.3 Types of partial discharge

2.3.1 Internal discharges

Figure 2.3 shows some examples of internal discharges in solid insulation. This PD type occurs in a void of solid dielectric and also shaped by the process of electrical treeing.

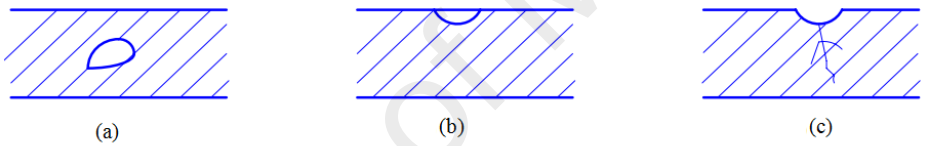

(a) Void apart from electrodes,
(b) Void adjacent to electrode,
(c) Void as pre-breakdown channel (Tree)

Figure 2.3: Sources of internal discharges in solid dielectrics (Kreuger, 1992)

2.3.2 Surface discharge

Surface discharge is a streamer type discharge that could start at high tangential field strength along the interface. There may be no difference between internal and surface discharge if the detected PDs are near to inception voltage. The difference can only observe when the voltage is increased, discharge happens along a longer surface. Thus, surface discharge increases in length and magnitude. Through this way, it may not be difficult to differentiate surface discharges from internal discharges (Kreuger, 1992).

2.3.3 Corona discharge

Corona discharge occurs near to the sharp point under high electric field during the measurement of partial discharge in cables. The sharp edges at the cable termination may cause corona discharge and could be enclosed by metallic round caps surrounding the sharp point at equal potential (Kreuger, 1992).

2.4 Partial discharge in a void

A void is a gas filled cavity in the insulation and may appear due to the errors in the manufacturing of insulation material. A void represents the weakest point in the insulation and it has low value of permittivity with lower value of electrical breakdown strength compared to surrounding insulation material. This enhances the electric field in the void at high applied electric field and PD may occur in the void. PD degrades the insulation via combination of thermal, chemical, mechanical and radioactive processes (Bartnikas, 1987). In order for a PD to occur in a void, the electric field in the void must exceed a critical value with the availability of free electron to initiate an electron avalanche. The schematic diagram of PD in a void is shown in Figure 2.4.

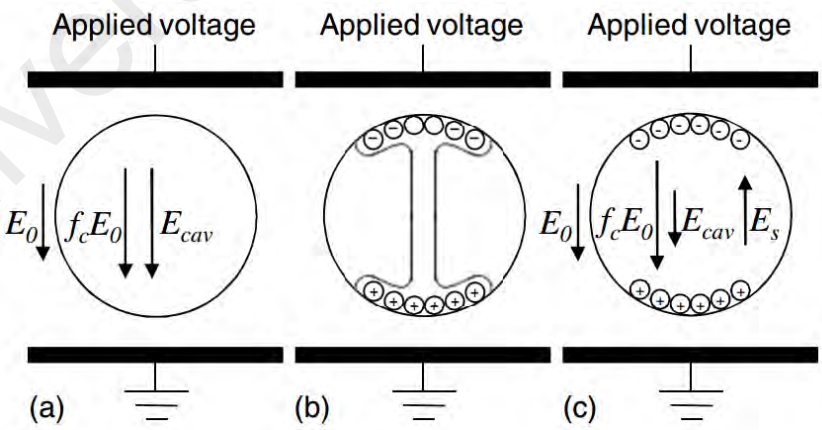

Figure 2.4: Schematic diagram of a PD Schematic diagram of a PD activity in the cavity: (a) before PD, (b) during PD and (c) after (Illias H. A. et al., 2011)

All fields (as shown in Figure 2.4 (a)) have same polarity as the applied voltage. Before PD happens, EF in the centre of the cavity, E_{cav} is equal to f_cE_0 where f_c is the modification factor of the field that has been applied in the cavity subjected to the permittivity of the material and cavity geometry. During PD event, when the discharge has gone through the cavity and reach to the opposite surface, charges propagate on the cavity wall as shown in Figure 2.4 (b). Due to this EF in cavity, E_{cav} decreased and discharge activity stops once E_{cav} less than the extension field $E_{ext.}$. After discharge event, free charges may move on the cavity surface subjected to the magnitude and the polarity of E_{cav} and filed due to surface charge, E_s (Illias H. A., et al., 2011). PD ionizes the gas in a void and resulting in charges to move in the electric field and becomes trapped on void surfaces. The charge builds up on void surfaces in the opposite direction of the applied field and ultimately leads to extinction of the discharge (Kuffel et al., 2000).

2.5 PD measurement methods

PD measurement has great importance to assess the insulation condition of high voltage equipment because PD causes high risk for the stability of an insulation system. PD measurement has been utilized to evaluate the design of insulation system and for quality test for new high voltage equipment. PD measurement has been widely applied in past 20 years to diagnose the insulation in cables, transformers, motors, switchgears and generators. Generally, there are three factors about PD events, its level, type and location. It is important to have data of PD together with information of the surrounding insulation material in order to plan repair or maintenance actions timely (Tenbohlen et al., 2008). It is also very important to know the reasons why PD measurement is done.

PD measurement is used for design, quality assurance and diagnostics test of the insulation system. There is a certain allowable or safe limit of PD magnitude to exist in

insulation during material testing. If the allowable limit is exceeded, there may be manufacturing deficiencies exist or due to poor workmanship. The main purpose of each test is to ensure that the equipment is reliable. If the levels of detected PD are high, it is likely that the insulation will fail precipitately (Stone, 2005).

In general, the measurement methods of PD in high voltage cable insulation is shown in Figure 2.5. The electrical method has high sensitivity and precision measurement but it has higher vulnerability to noise. The acoustical method has the advantage of being immune from electrical interference. However, acoustic emission attenuation within high voltage cables significantly reduces the measurement sensitivity and makes it impossible to be calibrated. Acoustical emission method is suitable for PD monitoring in power transformers and switchgears, where they are immune to excessive electrical noise that may exist at the measurement site (Tian Y. et al., 2005).

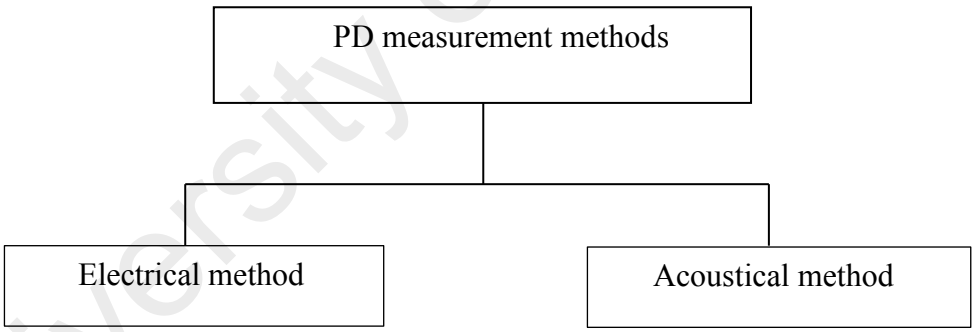

Figure 2.5 : Classification of PD measurement methods in high voltage cable insulation

In PD detection, high frequency pulses due to PD activity that travel along the conductor side of a cable and ground connection of the termination have a band width and rise time of nanoseconds range. These pulses can be either signal pulses or a cascade of fast pulses, depending on the types of defects in cable insulation. Hence, a sensor that is used to detect these pulse signals must be of high frequency type. There

are two common types of coupler used in detecting PD signals from cable insulation; inductive and capacitor couplers, as shown in Figure 2.6.

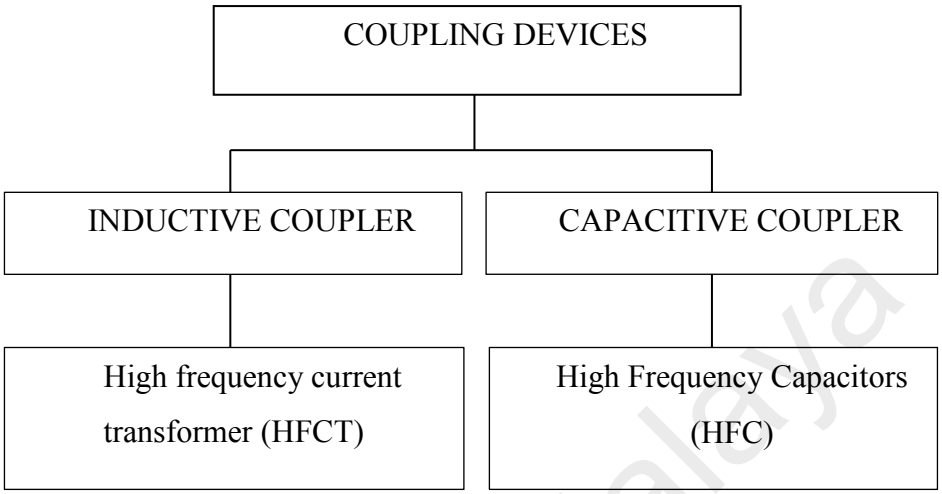

Figure 2.6: Types of coupling device in PD detection methods (Ahmed et al., 1999)

High frequency current transformer (HFCT) is one of the inductive coupler types. HFCT is usually used in online testing and placed around grounding leads of cable termination. HFCT consists of a doughnut shaped of ferrite core with coupling turns, which is sensitive to frequencies. These couplers detect the magnetic field disturbance induced by the PD pulses travelling in the ground loop (Ahmed, et al., 1999).

High frequency capacitor (HFC) is a capacitive coupler type. It is commonly used in offline testing and is connected in parallel with cable termination. These high frequency capacitors filter the 60 Hz component from very high frequency pulses associated with PD. As these capacitive couplers are connected directly to the high voltage side, they must be free of PD at the test voltage. In theory, online testing using capacitive coupler can be made possible by permanently installing the sensor next to the cable termination. However, permanent installation of capacitive couplers is not economically feasible (Ahmed, et al., 1999). Comparison about inductive and capacitive coupler is shown in Table 2.4.

Table 2.4: Comparison between inductive and capacitive (Ahmed, et al., 1999; Zhong et al., 2001; Zhou et al., 2009) coupler

INDUCTIVE COUPLER	CAPACITVE COUPLER
High frequency current transformer is an inductive coupler	High frequency capacitor is a capacitive coupler
It consists of a ferrite core with eight-coupling turns and is sensitive to a frequencies ranging from 10kHz to 200MHz	It consists of a metallic foil electrode in contact with the semi conducting screen at a metal screen cut.
It is connected around the cable itself (Ahmed et al., 1998)	It is connected directly to the high-voltage side of the termination; it must be PD free at the test voltage.
It is normally utilized during on-line PD testing	It is normally utilized during off-line PD testing

Many researchers have developed practical methods to measure PD during 1950-1980s and these methods are widely used today in laboratories and factories (Bartnikas et al., 1979; Kelen, 1976; Kreuger, 1989). Since the last 20 years, the nucleus of the research has been to enhance PD technology so that it can be applied practically to diagnostics testing to determine the insulation condition of power cables, transformers, switchgears, etc.

2.5.1 Conventional method

Conventional PD testing has been used to evaluate cable quality and usually performed offline in the laboratory using international standard (Ahmed, et al., 1998; IEC, 1996). This electrical testing was used to detect small discharges during the initiation of insulation deterioration (Tian Y, et al., 2002). Since many years, conventional testing has been used in order to assess the insulation of the cables as directed by IEC 60270. This electrical testing is usually performed offline in the

laboratory. After the introduction of polyethylene cables in distribution system in 1950s, different PD detection methods were developed to check the reliability of these cables (Wang et al., 2005). Table 2.5 shows an overview of various energizing methods used for PD diagnosis.

Table 2.5: Various energizing methods (Gulski, et al., 2005)

Voltage Type	Voltage Source
AC 50/60 Hz	Inductively tuned resonant circuits
AC 15-500 Hz	Frequency tuned resonant circuit
VLF 0.1 Hz	0.1 Hz sin wave generator and amplifier
DAC Damped AC voltages, 50-500 Hz	Damped oscillating voltage wave excitation sources

The measurement circuit for PD in conventional method (offline method) includes coupling capacitor (80-1000 pF range), which is connected in parallel with the test object and in series with PD detector and a recording instrument is connected to record the PD data for further analysis. Normally, offline diagnostic testing is done by disconnecting the power cable from the main circuit and connected to the external power source to energize it. The offline measuring circuit is shown in Figure 2.7.

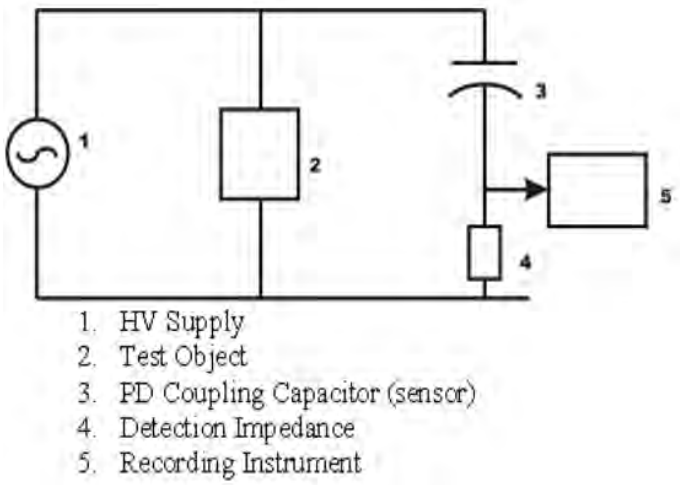

Figure 2.7: Schematic diagram of offline PD measurement (Stone, 2005)

In an off-line PD testing, the most common means of detecting the PD pulse is using a high voltage coupling capacitor connected to the high voltage terminal of the test object, as shown in Figure 2.7. When a PD occurs, there is a very fast flow of electrons within the defect site. This causes a voltage drop across the defect site. However, this voltage drop is compensated by charges that flow from the coupling capacitor to the electrodes at the defect site. The coupling capacitor has very high impedance to high AC voltage but very low impedance to high frequency PD pulse current. This results in a current flow within the circuit. Since the electrons are moving near to the speed of light across a small distance, the resulted current pulse has a very short duration, typically in a few nanoseconds (Bartnikas R, 2002). Any PD coupling devices or sensors, such as HFCT that are sensitive to high frequencies can detect the PD pulse currents.

PD detection normally consists of circuits which convert PD pulse currents from a sensor to a voltage signal because most measurement instrumentations are more sensitive to voltage than current. The conversion occurs via a resistor or more elaborate detection impedance. A resistor yields a wide band detection system with the output normally measured in mV or μV. However, if RLC detection impedance is used, the characteristics of the detector can be manipulated to integrate the PD pulse current to

yield a signal magnitude that is proportional to the apparent charge transfer in each discharge (Bartnikas R, 2002). The RLC detection impedance is very popular since the rate of deterioration of polymeric insulation is often directly proportional to the total number of electrons and ions that bombard the insulation surface, as commonly used in off-line PD testing (Stone, 2005).

2.5.2 Non-conventional method

This method is used for the online monitoring of cable insulation and its accessories by using PD detection technique through sensors such as directional, inductive and capacitor couplers (Ahmed, et al., 1998; Tian Y et al., 2004; Wang, et al., 2005). The online testing is very useful for cable termination and joints problems (Stone, 2005). PD measurement can be done while the cable is connected to the circuit or cable in service but the main problem in this method is noise interference during the PD measurement (Tian Y, et al., 2002).

Online PD measurement represents the true condition of insulation since measurements are taken under the actual operating condition of a cable. Hence, the result of online PD testing has higher reliability than the off-line testing. The actual operating conditions that affect the outcome of PD testing are the ambient temperature, thermal expansion, contraction characteristics, material properties, mechanical loading influence, current based power factor and harmonics frequency effects.

Online PD monitoring of high voltage is therefore an important and robust method of PD detection (Hao et al., 2007; IEC 60270 3rd Edition, 2000). Presently, online PD detection technology is less mature than that in laboratory due to several issues, they are; serious electromagnetic interference and back ground noise and insulation deterioration evaluation basis is insufficient (Wenjie et al., 2012).

Online PD measurement is much easier in extruded cable terminations since the cable below the termination plate is readily accessible. In theory, online testing using capacitive coupler can be made possible by permanently installing the sensor next to termination. However, this is not economically feasible due to the cost of the couplers and the reliability of transmission cable terminations. Therefore, capacitive coupling techniques is advantageous in offline testing (Ahmed, et al., 1999).

Online PD measurement has higher reputation in power supply industry because it does not cause any disruption to normal service and does not require any separate source to energize the cable. There is an availability of continuous monitoring to monitor PD behavior development over a long period in online PD measurement. However, online PD measurement can be affected by the presence of noise and disturbance that can modify or hide PD activity (Cavallini, Montanari, et al., 2005).

An example of online PD measurement circuit on power cables is shown in Figure 2.8. An artificially generated PD signal is applied to the power cable through calibrator. Then, the PD signals are produced and picked up by the HFCT sensor. HFCT sensor is coupled to spectrum analyzer which is used to measure PD activity and displayed by digital oscilloscope. A General Purpose interface bus (GPIB) is connected, which is used for attaching sensors and programmable instruments to a computer.

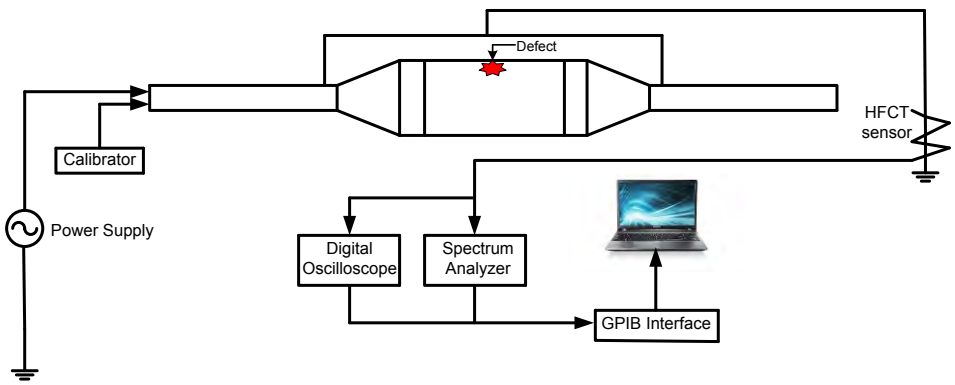

Figure 2.8: Online PD measurement system in cables (Kwang Jin Lim et al., 2008)

It is difficult to perform field measurement of PD by utilizing the conventional techniques in power cables. This technique does not have sufficient sensitivity for a long cable due to the high capacitance involved; it can only identify discharges in short remote cable lengths. By installing sensors permanently at cable joint, online continuous monitoring can be achieved. The spectrum analyzer method has been employed recently to measure the PD activity in GIS cables. Calibration without isolating the cable from the circuit and introducing PD pulses are not easy to perform. Hence, a pulse phase analyzer is used to identify PD and a digital signal oscilloscope is used to display the signals in a laboratory setup and these measurements are made while cable in service (Ahmed et al., 1997).

Online PD monitoring can detect newly arising defects within cable insulation during its normal operation. Online PD monitoring has two main advantages; there is no interruption to operational service of the cable and it provides continuous monitoring. In the past, online PD monitoring on power cables have been implemented by using inductive high frequency current transducers, acoustic emission sensors and high frequency capacitive sensors (Tian Y, et al., 2002). These sensors are installed near to cable joint to detect PD signals. A measuring equipment receives PD signals through coaxial cable for data acquisition and processing for further analysis. However, the main problem of this signal transmission is the attenuation and electromagnetic interference. To overcome this problem, optical fibre system has been used for the transmission of PD signals (Auckland et al., 1995).

2.6 Past PD measurements in voids

2.6.1 PD measurements in a cylindrical void

In the past, PD measurements were performed in an artificial cavity. In one of the literatures, PD measurements were taken on a disc shape cavity which was prepared by

pressing three polycarbonate plates (Forssen et al., 2008a). A hole was created by drilling one of the plates to form a cavity and was placed between other two plates. PD measurements were taken on the test object at different applied voltage and frequency. Referring to the measurement results, the PD events in the cavity clearly vary with frequency of the applied voltage. When the frequency of 8 kV applied voltage was decreased from higher to a lower value, the value of the maximum apparent charge reduces. The change in the maximum charge magnitude with frequency may be due to the statistical effect, which is increased at higher frequency. The wide spread in PD magnitudes were observed at higher frequency. This shows that the change in the applied voltage during time lag is significant.

The measured PD patterns at 10 kV were similar to that of 8 kV at lower frequency (Forssen, et al., 2008a). At higher frequency, more number of PDs at 10 kV with lower maximum charge magnitude was obtained as compared to 8 kV. The measurement results have shown that the PD event in the cavity depends on frequency of the applied voltage. It is clear that the frequency dependence of the PD event changes with the applied voltage. The number of PDs per cycle at 8 kV remains unchanged while PD magnitude increases as the frequency was increased. In contrast, the number of PDs per cycle at 9 and 10 kV increases with the frequency but the PD magnitude is almost constant. The PD magnitude at lower frequency is found nearly same for all applied voltages (8, 9 and 10 kV) but not similar at higher frequency. Referring to the measurement results, PDs are more concentrated at 9 and 10 kV, which indicates that the statistical time lag does not influence the PD event significantly at these voltages. Hence, the statistical time lag must be shorter at 9 and 10 kV as compared to 8 kV. This is expected since the statistical time lag decreases as the electric field increases.

The PD measurements were taken on insulated cavities with different diameters to observe the effect of cavity diameter on PDs (Forssen, et al., 2008a). The measurements were taken at different cavities with diameter of 1.5, 4 and 10 mm respectively at 10 kV and variable frequencies. The lowest inception voltage (~ 7 kV) was obtained for the cavity with diameter of 10 mm and this may be due to differences in the electric field enhancement. Referring to the measurement results, PD event in the cavity is almost the same as the frequency of the applied voltage was increased and the number of PDs is almost constant when the frequency varies and there is wide spread in PD magnitude at all frequencies. The concentration of PDs was observed for all diameters at lower frequency. The actual number of PDs per cycle increases as the frequency of the applied voltage was increased. The same number of PDs was witnessed for small size of the cavity at all frequencies. However, for larger cavity diameter, the number of PDs per cycle decreases as the frequency was decreased from 100 Hz to 0.01 Hz. For larger size of the cavity, the surface charge decay via recombination is slow and the higher number of PDs per cycle with larger cavity diameter is mainly due to the PD inception voltage decreases with increasing cavity diameter.

When PRPD patterns were captured at 11 kV and the frequency was decreased from 100 to 0.01 Hz, PD events in the cavity evidently change with the applied frequency (Forssen, et al., 2008a). The spread in phase and magnitude of the PDs varies between different applied frequencies. Additionally, the number of PDs per cycle is higher at 100 Hz compared to lower frequencies. In real practice, the number of PDs is even higher than the recorded in PD measurement because some of PDs are discriminated by the measurement system.

2.6.2 PD measurement in spherical void

PD measurements were also performed under various voltage amplitudes, frequencies of applied voltage, cavity sizes and material temperature (Illias H. A et al., 2011b). The test sample that has been prepared in the laboratory for the experiment is shown in Figure 2.9. PD measurements were taken through PRPD under different applied voltage for spherical cavity of 1.4 mm diameter. From the measurement results, it was found that the number of PDs per cycle, total charge magnitude per cycle and the magnitude of maximum charge increases except the magnitude of mean charge with increasing the applied voltage.

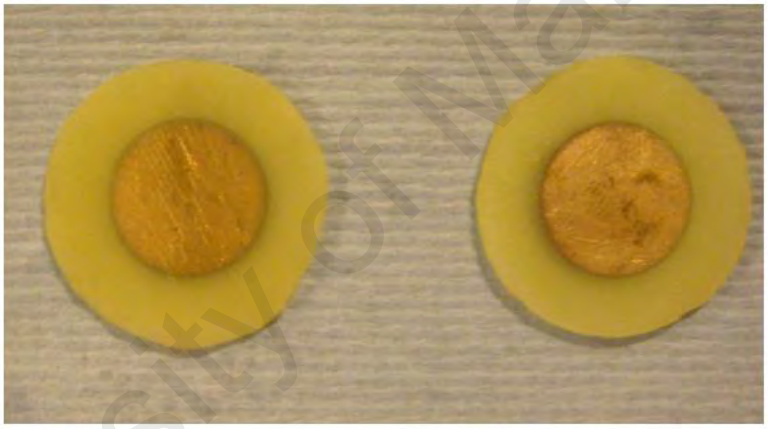

Figure 2.9 : Test object used for PD measurement spherical cavity (Illias, 2011)

As the applied voltage was increased, the electric field was enhanced and initial electron generation rate was increased, which corresponds to a larger number of initial free electrons in the cavity (Illias H. A, et al., 2011b). Hence, the statistical time lag decreases, resulting in more number of PDs occurring in the earlier phase of the applied voltage. Therefore, more number of PDs per cycle as the applied voltage amplitude was increased. The total charge magnitude also increased as the applied voltage was increased due to higher PD repetition rate. However, the magnitude of mean charge value decreases when the applied voltage was increased. The statistical time lag was reduced with increasing applied voltage and due to this more number of PDs with lower

charge magnitude. The value of maximum charge magnitude increases when the applied voltage was increased because of lager voltage drop across the cavity when a PD occurs.

PD experiments were also performed on spherical cavity having diameter of 1.55 mm as a function of frequency at 14 kV AC sinusoidal voltage. As the frequency of applied voltage was decreased, the number of PDs per cycle and the total magnitude of charge per cycle decrease but the magnitude of maximum charge remained unchange whereas the value of mean charge increases. It was observed from the measurement that the order of applied frequency did not affect PD event (Illias H. A, et al., 2011b).

When the frequency of applied voltage was increased, higher number of PDs per cycle was obtained due to the reduction in charge decay on the cavity surface between consecutive discharges. At higher frequencies, more charges are available on the surface of the cavity for the next PD to occur. Hence, more PD events occurred immediately once the level of inception voltage, U_{inc} (~4.53 kV) is exceeded, causing higher repetition rate of PD for higher applied frequencies.

As the frequency of applied voltage was increased, the total charges were increased slightly because of higher number of PDs per cycle at higher frequency. However, the increase in total charge is not high due to the reduction in the number of discharges with higher charge magnitudes. At lower frequencies, the effect of surface charge decay is more significant, reducing the electron generation rate and increasing statistical time lag. Hence, more PDs occur at voltages higher than inception voltage, resulting in a reduced number of PDs with larger charge magnitudes.

The magnitude of mean charge decreases when the frequency of applied voltage was increased due to more discharges having low magnitudes (Illias H. A, et al., 2011b).

The magnitude of the maximum charge is not frequency dependent because the applied voltage amplitude is unchanged, resulting in the same maximum voltage drop across the cavity when a PD occurs. Referring to the charge magnitude-phase axes of the ϕ-q-n plots, for larger cavity, the tail of the 'rabbit-ear' like pattern is distributed but for smaller cavity, it is well defined over a larger phase range. PDs near the minimum charge magnitude for larger size of the cavity are lower in number compared to the smaller cavity.

Referring to the PD measurement data, less number of PDs was observed for larger size (~2.35 mm) of the cavity. This may be due to a higher rate of charge decay via surface conduction. However, the total number of charge, magnitude of mean, maximum and minimum per cycle are higher for larger size of the cavity because the maximum avalanche propagation length parallel to the applied field and the resulting avalanche head perpendicular to the applied field are larger. The inception field, E_{inc} (~2.83 kV/mm) was obtained lower for larger size of the cavity compared to smaller cavity (~1.1 mm) (Illias et al., 2012).

Referring to the PD measurements under different material temperature, when the temperature of the material was increased, each PD data increases except for the value of the maximum charge magnitude. The higher repetition rate of PDs at higher material temperature could be due to an enriched electron generation rate. The value of minimum charge magnitude increases as the material temperature was increased because of higher inception field. However, the maximum charge magnitude decreases with increasing material temperature because of higher electron generation rate, decreasing the statistical time lag and subsequently PDs are expected to occur at lower field in the cavity. At higher temperatures, the 'rabbit-ear' like pattern on the charge magnitude-

phase axes happens over a narrower phase range whereas the number of PDs near $q_{\min}$ rises (Illias, et al., 2012).

2.7 Past PD modelling

2.7.1 PD in a cylindrical void

In one of the past literatures, the modelling of PD in cylindrical void was done at different frequencies of the applied voltage (Forssen et al., 2008b). The main aim of this work was to present explanation of the PD frequency dependence based on the physical conditions at the cavity. A physical model of PD in a cavity has been developed that was used to reproduce the important features of measured PD patterns and simulate the PD sequence dynamically at variable applied frequencies. A PD model was developed by using Comsol Multiphysics 3.3a software in 2D axial symmetric based on the test object with spherical electrode, as shown in Figure 2.10. The simulation for the sequence of PDs in the cavity was done for 100 to 500 applied voltage cycles with amplitude of 11 kV at variable frequency in the range of 0.01 to 100 Hz.

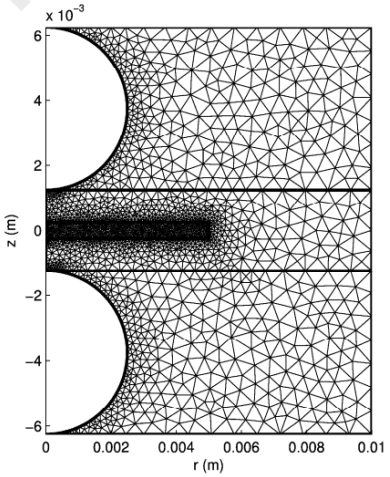

Figure 2.10: 2D- axial symmetric model geometry with mesh (Forssen, et al., 2008b)

The main aim of such work was to develop a physical model of PD in the cavity that reproduces the important features of PD patterns that have been measured at variable applied frequencies. The developed model consists of these parts; the calculation of the

electric potential distribution in the test specimen at each time step, the electron generation in the cavity, the discharge process, the apparent charge and surface charge decay (Forssen, et al., 2008b).

For the calculation of electric potential distribution, it is supposed that all PD events occur in the centre of the cavity where the electric field is high as compared to its surrounding area and it is also assumed that the charge move on the surface of the cavity due to conduction. The potential distribution in the test object can be determined from equations (2.1) and (2.2) through Finite Element Method (FEM),

$$\nabla \cdot (-\sigma \nabla V - \frac{\partial}{\partial t}(\varepsilon_0 \varepsilon_r \nabla V)) = 0 \tag{2.1}$$

$$\nabla \cdot (-\sigma_{surf} \nabla V_{surf}) = 0, \quad V = V_{surf} \text{ on the surface of the cavity} \tag{2.2}$$

where V is the electric potential, ε_r is the relative permittivity, ε_0 is the vacuum permittivity, σ is conductivity, V_{surf} is the potential on the cavity surface and σ_{surf} is the conductivity of the cavity surface. It is assumed that the generation of free electrons in the cavity is dominated by surface emission from cavity walls. The total generation of free electrons N_e is modelled as

$$N_e(t) = N_{e0} \exp(|U_{cav}(t)/U_{crit}(t)|) \tag{2.3}$$

where U_{cav} is voltage over the centre of the cavity, U_{crit} is minimum voltage for discharge and the value of N_{e0} is a constant. Therefore, the electron generation rate increases with increasing electric field. The probability that a free electron is generated in the cavity in the time interval $[t,t+\Delta t]$ and is assumed to be $N_e(t)\Delta t$, provided that $|U_{cav}(t)| > U_{crit}$. The equivalent distribution function for PD is

$$F(t) = 1 - \exp\left(- \int_0^t N_e(t')dt' \right) \tag{2.4}$$

The time point of PD in the cavity is simulated from above distribution function by use of a random number R ($0 \leq R \leq 1$). PD will occur when F is greater than R; otherwise there will be no discharge event.

In the developed model, the process of discharge in the cavity is modelled dynamically by increasing the conductivity of the cavity resulting current flow through the cavity and a corresponding decrease in U_{cav}. If the value of U_{cav} drops below a certain level called U_{ext}, then the conductivity of the cavity is decreased and the discharge extinguishes. In the presented model, the calculation of apparent charge is done numerically by time integration of total current through test object. The total current can be determined by integrating the current density over the surface of the lower electrode. The surface charge decay in the cavity is modelled by the conduction on the surface of the cavity governed by equation (2.2). Once the PD has occurred in the cavity, then the value of cavity surface conductivity σ_{surf} is set to higher value $\sigma_{surfhigh}$ (~3 x $10^{-15}\,S$ for (f = 0.01 Hz) and ~2 x $10^{-11}\,S$ for (f ≥ 0.1 Hz)) and this higher value of the cavity surface conductivity $\sigma_{surfhigh}$ is maintained until the total amount of charge Q drops below a critical level Q_{crit} (~10 pC). After that, the value of σ_{surf} is changed back to its initial low value $\sigma_{surflow}$ ($\sim 10^{-15}\,S$). The conductivity is the same over the whole surface of the cavity (Forssen, et al., 2008b).

The time dependent electric field distribution in the test object is calculated through Finite Element Method (FEM). The main advantage of FEM is its capability to handle complex geometries. The simulation results are in reasonable agreement with measurement results at the same voltage amplitude and frequencies. Referring to the

simulation results, the conductivity of the cavity surface, the electron emission from the surface of the cavity and PD extension voltage may vary with the frequency of applied voltage. It is also concluded from the simulation results that the surface charge decay in a cavity via conduction on the surface of the cavity cannot be modelled by keeping the conductivity of the cavity surface constant. Instead, the results incriminate that the conductivity of the cavity surface is subjected to the total charge present on the surface (Forssen, et al., 2008b).

2.7.2 PD in a spherical void

In the past, a PD model for a spherical cavity within a homogeneous dielectric material was developed through Finite Element Analysis (FEA) software (Illias H. A, et al., 2011b). The developed model was used to simulate PD event in the cavity for different stress conditions and cavity conditions. Two modes, 'Meridional Electric Current' and 'Heat Transfer by Conduction' in the COMSOL Multiphysics software was chosen to study the distribution of electric field and temperature within the cavity respectively. The two-dimensional (2D) axial symmetric model geometry that has been developed using FEA software based on the test specimen is shown in Figure 2.11. An AC sinusoidal voltage was applied to the upper electrode whereas the lower electrode was constantly grounded. The developed model was used to solve electric potential and temperature. The distribution of the electric field was determined using Equation (2.5) (Illias, et al., 2012),

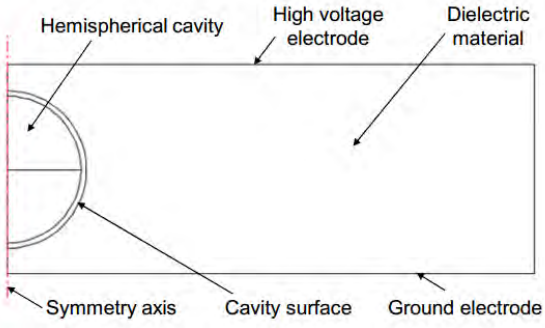

Figure 2.11: 2D-axial symmetric model (Illias H. A, et al., 2011b)

$$\sigma \nabla V + \varepsilon \nabla \left(\frac{\partial V}{\partial t} \right) = 0 \tag{2.5}$$

where V is the electric potential, ε_r is the permittivity and σ is the conductivity.

From the developed model geometry, the uniform field distribution was observed when there was no PD. When the size of the cavity is large as compared to thickness of the dielectric material; the distribution of electric field in whole cavity is no longer uniform. The electric field on the surface of the cavity nearest to the electrode is fairly lower as compared to the field at the centre of the cavity due to the impact of the electrode. However, the electric field in the cavity is symmetrical along the *r* and *z*-axes (Illias H. A et al., 2011a). Due to this, FEA model is used continuously during the simulation to compute the field distribution in the cavity. Symmetry of both electric field and charge distributions in the cavity along the *r* and *z* axes is assumed before and after PD occurrences and this was attained in the FEA modeling by assuming that the whole cavity is affected during PD activity (Illias, et al., 2012).

From the developed model, only the electric field in the centre of the cavity, E_{cav} was extracted. Once E_{cav} exceeds the inception field, E_{inc}, an initial free electron is needed to initiate the PD event. The inception field E_{inc} can be calculated by using

$$E_{inc} = (E_1/p)_{cr}\, p(1 + B/\sqrt{pd}) \tag{2.6}$$

where $(E_1/p)_{cr}$ and B are the parameters of ionization for the gas, d is the diameter of the cavity and p is the pressure in the cavity. The inception field is constant for cavity diameter, d. For air, $(E_1/p)_{cr}$ is 24.2 $VPa^{-1}m^{-1}$ and B is 8.6 $Pa^{1/2}m^{1/2}$ (Illias H. A, et al., 2011b).

To model an initial free electron by using total electron generation rate (EGR), $N_{et}(t)$ is defined as the total number of free initial electrons generated in the cavity per unit time. $N_{et}(t)$ is the summation of EGR due to surface emission, $N_{es}(t)$ and to volume ionisation, N_{ev},

$$N_{et}(t) = N_{es}(t) + N_{ev} \tag{2.7}$$

It is presumed in the model that $N_{es}(t)$ is dominated by charge detrapping from cavity surface, where the amount of charge detrapping for a PD likely to occur is reliant on the charge magnitude of the earlier PD. Therefore, primarily, $N_{et}(t)$ only depends on N_{ev}. Once the first PD has occurred, $N_{et}(t)$ depends on both $N_{es}(t)$ and N_{ev} (Illias, et al., 2012).

In order to have a simplified PD model, $N_{es}(t)$ is defined as the number of free electrons generated in the cavity per unit time via surface emission. If N_{es0} is the number of free electrons generated in the cavity per unit time, then the number of free electrons generated in the cavity per unit time due last PD, N_{PD} can be defined as

$$N_{PD} = N_{eso}\,|E_{cav}(t_{PD})/E_{inc}| \tag{2.8}$$

where $E_{cav}(t_{PD})$ is E_{cav} of the earlier PD at a time t_{PD}. It is assumed that N_{PD} is linearly proportional to E_{cav}/E_{inc}. $N_{es}(t)$ is assumed to be increased exponentially with

the product of electric field in the cavity, $E_{cav}(t)$ and temperature of the material T_{mat} (Illias, et al., 2012). This is based on the assumption that surface emission is enhanced by the electric field and temperature of the material. Therefore, when a PD probably to occur, with the consideration of the charge decay effect since the earlier PD and the field and temperature-dependent terms, $N_{es}(t)$ can be defined as

$$N_{es}(t) = N_{PD}\, exp\left[\frac{-(t-t_{PD})}{\tau_{dec}}\right] exp\left|\frac{E_{cav}(t)}{E_{inc}}\frac{T_{mat}}{T_{amb}}\right| \tag{2.9}$$

where τ_{dec} is the charge decay time constant and T_{amb} is the ambient temperature. $\frac{E_{cav}(t)}{E_{inc}}$ and $\frac{T_{mat}}{T_{amb}}$ represent a simplified field and temperature dependency (Illias, et al., 2012). The availability of an initial free electron is modelled using the likelihood of a PD occurrence, $L(t)$ which is compared with a random number, *R*. If $L(t)$ is higher than *R*, a PD will occur at the given time instant (Illias, et al., 2012). Assuming that $L(t)$ is proportional to the total EGR, $N_{et}(t)$ and the time-step interval, Δt, $L(t)$ is defined as

$$L(t) = N_{et}(t)\,\Delta t \tag{2.10}$$

Once the PD event has occurred, the temperature in the cavity increased due to the electron ionisation process. It is assumed in the developed FEA model that the temperature in the cavity is affecting the inception field, E_{inc}. Hence, only the temperature in the centre of the cavity, $T_{cav}(t)$, is extracted.

It is assumed that the discharge occurred along the center axis of the cavity and affects the entire cavity. When partial discharge is modeled dynamically, the discharge activity can be denoted by changing the cavity state from non-conducting to conducting. This can be modeled by increasing the conductivity of the cavity from its initial conductivity, σ_{s0} (~1x10^{-18} S/m) to maximum cavity conductivity, $\sigma_{cav\max}$. $\sigma_{cav\max}$ is the conductivity of the cavity which decreases the voltage across the centre of the cavity

until it becomes less than the extinction voltage, U_{ext} (~4.68 kV) during the process of discharge (Illias H. A, et al., 2011b). The maximum conductivity of the cavity $\sigma_{cav\max}$ can be determined by using

$$\sigma_{cav\max} = (\alpha e^2 N_e \lambda_e) \Big/ (m_e c_e) \tag{2.11}$$

where α is the coefficient related to the distribution of electron and mean free path (~0.85), e is the electric charge of the electron, m_e is the mass of the electron, λ_e is the mean free path of the electron (~4 μm), c_e is the thermal velocity of the electron $(\sim 3\times 10^8 ms^{-1})$ and N_e is density of the electron, which is defined as

$$N_e = n_e \Big/ (4/3\pi r^3) \text{ , where } n_e = q_{\max} \Big/ e \tag{2.12}$$

where n_e is the number of electrons in the streamer channel, r is the radius of the cavity and $q_{\max}$ is the magnitude of maximum charge, which can be obtained from the measurement results (Illias H. A, et al., 2011b).

Charges accumulated on the surface of the cavity after a PD may remain free on the surface of the cavity, which are supposed to move along the wall of the cavity via surface conduction. In the developed model, this mechanism can be represented by a field-dependent cavity surface conductivity, σ_s. The cavity surface conductivity, σ_s is subjected to the direction of $E_{cav}(t)$ and the field due to the surface charge $E_s(t)$. The amount of free surface charge after a PD, $q_{sfreePD}(t_{PD})$ can be calculated from the FEA model by integration of field displacement, $D(t_{PD})$ over the lower or upper cavity surface boundary, S

$$q_{sfreePD}(t_{PD}) = \int_S D(t_{PD}) \bullet dS \tag{2.13}$$

Therefore, the field due to free surface charge immediately after a PD event, $E_{sfreePD}(t_{PD})$ can be determined using

$$E_{sfreePD}(t_{PD}) = \left| q_{sfreePD}(t_{PD}) / q_{PDtotal}(t_{PD}) \cdot E_{sPD}(t_{PD}) \right| \tag{2.14}$$

where $q_{sfreePD}(t_{PD})$ is the total PD real charge up to time t_{PD} and its equivalent field is $E_{sPD}(t_{PD})$. It is calculated using

$$q_{PDtotal}(t_{PD}) = \sum_{i=1}^{m} (q_{PD})_i \tag{2.15}$$

where m is the number of PD events and $(q_{PD})_i$ is PD real charge magnitude of i^{th} PD event. When $E_s(t)$ reaches $E_{sfreePD}(t_{PD})$ during surface charge decay, no more surface charge can decay through conduction along the cavity wall (Illias H. A, et al., 2011b). Table 2.6 shows the PD characteristics in the case of field non-uniformity.

Table 2.6 : PD characteristics in the case of field non-uniformity

Definition	PD characteristics
Electric field distribution within the model is determined using	$\vec{\nabla} \bullet \varepsilon_0 \varepsilon_r \vec{E} = 0$ where ε_0 and ε_r is the vacuum and relative permittivity.
Electric field distribution before PD activity	Non Uniform
Electric field distribution after PD activity	Non Uniform
Distribution of charges on void wall	Non Uniform

2.7.3 Analytical model of PD

In the past, a model of PD has been developed that simulates streamer type discharge (Niemeyer, 1995). The developed PD model details the mathematical model of initial electron generation equations, model of streamer process and the approximation of PD charge magnitude. The electric field in the cavity is obtained through Poisson's equation and the field enhancement in the cavity is averaged to obtain a field enhancement factor. This factor is used to approximate the field enrichment due to field that has been applied and due to cavity surface charge. After that, the simulation results of the developed model are compared with measurement. Poisson's equation is solved because of field effect due to surface charge on the net electric field in the cavity. The initial free electron generation for a PD to occur has been categorized into surface emission and volume ionization, where related equations involving to physical parameters of the material have been derived.

The calculation of real charge magnitude of PD was done by using $c\Delta U_{PD}$, where c is the capacitance of the cavity and ΔU_{PD} is the voltage drop across the cavity because of PD (Niemeyer, 1995). The apparent charge due to a PD is measured as the charge induced on the measurement electrode, which depends on the location of the cavity within the material, the shape of the cavity, the pressure of the gas and the orientation of the cavity against the applied field (Crichton et al., 1989; McAllister, 1997; Pedersen et al., 1991; Schifani et al., 2001). The simulation results are in reasonable agreement with measurement data with some differences in PD phase and magnitude. Another model of PD uses the similar field enhancement approximation method to simulate mechanism of PD at high temperature within a cavity in an epoxy resin (Schifani, et al., 2001). A discharge model was developed in the past to simulate a streamer type PD in the cavity within an epoxy resin. The model that has been developed used to characterize PD in voids and the change in behaviour due to aging (Gutfleisch et al., 1995). Although these

models deliver worthy explanations of PD event, the simulation results are compared with experimental results for a single value of applied stress.

2.8 PD measurement in underground cable

Underground cables have a key role in urban power grids. Thus, any failure in power cables may lead to service disruption to consumers and financial losses. Regardless of strong quality controls throughout manufacture process in the factory, defects may still exist in the power cable system during installation (Ruay-Nan et al., 2011).

Nowadays, utilities are involved in operating their systems efficiently with minimum expenditure. Failure statistics show that outages due to weak spots in the cable system which affects the reliability of whole power grids. Table 2.6 shows failure statistics in MV grids. Refereing to Table 2.6, the failure in medium voltage grids is mainly contributed by cable system with 59% (Gargari et al., 2011).

Table 2.7: Failure statistics in medium voltage grid (Gargari, et al., 2011)

Failure caused by	Percentage
Cable circuits	59%
Digging	17%
MV transformers	2%
Secondary installations	4%
Other	14%

Modem underground power cables are mostly manufactured with polymeric insulation that is vulnerable to degradation and failure due to PDs. PD events may occur due to contamination, mechanical damages and imperfection caused during

installation. Generally, XLPE cables are used in medium voltage underground cables. Although their resistance to PD is less, it is reliable as compared to other insulating materials. Because of its less resistance to PD, failure risk of XLPE cable is high. Therefore, PD measurement is very important to monitor the insulation of the underground cables to avoid sudden failure (Escorsa et al., 2008; Vakilian et al., 2006).

In one of the past literatures, PD measurements on two 11 kV XLPE cables were done. In this study, a new sensitive internal sensor for PD signal, the semiconducting length with PD simulation model was introduced. It was found that by using semiconducting layer as PD internal sensor, the monitoring of power cable insulation is possible through PD detection (Vakilian, et al., 2006).

Another study was conducted in one of the past literatures. The authors have examined PD event in four 11 kV, PILC type underground cables for the period of 3 months. The on-line PD based monitoring was used to collect the data from power cables using high-frequency current transformers (HFCT). From the results of the study, it was found that the electrical noise associated with PD signal is one of the major issue in the on-line PD based monitoring and it must be removed for the identification of PD signal (Zhou, et al., 2009).

In one of the past literatures, sixty one well aged XLPE underground cables were tested in the laboratory. In this study, authors have tested these power cables through PD detection and location system. The test results are given in Table 2.7. Table 2.7 comprises of applied voltage, the inception voltage of PD and the discharge magnitude if site of the PD was located. All tests were conducted in a normal laboratory atmosphere with a background noise of 1 to 3 pC (approximately).

Table 2.8: Table: Sample log for PD location (McBride et al., 1994)

Test No	Findings	Inception Voltage (kV)	Applied Voltage (kV)	Approx. PD Level (pC)
1	No PD	---	11	---
2	No PD	---	11	---
3	Nick	---	12	---
4	Nick	---	10	---
5	PD	13.4	13.4	100
6	No PD	---	14.8	---
7	No PD	---	14.8	---
8	PD	8.0	9.7	25
9	No PD	---	14.8	---
10	Nick	---	10.2	---
11	No PD	---	14.8	---
12	Nick	---	9.1	---
13	No PD	---	14.8	---
14	PD failure	19.3	19.3	30
15	No PD	---	25	---
16	No PD	---	25	---
17	PD failure	31.6	31.6	334
18	No PD	---	34.7	---

19	No PD	---	34.1	---
20	No PD	---	29.4	---
21	No PD	---	34	---
22	PD failure	34	34	12
23	Failure	---	33.4	---
24	No PD	---	34	---
25	PD Ext	35	35	62
26	No PD	---	35	---
27	No PD	---	34.6	---
28	No PD	---	35	---
29	No PD	---	15	---
30	No PD	---	15	---
31	Nick	---	15	---
32	No PD	---	15	---
33	Nick	---	7.9	---
34	No PD	---	15	---
35	No PD	---	15	---
36	Nick	---	15	---
37	No PD	---	20	---
38	PD Failure	14	14	84

39	No PD	---	13.3	---
40	No PD	---	15	---
41	No PD	---	9.5	---
42	No PD	---	15	---
43	No PD	---	15	---
44	No PD	---	15	---
45	PD Ext	12	20	44
46	No PD	---	15	---
47	PD Ext	14	14	22
48	No PD	---	15	---
49	No PD	---	15	---
50	No PD	---	20	---
51	No PD	---	20	---
52	No PD	---	20	---
53	No PD	---	20	---
54	No PD	---	14	---
55	Failure	---	27	---
56	PD Failure	18.5	6.0	938
57	PD Failure	19.4	19.4	374
58	PD	16	16	---

59	No PD	---	20	---
60	PD	14.0	9.1	46
61	PD	12.4	11.4	91

When PD event was not detected, there were no pulses recorded above background noise level. After observing and testing sixty one severely aged test specimens, no specimens were found with an inception voltage of PD at or lower than their normal operating voltage. The test voltages of PD in the experiment were raised higher than operating voltage to locate the sites of potential failure. All sixty cables were well aged but only there were only fourteen specimens in which PD location was detected. Only two samples at no 5 and 58 in the Table 2.7 tested contained PD locations which neither extinguished nor failed. The sample Test 5 was inspected constantly with minor change in the inception voltage during the aging test and test no 58 was stayed in the aging test for many weeks deprived of failure. Seven power cables were failed while monitoring and locating PDs. The data of these failed power cables is given in Table 2.8. From the power cable failure data collected through PD testing, possibly failure sites can be projected. This site estimation skill permits the inspection of the area around the site of PD prior to failures.

Table 2.9: Cable failures during PD location (McBride, et al., 1994)

Test No	Cable Length (ft)	Estimated PD location (ft)	Actual Failure Location (ft)	Failure Voltage (kV)
8	53.5	25.4	26.0	24
14	58	39.4	37.5	19.3
17	60.7	16.9	20.3	31.6
22	51.3	43.3	40.3	34
38	78.5	12.3	18	14
56	36.1	32.8	31.6	6
57	52.4	47.7	49.6	19.4

In the work, two active sites of PD were located. One of the sites illustrated definite proof of potential failure. This PD site had a big water tree with proof of PD at the tree tips and a big hole in the center. Immediately next to this water tree, an electrical channel had stabbed the insulation material and bridged the entire insulation. The other site had a voids and was extremely contaminated with water trees (McBride, et al., 1994).

2.9 Summary

In high voltage system, the measurement of partial discharge is one of the important and recognized diagnostic tools to detect defects in power cable insulation to avoid sudden failure of the whole power system. This chapter has presented overview on significance of PD measurement in power cables. Two PD measurement methods such as conventional and non-conventional are also detailed in this chapter. Apart from that, this chapter has discussed past PD measurements performed in an artificial cavity under

various applied stress conditions. The different PD models that have been developed in the past are also detailed in this chapter. Finally, this chapter has discussed PD measurement in underground cables.

CHAPTER 3: METHODOLOGY

3.1 Introduction

This chapter presents the methodology of this work. The cable insulation geometry model has been developed using Finite Element Analysis (FEA) method. The developed model consists of a cylindrical void within a cylindrical insulation-shaped model geometry. Two-dimensional cylindrical insulation-shaped model geometries using FEA method and equations related to this model are explained. The modelling part is also subdivided into different sections; FEA model development, equations, charge accumulation on the surface, charge decay after PD occurrence and generation rate of electron.

This chapter also presents the preparation of the test specimens that have been used for the measurement of PD. Different measurements that have been undertaken by using prepared test specimens in the University of Malaya High Voltage Laboratory (UMHVL) are also detailed. The measured PD results are compared with simulation results under different stress conditions and void diameters. This allows identification of the key parameters affecting PD activity from the PD simulation model of cable insulation geometry under different stress conditions to be achieved. Finally, an optimisation method, the particle swarm optimisation (PSO), which is used to determine the parameters of the PD model is described.

3.2 Proposed PD physical model

3.2.1 Model geometry

Figure 3.1 displays the geometry of the cylindrical insulation-shaped model which was developed based on the test object that has been created in two-dimensional (2D). The model was created in Finite Element Analysis method using COMSOL software

and interfaced with MATLAB programming code. In COMSOL software, the 'Electrostatics' module was chosen to solve the electric field distribution in the cable insulation model. All assigned constants and settings of the cylindrical insulation-shaped model that have been used for simulation are shown in Table 3.1 and Table 3.2. The cable insulation model comprises of a dielectric material with outer radius of 12.5 mm (representing insulation layer), inner radius of 3 mm (representing conductor) and a 1.5 mm void radius located in the middle of the dielectric. Figure 3.3 shows the unstructured mesh with triangular elements in the cylindrical insulation-shaped model. Eq. (3.1) is applied to determine the distribution of the electric field, E within the model, where ε_0 and ε_r are the vacuum and relative permittivity,

$$\vec{\nabla} \bullet \varepsilon_0 \varepsilon_r \vec{E} = 0 \tag{3.1}$$

Under high voltage stress, the distribution of the electric field is not uniform in the insulation material and void from the high voltage conductor to the ground layer. Therefore, PD occurrences are influenced by the non-uniform field distribution within the void. The surface was grouped into two regions as shown in Figure 3.1; the surface region nearer to the high voltage electrode is called lower void surface while the other surface is called upper void surface. Both surface regions do not have equal area. To represent the distribution of charges on the void surface after a discharge happens in a non-uniform electric field (EF), the lower and upper void surface regions were divided equally into four sections as shown by the red dashed lines in Figure 3.1. From Figure 3.1, the area of one section, S_s for each region is

$$S_s = \begin{cases} \dfrac{\text{Total area of high voltage region}}{4\,\text{sections}} \\ \dfrac{\text{Total area of grounded region}}{4\,\text{sections}} \end{cases} \qquad (3.2)$$

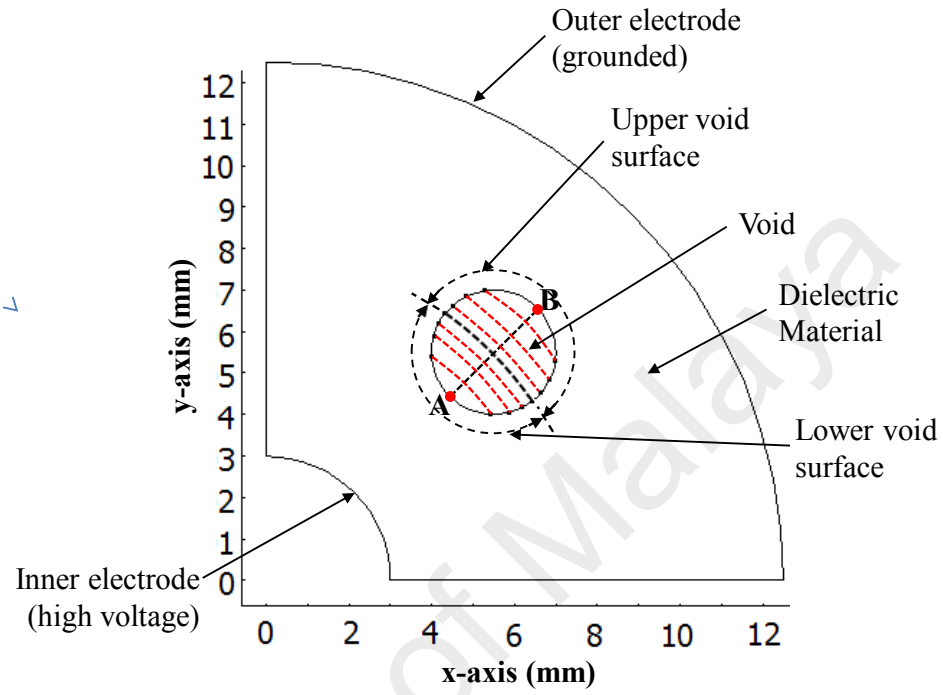

Figure 3.1: 2D cylindrical insulation-shaped model geometry

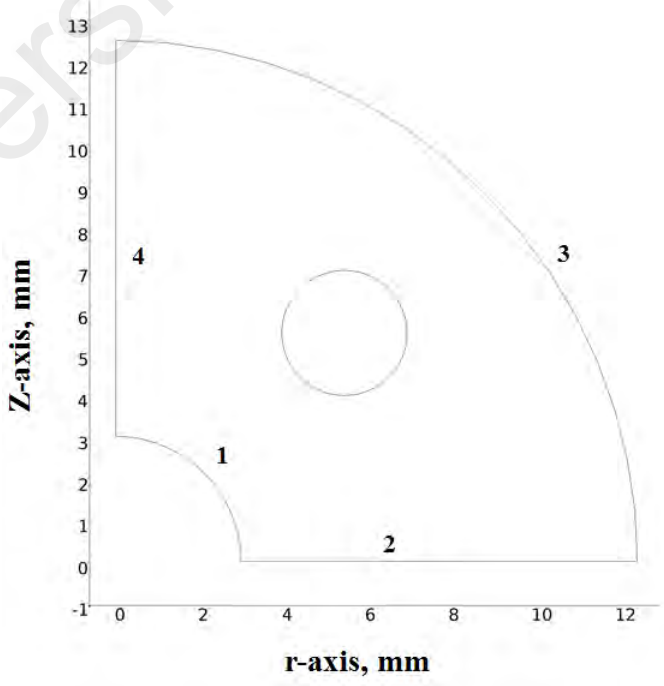

Figure 3.2: Boundary condition of the model geometry

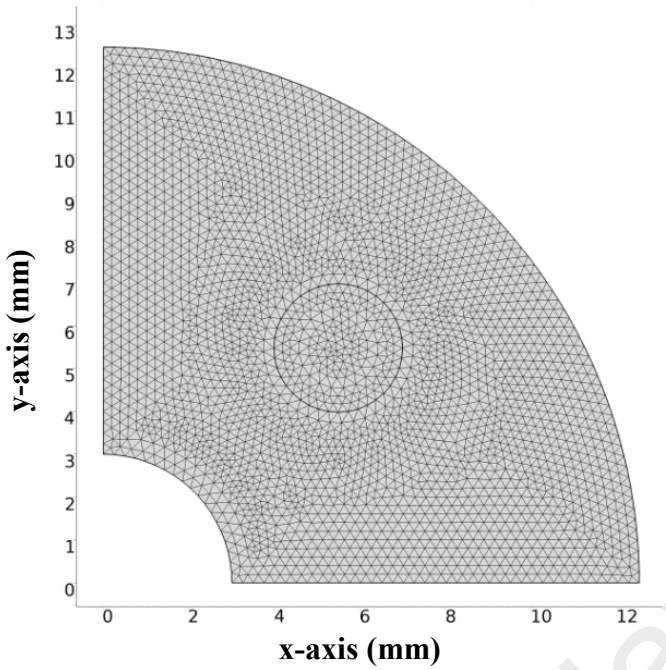

Figure 3.3: 2D cylindrical insulation-shaped model geometry with mesh

Table 3.1: Assigned constants for the model

Name	Symbol	Expression
Applied voltage amplitude	U_{app}	21 kV
Frequency of applied voltage	f	50 Hz
Material relative permittivity	ε_{rmat}	2.3
Void surface permittivity	ε_{rv}	1

Table 3.2: Boundary settings of the model

Boundary line	Boundary condition	Expression
1	Electric potential	$V = U_{app} \bullet Sin(2 \cdot pi \cdot freq \cdot t)$
2, 4	Electric insulation	$\vec{n} \bullet \vec{J} = 0$
3	Ground	$V = 0$
All interior boundaries	Continuity	$\vec{n} \bullet (\vec{J}_1 - \vec{J}_2) = 0$

3.2.2 Charge accumulation on the surface

Referring to Figure 3.1, it is assumed that PDs occurs from point A to point B. These two points are located on the line crossing from the centre of the conductor to the void centre. As such, the field magnitude within the void along the PD charge movement across the void surface between points A and B is not uniform. Hence, if a discharge happens in the void, the average field magnitude, E_{ave} along the line between points A and B is checked if it is higher than the inception field, $E_{inc} = 2.8$ kVmm^{-1}.

When a PD occurs between points A and B, electrons move towards either point A or B while, positive ions move towards the opposite direction of the electrons. Once the respective charges have reached points A and B, it is assumed that the charges propagate along the void surface away from points A and B.

The propagation of charges along the void wall is represented by increasing the density of charge along the surface section. When a PD happens under the direction of E_{ave} from the high voltage surface to ground surface, a density of charge, $-\rho_s$ is first

increased on the section adjacent to the point A while ρ_s is added on the section adjacent to the point B. Addition of ρ_s and $-\rho_s$ causes E_{ave} to decrease. The propagation of charges along the void wall stops once E_{ave} is less than the extinction field, E_{ext}. If E_{ave} remains larger than E_{inc}, new ρ_s and $-\rho_s$ are added on the next section of the void surface region. When a PD occurs under the direction of E_{ave} from the ground surface to high voltage surface the opposite is done, a charge density, ρ_s, is first added on the section adjacent to the point A while $-\rho_s$ is added on the section adjacent to the point B. If E_{ave} is still higher than E_{ext} once charges have propagated on all sections of the high voltage and ground surface regions, ρ_s and $-\rho_s$ are added again on the sections adjacent to points A and B. The process is repeated until E_{ave} reduces lower compared to E_{ext}. When the next discharge event happens, ρ_s and $-\rho_s$ are added to the charge density on the void wall from the last PD activity.

Once PD stops, the accumulation of charges on all regions can be used to calculate the magnitude of real charge, q_{real} by

$$q_{real} = A\sum \rho_s \tag{3.3}$$

where A is the area of one surface section and $\Sigma\rho_s$ is summed density of charge that has been introduced on the void wall. The real charge density calculated using eq. (3.3) was found to be within reasonable agreement compared to the calculation using real charge equation in (Gutfleisch, et al., 1995; Niemeyer, 1995), as follows,

$$q_{real} = \varepsilon_o \pi r_v^2 (1 + 2\varepsilon_r)\Delta E_{ave} \tag{3.4}$$

where ε_0 is the vacuum permittivity, r_v is the void radius, ε_r is the material permittivity and ΔE_{ave} is the change of field within the void due to PD, which equals to the void field when a PD happens minus the void field when a PD stops.

The charge magnitude (apparent), q_{app} can be found by integrating the difference of density of charge on the grounded conductor before and after a PD occurs, $\rho_{se}{}^{a}$ and $\rho_{se}{}^{b}$ over the surface area, S, where

$$q_{app} = \int \left(\rho_{se}^{b} - \rho_{se}^{a}\right) dS \tag{3.5}$$

3.2.3 Charge decay

After a PD occurs, the distribution of charges turns not uniform due to the density of charge variation on void surface. It is assumed that charges on the void wall are free to propagate along the void surface through conduction. When charges of opposite polarity meet, recombination happens, causing the surface charge decay. The free charges movement on the void wall is subjected to the polarity of average field in the void, E_{ave} and the surface charge field, E_{sc} polarity. If both E_{sc} and E_{ave} have the same polarity, free charges on each surface section move away from points A and B via conduction on the void wall. This results in the amount of charge nearer to points A and B becomes lower and the amount of charge increases at void sections further from points A and B.

The charge conduction through the wall of the void is commonly represented by enhancing the surface conductivity of the void, σ_{vs} from a small to a large value $(\sim 0 - 10^{-4})\ S/m, (\sim 1x\ 10^{-13} - 5x10^{-3})\ S/m$, as have been adopted in the past PD models (Forssen, et al., 2008b; Illias, et al., 2012) .When the charge movement on the void wall does not occur, σ_{vs} is always set to 0. A sudden increment of σ_{vs} from zero to a higher value in the model is not related to physical mechanism of surface degradation due to bombardment of charges on the void surface. Instead, it is adopted to model the

movement of charges by surface conduction because a higher surface conductivity will reduce the electric field due to the charges on the surface against time.

The decrement of surface charge density, $\Delta\rho_{sn}$ from n-th void section is calculated using

$$\Delta\rho_{sn} = (1/A_n)\sigma_{vs}E_{ave}d_v\Delta t \tag{3.6}$$

where A_n is the area of n-th void section, d_v is the void diameter and Δt is the time step without discharge. Hence, charge reduction from n-th void section causes its charge density, ${\rho_{sn}}^t$ to become

$${\rho_{sn}}^t = {\rho_{sn}}^{t-1} - \Delta\rho_{sn} \tag{3.7}$$

Where t is the current time step in the simulation while t-1 is the previous time step.

Since the charge moves away from points A and B, $\Delta\rho_{sn}$ is added on the section adjacent to n-th section,

$${\rho_{s(n+1)}}^t = {\rho_{s(n+1)}}^{t-1} + \Delta\rho_{sn} \tag{3.8}$$

The impact of various distribution of charge density on the void wall will influence the void electric field distribution, hence, affecting the next discharge occurrence.

3.2.4 Partial discharge occurrence

The inception field, E_{inc} can be determined through comparison between the simulation and measurement data. E_{inc} equals to the average field within the void, E_{ave} without surface charge when the applied voltage equals to the inception voltage, U_{inc}. U_{inc} is determined from the measurement, where the first ever PD occurs in the test sample. There are two conditions for a discharge event to happen within a void,

1- The field magnitude in the center of the void has to be larger compared to the inception field, E_{inc}
2- A free electron is needed to start a discharge

A free electron is represented by the summed electron generation rate (EGR), $N_{et}(t)$ or the summed amount of generated free electrons in the void per second. The summed EGR is the addition of EGR due to volume ionization, N_{ev} and surface emission, $N_{es}(t)$, where

$$N_{et}(t) = N_{ev} + N_{es}(t) \tag{3.9}$$

Initially, the total EGR depends on the volume ionization, N_{ev} but after the first PD event, EGR is dependent on N_{ev} and $N_{es}(t)$. To reduce the complexity of the model describing PD behaviour, it is assumed that the total electron generated in the void due to surface emission depends on charge de-trapping from the void surface due to last discharge. Surface emission is the major source of EGR (Gutfleisch, et al., 1995; Niemeyer, 1995). For subsequent discharge, it is assumed that the charge de-trapping is subjected to the field in the void center of the last discharge occurrence, $E_{ave}(t_{PD})$, where t_{PD} is the last PD time. If N_{es0} is the generated free electrons within the void per second at E_{inc}, then, the generated electrons within the void per unit time due to last discharge, N_{PD}, can be given by

$$N_{PD} = N_{es0}|E_{ave}(t_{PD})/E_{inc}| \tag{3.10}$$

From (3.10), it is assumed that N_{PD} is linearly proportional to E_{ave}/E_{inc}. Therefore, $N_{es}(t)$ can be defined by including the effect of charge decay from the last discharge event,

$$N_{es}(t) = N_{PD}\exp[-(t-t_{PD})/\tau_{dec}]\exp|E_{ave}/E_{inc}| \tag{3.11}$$

where $(t - t_{PD})$ is the time passed since earlier PD and τ_{dec} is the charge decay time constant. $|E_{ave}/E_{inc}|$ represents the field-subjected of $N_{es}(t)$. In this work, N_{es0} is subdivided into lower and higher values, N_{es0H} and N_{es0L}. The value of N_{es0L} is applied when the E_{ave} polarity changes between two PDs while N_{es0H} is used when there is no change in the polarity. The generation rate of electron through surface emission increases when the void field is larger.

An electron availability is represented through the discharge probability occurrence, $P(t)$, with the assumption that $P(t)$ is linearly dependent on the total EGR, $N_{et}(t)$ and the time step, Δt_0 during no discharge event. $P(t)$ is checked with a number randomly generated, R. Then, a PD may happen when $P(t)$ is higher compared to R. $P(t)$ is found by

$$P(t) = \Delta t_0 N_{et}(t) \tag{3.12}$$

All simulation parameters are shown in Table 3.3. The value of Δt_0 is set short to have reasonable time for simulation. The value of Δt_1 is set very small to model very short discharge period. The material relative permittivity, ε_{rmat} is 2.3, which is same as used in the laboratory experiment. The relative permittivity of the void, ε_{rv} is set as 1 because it was assumed that the void consists of air. Finally, the value for the time constant of charge decay, τ_{dec} is 1.5 ms. The values for N_{ev}, N_{es0L} and N_{es0H} depend on each other, depending on the experiment conditions. Their values are chosen by matching the simulation and measurement data. Improper selection of the values may result in non-matching between the simulation and measurement results. In example, when EGR is very large, the PD occurrences per cycle might be very high than the measurement while if EGR is very low, PD occurrences might be very small than the measured value. The value of ρ_s is set as $1\text{x}10^{-4}$ Cm^{-2} throughout the simulation to obtain good precision of discharge magnitude with reasonable simulation time. The selection

of ρ_s is similar to how Δt_1 is selected. Values for σ_{vs}, E_{inc}, E_{ext}, N_{es0H}, N_{es0L} and N_{ev} are determined through comparison between simulation and measurement results.

Table 3.3: General simulation parameters

Definition	Symbol	Value	Unit
Insulation diameter	d_{mat}	25	mm
Conductor diameter	d_{cond}	6	mm
Void diameter	d_v	3 to 5	mm
Material relative permittivity	ε_{rmat}	2.3	-
Void surface permittivity	ε_{rv}	1	-
Applied voltage	U_{app}	21 to 24	kV
No discharge time step	Δt_0	100	us
Discharge time step	Δt_1	1	ns
Simulation cycle	Cycle	500	-
Voltage frequency	f	50	Hz
Time constant of charge decay	τ_{dec}	1.5	ms
Surface charge density	ρ_s	$1x10^{-4}$	Cm^{-2}
Conductivity of the void surface	σ_{vs}	-	Sm^{-1}
Extinction field	E_{ext}	-	$kVmm^{-1}$
Inception field	E_{inc}	-	$kVmm^{-1}$
EGR from volume ionization	N_{ev}	-	s^{-1}
EGR from surface emission (lower)	N_{es0L}	-	s^{-1}
EGR from surface emission (higher)	N_{es0H}	-	s^{-1}

3.3 Test specimens

3.3.1 Low density polyethylene (LDPE)

Polyethylene is used as dielectric material in power cables for the last four decades due to its superior electrical insulating properties and reputable thermo-mechanical

behavior (Alapati et al., 2012; Huuva et al., 2009; Khalil, 1996; Mori et al., 1998). In this work, low density polyethylene (LDPE) is used as dielectric material of the test object due to its high dielectric strength, low relative permittivity (2.3) and low dielectric losses (Argaut et al., 1993). LDPE has less stiffness but better ductility as compared to HDPE. The breakdown strength of LDPE is approximately 20-160 $\mathrm{kV.mm^{-1}}$, subjected to the conditions surrounding the material (Braunsberger, 2007; Lide, 2008; Vaughan et al., 2003). Cross-linked polyethylene (XLPE) was not used in this work because of no supplier of this product in Malaysia.

3.3.2 Preparation of test specimens

Test samples that have been prepared in the laboratory for PD measurement is shown in Figure 3.4. The material used as the insulation is Low Density Polyethylene (LDPE) with a relative permittivity, ε_r of 2.3. First, a steel rod of 6 mm diameter was cut into 15 cm length. The rod represents a high voltage conductor of a power cable. Then, a cylindrical-shaped LDPE insulation material of 6 cm length and 25 mm diameter was introduced around the steel rod. The cylindrical-shaped insulation was prepared by melting LDPE granules completely around the steel rod in a cylindrical mould of 25 mm diameter. The melted LDPE was left to cooling and turned into a solid before the mould was removed. After that, an artificial void with diameter of 3 mm was created by drilling the hole in the middle of the insulation from one end of the sample. The radial position of the void is at the middle of the LDPE insulation thickness, which is at r = 7.75 mm from the centre of the conductor. From the test object shown in Figure 3.4, the radius of the LDPE insulation is 12.5 mm. Hence, the middle point in the LDPE insulation from the centre of the conductor is at 7.75 mm.

Then, the drilled hole was filled tightly with a piece of LDPE insulation by leaving a gap of 5 mm after cleaning with Turpentine material in order to avoid imperfection.

Hence a cylindrical void of 3 mm diameter and 5 mm length was created. To replicate a layer of ground wire in actual cable geometry, a piece of copper sheet of 5 cm length was tightly glued around the LDPE insulation material. This sheet is called as the outer electrode of the test specimen. Finally, the overall test specimen was soaked in silicon oil to avoid external discharges surrounding the test object. Silicon oil has dielectric constant of 2.5 and it was used because of its higher breakdown strength compared to air ($3\ \mathrm{kV.mm^{-1}}$). A 50Hz, AC sinusoidal voltage, U_{app} was connected to the high voltage electrode and the outer electrode was connected to the ground. Before connecting any test specimen, the measurement system was checked and found to be PD

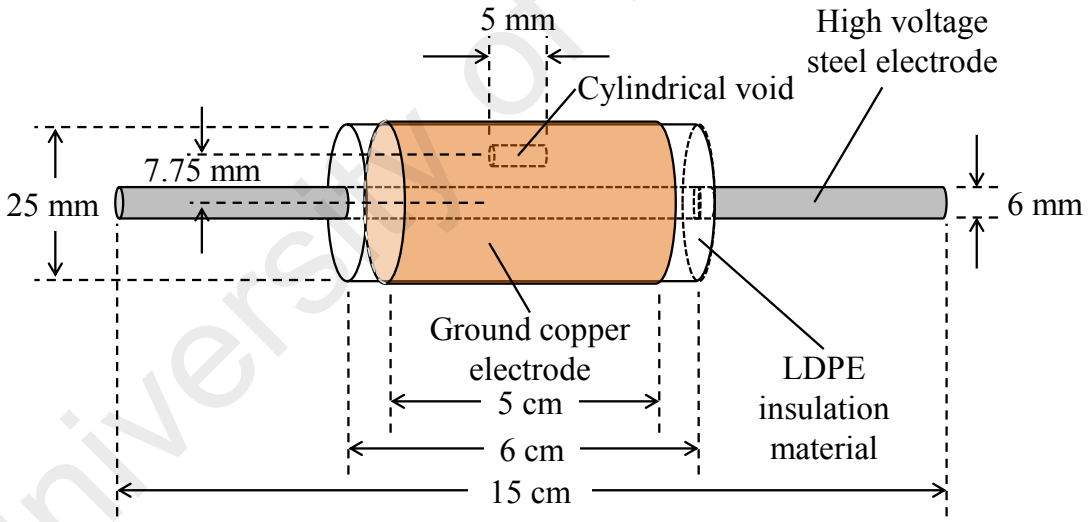

Figure 3.4: Test object schematic diagram (not drawn according to the actual scale)

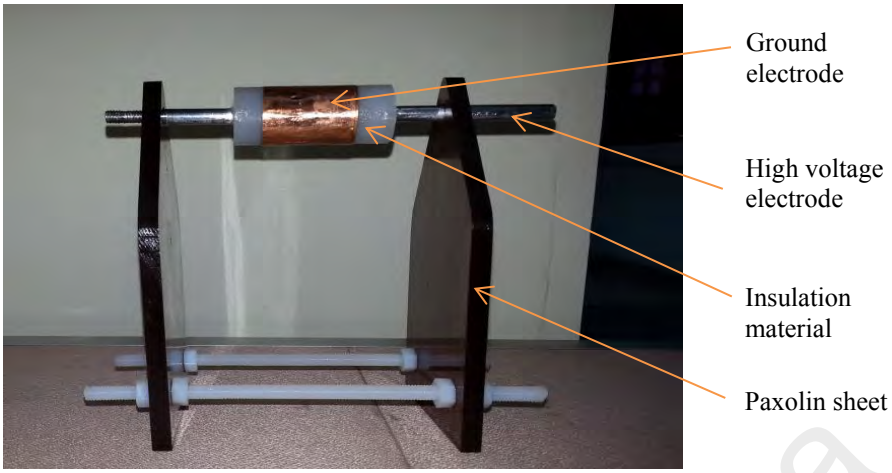

Figure 3.5: Prepared test object

3.4 Measurement technique

In general, phase resolved partial discharge analysis (PRPDA) technique is adopted for analysis of PD measurement. The equipment in PRPDA measurement measures the magnitude of apparent charge and the phase of each PD occurrence and obtained the PRPD pattern by sorting and counting each charge magnitude q occurring at phase, ϕ of the applied voltage.

PRPDA technique is used to analyse PD measurements that have been recorded. In this technique, the apparent charge with its phase position is recorded for each detected PD. The values that have been recorded are separated into phase and charge channels and sorted into matrix as shown in Figure 3.6 (a). The x and y-axes of the columns show the phase and charge channels respectively and the elements represent the number of detected PDs with certain phase and charge.

Referring to Figure 3.6 (b), the x-axis and y-axis show the phase and apparent charge whereas the color bar shows the detected PDs with the combination of phase and charge. The PRPDA technique is diagnostics tool used to classify different types of PD source from its PD pattern (Gulski et al., 1992). The representation of PRPD pattern in

2D has the advantage over 3D ϕ-q-n plot. In 2D PRPD pattern the phase and the apparent charge magnitude can be clearly seen as compared to 3D ϕ-q-n plot.

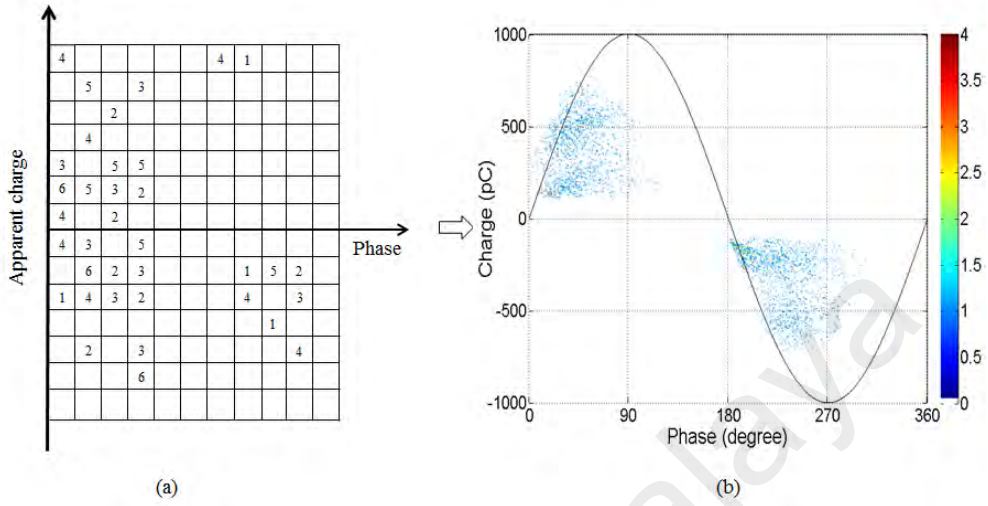

Figure 3.6: (a) Resultant matrix of PRPDA and (b) PRPD example

3.5 Experimental setup

The mtronix MPD 600 system developed by OMICRON is used for the measurement of PD. Figure 3.7 shows the experimental setup used for the PD measurement under AC voltage. The test setup includes a PD-free step-up transformer, measuring impedance (equivalent RLC circuit), a test specimen, a coupling capacitor, a USB controller and a PD detector connected to computer (PC) to explore the PD events for further analysis. For measurement under impulse voltage, DC and impulse voltage setups were included between the PD-free transformer and the test object.

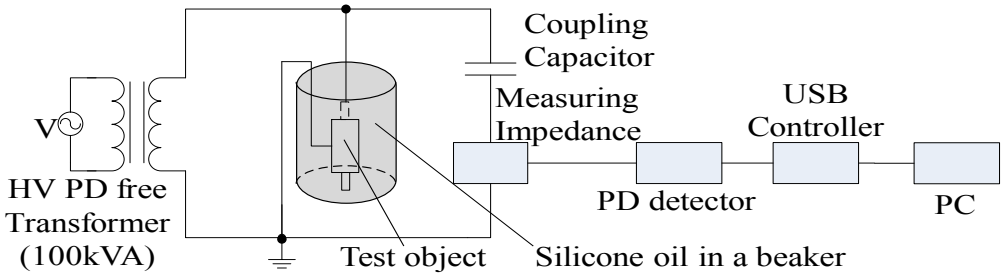

Figure 3.7: Setup of PD measurement under AC voltage

The PD detection concept is based on measuring the current pulse across the test sample. When a discharge occurs in the test sample, charges from the coupling capacitor (coupling capacitor = 1 nF) are transferred to the test sample in order to balance the voltage drop across the test sample. As a result, a current pulse, $i_o(t)$ of short time duration of nanoseconds range flows in the circuit and a voltage pulse, $V_o(t)$ is generated across the coupling device. The amount of charge transferred is known as apparent charge. The magnitude of apparent charge is determined by the induced number of dipole moment of real charge from PD in a void that produces a sudden change in the capacitance of the test sample (Boggs, 1990; Kuffel, et al., 2000).

The measuring impedance (a coupling device) measures the short duration voltage pulse, $V_o(t)$ when a PD occurs. Such device has the output frequency in the range of 20 kHz to 6 MHz. Such device consists of a simplified RLC circuit connected in parallel. The output from this device is connected to PD detector that detects the magnitude of discharge pulse and applied voltage amplitude through its PD impulse input and voltage input respectively. Finally, the output from PD detector is connected to USB controller through fibre optic cables and the all the data is sent to the PC for user to display, save and analyse PD activities.

The system needs to be calibrated every time the mtronix software is restarted. The calibration through MPD 600 was done digitally. During charge calibration, the calibrator was connected in parallel with test sample where calibration charge was injected to the electrode with the range of 1 to 100 pC, where 1 pC is equivalent to 1 mV pulse. The charge calibration was completed once the target value of the charge in calibration settings is equal to a specific charge value sent from the calibrator. Through this method, the charge calibration can be done more precisely. The actual experimental setup is shown in Figure 3.8.

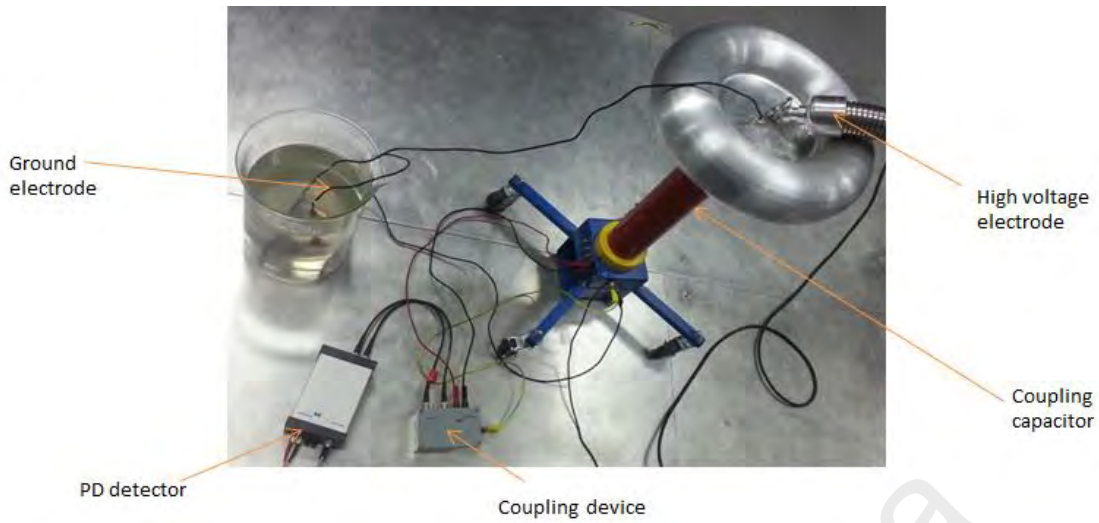

Figure 3.8: Test setup

3.6 PD measurements

It is important to ensure that the oil in the beaker is bubble-free because the presence of bubbles in the oil might affect the measurement results and there are no sharp edges to avoid corona discharges. Before PD measurement, the whole test setup was tested to make sure that it was PD-free. It was found the test setup is PD-free up to 28 kV. PD measurements were taken for several voltage cycles to obtain sufficient data. Table 3.4 shows the summary of PD measurement tests that have been performed.

Table 3.4: Summary of PD measurements

No	Sample		Measurement
	Void diameter	Void length	
1	3 mm	5 mm	PD as a function of applied voltage (50 Hz, 21 kV-24 kV AC sinusoidal)
2	3mm 4mm 5mm	5 mm	PD as a function of void diameter (50 Hz, 21 kV AC sinusoidal)
3	4 mm	5 mm	PD as a function of applied frequency (50 Hz-5 Hz, 8 kV AC sinusoidal)
4	4 mm	5 mm	PD as a function of peak impulse voltage magnitude (1.2/50 us rise/tail time, 18-21 kV) and for rectangular void (1.2/50 us rise/tail time, 60-90 kV)
5	4 mm	5 mm	PD as a function of peak triangle voltage magnitude (7.5-8.25 kV)
6	5 mm	5 mm	PD as a function of insulation material temperature (30℃, 40℃, 50℃ and 60℃)

Referring to Table 3.4, sample 1 was used for PD measurement as a function of applied voltage. The measurements were taken at 21, 22, 23 and 24 kV of 50Hz

frequency. Sample 2 was used to study the PD as a function of different void size, where the measurements were taken at 50Hz, 21 kV AC sinusoidal.

Sample 3 was tested at different frequency of the supply voltage. The order of the applied frequencies was 50, 40, 30, 20, 10 and 5Hz. Initially, the magnitude of 50 Hz was applied to test the sample in order to reduce the time required for the first electron to generate first discharge. The minimum frequency of 5Hz was chosen for the measurement because PD system is not stable at frequency below 5Hz. The maximum frequency of 50 Hz was chosen because the output from the high voltage amplifier became distorted at higher frequencies due to the high voltage filter. Measurements were obtained for 500 cycles at each frequency and were taken continuously without any interruption between two consecutive applied frequencies. The experimental setup for this measurement is similar as shown in Figure 3.7 except that high voltage PD-free transformer was replaced with high voltage amplifier and high voltage filter.

Sample 4 was used to measure PD as a function of peak impulse voltage magnitude. A standard 1.2/50 us rise/tail time was used and the peak magnitude was varied at 18, 19, 20 and 21 kV. Sample 5 was used for PD measurement as a function of peak triangle voltage magnitude. The measurements were done at 7.5, 7.75, 8.0 and 8.25 kV at 50 Hz frequency.

Finally, Sample 6 was used for PD as a function of insulation material temperature. The measurements were taken at 30℃, 40℃, 50℃ and 60℃ at 50Hz, 10 kV AC sinusoidal.

3.7 Particle swarm optimisation (PSO)

(Kennedy et al., 1995) introduced PSO technique in 1995, inspired from social behavior of organism, such as birds flocking and fish school. PSO has been proved as a

robust and fast technique in solving nonlinear, multi objective problems (Liu et al., 2008). This technique is initialized by generating a population of random solution. The whole population is known as swarm and each individual is called as particle. Each particle provides a solution to the optimization problem. Each particle flies in the search space towards the global best position according to its own experience and experience of neighboring particles. In PSO, each solution is associated with a velocity vector, which is constantly updated with respect to individual particle's experience and the companion of the particle experiences. The best value of the group is always shared with all particles. Thus, it is expected that particle moves toward better solution areas.

In an *n*-dimensional search space, let the position (x) and velocity (v) of the i^{th} individual be represented as the vectors:

$$\left.\begin{aligned} x_i &= (x_{i1},...,x_{id},...,x_{in}),\\ v_i &= (v_{i1},...,v_{id},...,v_{in}) \end{aligned}\right\} \tag{3.13}$$

For each particle, a fitness value f based on its position could be calculated. Generally, this fitness value is the function value of the aim function of the optimisation problem. The best previous experience of the i^{th} particle is stored and represented as:

$$Pbest_i = (Pbest_{i1},...Pbest_{id},...Pbest_{in}) \tag{3.14}$$

The best value obtained by the group is saved and represented as

$$gbest_i = (gbest_{i1},...gbest_{id},...gbest_{in}) \tag{3.15}$$

The particle's position and velocity in the next generation can be computed as

$$v_{id}^{(t+1)} = w.v_{id}^{(t)} + c_1 \times rand_1 \times (pbest_{id} - x_{id}^{(t)}) + c_2 \times rand_2 \times (gbest_{id} - x_{id}^{(t)}) \tag{3.16}$$

$$x_{id}^{(t+1)} = x_{id}^{(t)} + v_{id}^{(t+1)} \tag{3.17}$$

where, $i=1, 2....m$ is the index of each particle, t is the iteration number. The constants $c_1$and c_2 are known as weighting factors. Weighting factors help to move each particle toward *pbest* and *gbest* positions. w is the inertia weight, which is introduced for improving the performance. The value of inertia weight, which provides better global results in fewer iteration is in the range of 0.9 to 1.2 (Shi et al., 1998). Mathematically, it is set as

$$w^{(i+1)} = \frac{w^{\max} - w^{\min}}{i_{\max}} \times i \tag{3.18}$$

where, i_{max} shows the maximum number of iterations and i shows current iteration number. The value for c_1 and c_2 is often used as 2.0 (Eberhart et al., 2001; Kennedy, et al., 1995).

In this work, PSO technique is applied in the simulation under different amplitude, frequency and waveshape of the applied voltage, void sizes and temperature of the insulation material to determine the PD model parameters related to electron generation rate, which are N_{es0}, N_{es0H} and N_{ev}. Figure 3.8 shows flowchart of the code. In First step, the workspace in MATLAB is cleared. After that all parameters used in the simulations are defined and initialized. Then, the electric field in void, E_v is extracted from the FEA model and the inception field, E_{inc} in the void is calculated. If the electric field in the void, E_v is higher than the inception field, E_{inc} then, the parameters related to total Electron generation rate, N_{es0L}, N_{es0H} and N_{ev} are determined through PSO as shown in Figure 3.8. The global best values for the total EGR (N_{es0L}, N_{es0H} and N_{ev}) are obtained from PSO. After that a probability, P of a PD occurrence is calculated through Equation 3.12 and checked with a number randomly generated R. PD may happen when P is

higher compared to R. The PD occurrence phase and magnitude charge are save in the workspace. The cycle repeats till a stated number of cycles is reached. Then, the developed code calculates the number of PD occurrence per cycle, total charge per cycle, mean charge, magnitude of maximum and minimum charge and phase resolved partial discharge (PRPD) pattern in 2D is obtained. If the number of PD occurrence per cycle obtained is equals ±0.1 measured PD per cycle then, the data and PRPD pattern will be saved in the workspace. The comparison between measurement and simulation results under different amplitudes, frequency and waveshape of the applied voltage, void sizes and material temperatures is shown in chapter 5.

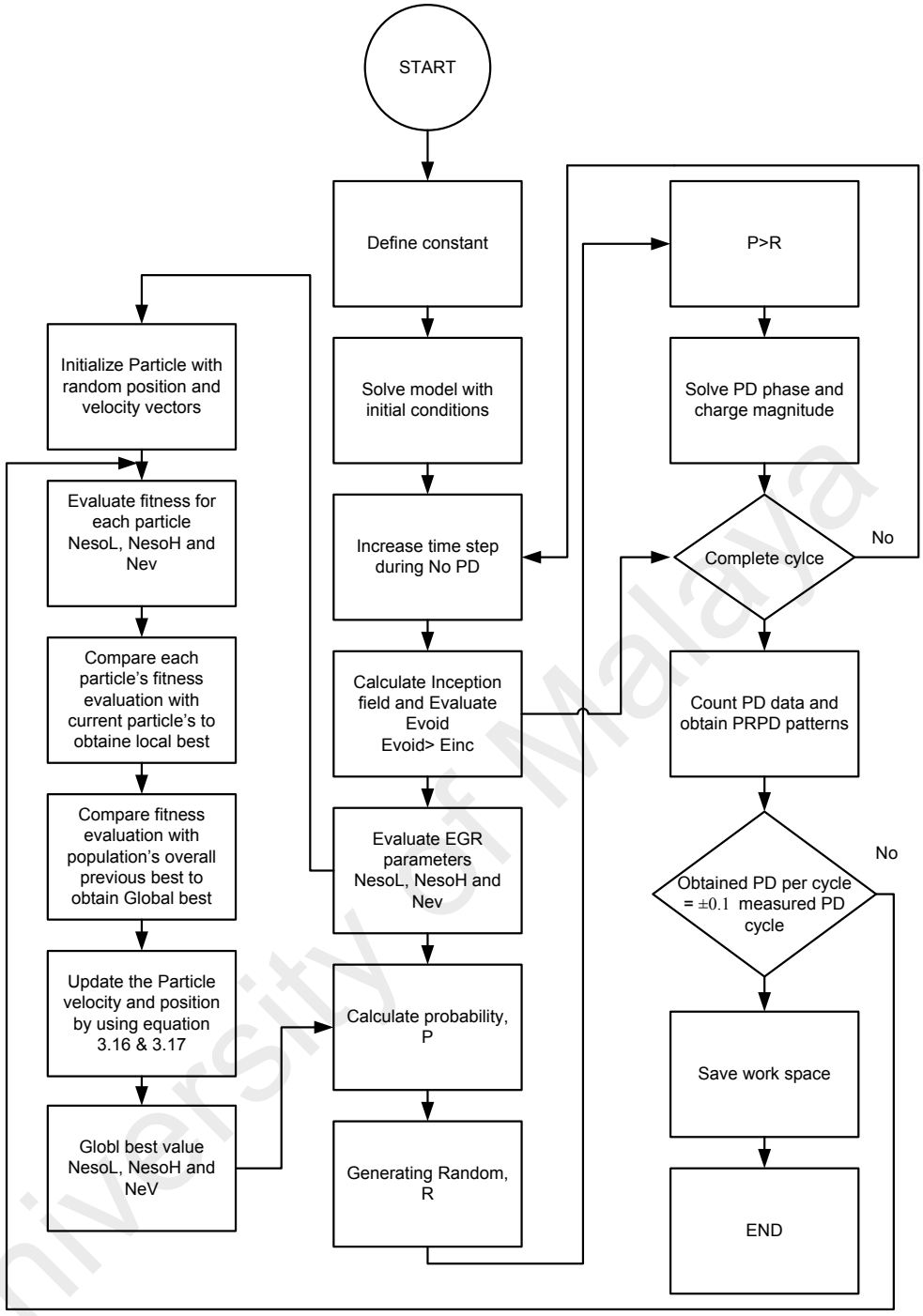

Figure 3.9: Flow chart of the code

3.8 Summary

A physical model of PD activities within an artificial void in cable insulation geometry developed in Finite Element Analysis has been explained in this chapter. The preparation of the test samples using insulation material of Low Density Polyethylene (LDPE) is also explained. PD measurement methods under different voltage amplitude,

void diameter, frequencies of the applied voltage, peak impulse voltage, peak triangle voltage and material temperature are also presented. PD data taken are represented by the total number of PD per cycle, total number of charge per cycle, magnitude of mean and maximum charge. The comparison between measurement and simulation results are shown in detail in Chapter 5 in order to identify the key parameters affecting PD activity in cable insulation geometry under different stress conditions.

CHAPTER 4: MEASUREMENT RESULTS OF PD ACTIVITY

4.1 Introduction

In this chapter, all measurement results are presented. PD measurements have been performed under different amplitude, frequency and waveshape of the applied voltage, void sizes and temperature of the insulation material. The measurement results are summarized via PRPD pattern. The total number of PDs, total charge magnitude and mean and maximum charge under different stress conditions and void size are also recorded.

4.2 PD under different applied voltage amplitudes

PD events within an artificial void of 3 mm diameter in cylindrical insulation-shaped geometry were measured at 21 to 24 kV AC sinusoidal applied voltage. Figure 4.1 shows the measured PRPD patterns for various applied voltage while the summarised measured PD data are given in Table 4.1. Referring to the PD data from the experiment, the PD occurrences per cycle, total charge magnitude per cycle and the magnitude of maximum charge are larger as the applied voltage increases. The mean charge reduces as the voltage amplitude is increased.

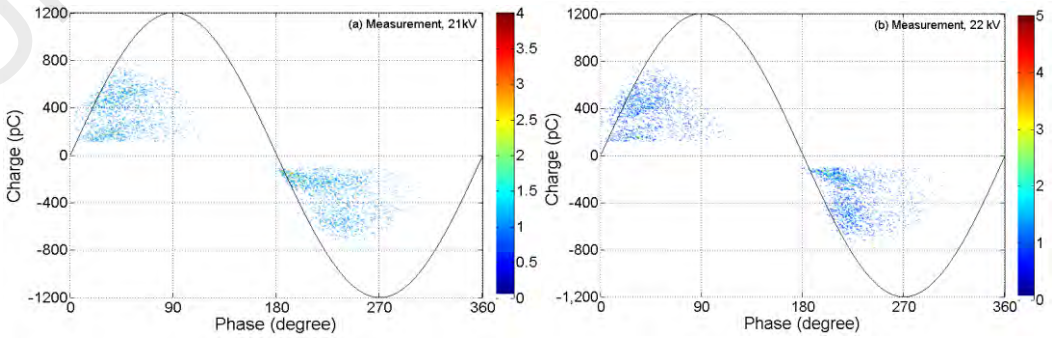

(a) 21 kV (b) 22 kV

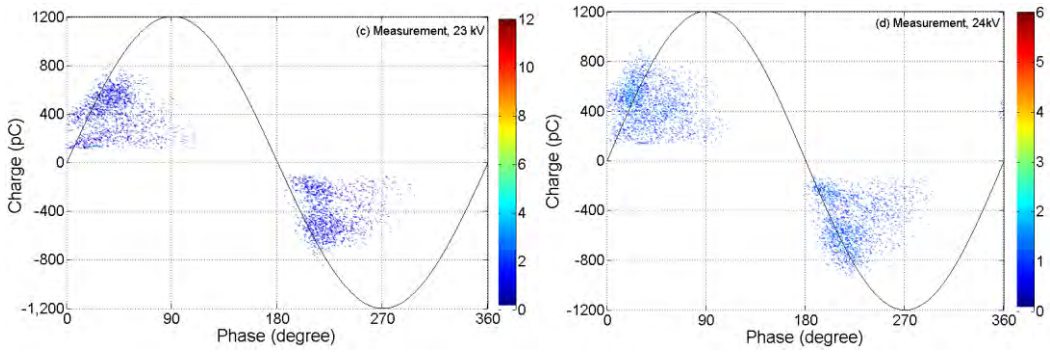

(c) 23 kV (d) 24 kV

Figure 4.1: PRPD patterns for various applied voltage at 50 Hz from the measurement

The electric field (EF) within the void increases as the applied voltage is higher. Due to this, the amount of free electrons generated within the void is larger. Hence, the statistical time lag, which is defined as the time delay of getting free electron for discharge event to happen, is reduced and PDs are happening at earlier applied voltage phase (Illias H. A, et al., 2011b). Therefore, higher repetition rate of discharge events is obtained. For the same reason, the total discharge magnitude per cycle increases with the applied voltage magnitude. The magnitude of the maximum charge increases when the voltage amplitude is higher since larger amplitude of the applied voltage guarantees a higher voltage decrement in the void when a discharge happens. The minimum charge magnitude does not depend on the voltage amplitude since the inception field and extinction field do not change with the applied voltage.

Table 4.1: Measured PD data for various applied voltages

Applied Voltage (kV)	21	22	23	24
Total PDs per cycle	3.2	3.6	4.2	4.6
Total charge per cycle (pC)	1194	1335	1498	1596
Mean charge (pC)	373	370	356	347
Maximum charge (pC)	779	780	823	835
Minimum charge (pC)	110	110	110	110

Referring to the experimental results as shown in Figure 4.1, the PD behaviour between positive and negative-half cycles is almost symmetrical since the void is positioned in the centre of the cylindrical insulation-shaped geometry although the distribution of field within the void and insulation is non-uniform without the presence of the first discharge. The patterns do not change much with the applied voltage except more PDs can be observed at higher voltage amplitude due to higher electron generation rate, EGR. Although no clear separation, PDs which occur along the rising edge of positive and negative voltage cycles up to 800 pC and from 0^o to 90^o and 180^o to 270^o can be slightly seen.

PD activities within an artificial void of 4 mm diameter in a cylindrical insulation-shaped geometry were also measured at 15 to 18 kV AC sinusoidal applied voltage. Figure 4.2 shows the measured PRPD patterns for various applied voltage while the summarised measured PD data are given in Table 4.2. Referring to the PD data from the experiment, the PD data occurrence per cycle, total charge magnitude per cycle and the magnitude of maximum charge are also larger as the applied voltage increases. The mean charge is not consistent as the voltage amplitude is increased. Referring to the experimental results as shown in Figure 4.2, the PRPD pattern is almost symmetrical since the void is positioned in the centre of the cylindrical insulation-shaped geometry.

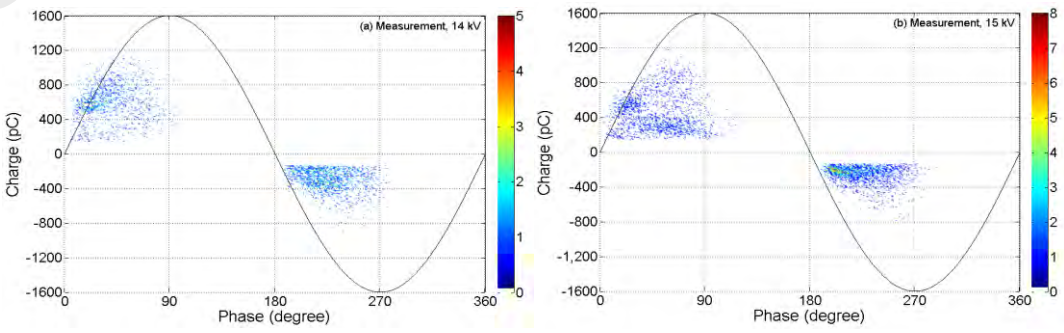

(a) 14 kV (b) 15 kV

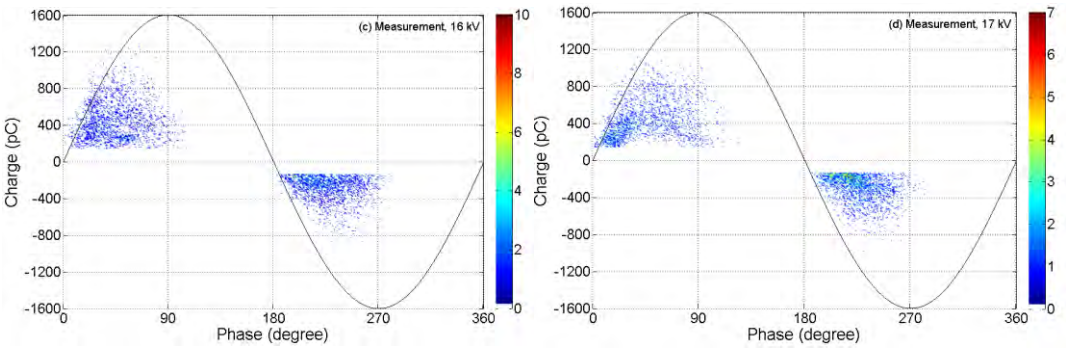

(c) 16 kV (d) 17 kV

Figure 4.2: PRPD patterns for various applied voltage at 50 Hz from the measurement

Table 4.2: Measured PD data for various applied voltages

Applied Voltage (kV)	14	15	16	17
Total PDs per cycle	2.8	3.7	4.1	4.3
Total charge per cycle (pC)	1204	1280	1497	1505
Mean charge (pC)	430	370	356	350
Maximum charge (pC)	999	1019	1062	1082
Minimum charge(pC)	140	140	140	140

4.3 PD under different void sizes

This test was done to observe how the diameter of the void influences the PD activity in the test object. The PD activity in an artificial void of diameter of 3, 4 and 5mm respectively is measured at 50 Hz, 21 kV AC voltage, as shown in Figure 4.3 while the PD data is given in Table 4.3.

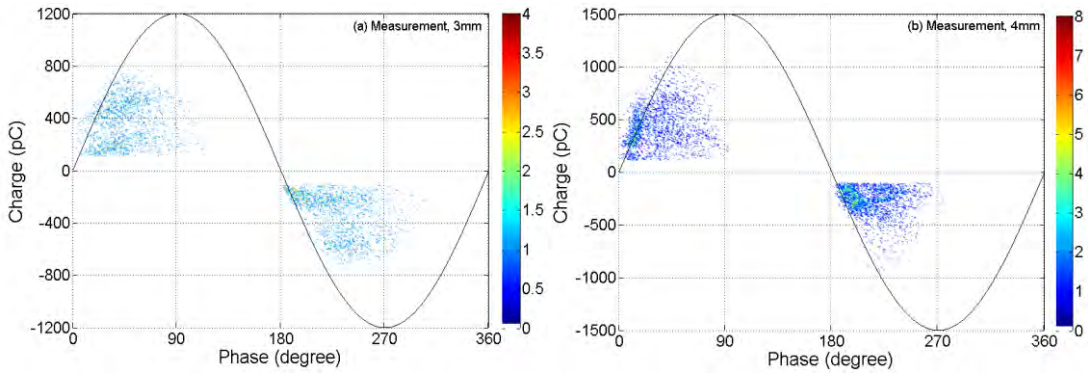

(a) Void diameter = 3 mm (b) Void diameter = 4mm

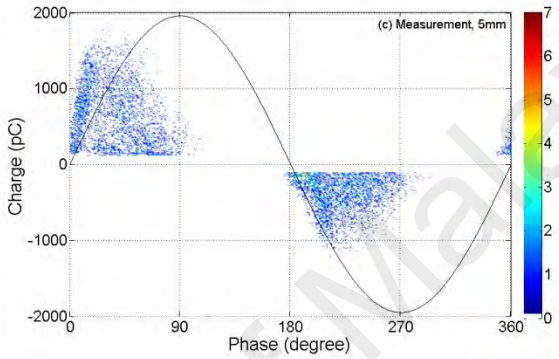

(c) Void diameter = 5 mm

Figure 4.3: PRPD patterns from the measurement at 50 Hz, 21 kV for various void diameters

Table 4.3: Measured PD data for various void sizes

Void diameter (mm)	3	4	5
Total PDs per cycle	3.2	4.8	6.8
Total charge per cycle (pC)	1194	1665	3516
Mean charge (pC)	373	347	513
Maximum charge (pC)	779	1037	1522
Minimum charge (pC)	110	110	110

Referring to Table 4.3, the total PD occurrences per cycle increases as the void size is larger and this is due to higher generation rate of electrons in the void. The magnitude

of the total charge and the magnitude of maximum charge increase with the void diameter because the avalanche head can develop larger within large size of the void. Again, the minimum charge magnitude does not change with the void size.

The PRPD patterns (Figure 4.3) show that PD activity is almost symmetrical between positive and negative-half cycles. This is due to the void is positioned in the centre of the cylindrical insulation-shaped geometry even though the distribution of field in the void is non-uniform. When the size of the void is larger, more PDs occur but in general, the patterns do not change significantly. The earliest phase of PD occurrence is shifted forward as the void size is larger, as can be seen in 5 mm void diameter compared to 3 and 4 mm diameter.

4.4 PD under different applied frequency

The measured PD data under different applied frequency is shown in Figure 4.4. The test sample used for this experiment consists of an artificial void of 4 mm diameter in cylindrical insulation-shaped geometry. PDs within the test sample were measured at 8 kV AC sinusoidal voltage. Referring to Table 4.4, the total PD per cycle, total charge magnitude and maximum charge magnitude are higher at 50 Hz frequency but the mean charge magnitude is not consistent.

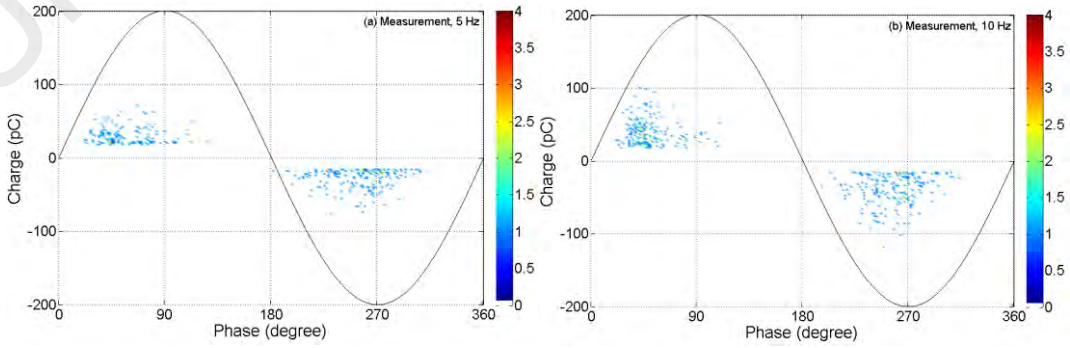

(a) 5 Hz (b) 10 Hz

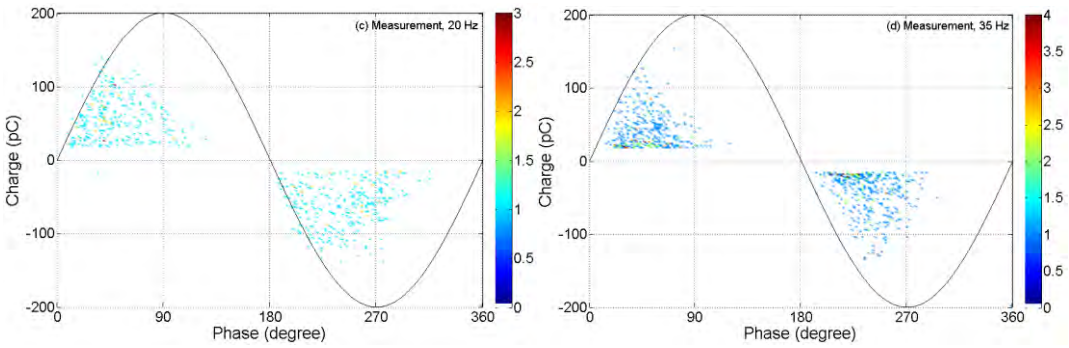

(c) 20 Hz (d) 35 Hz

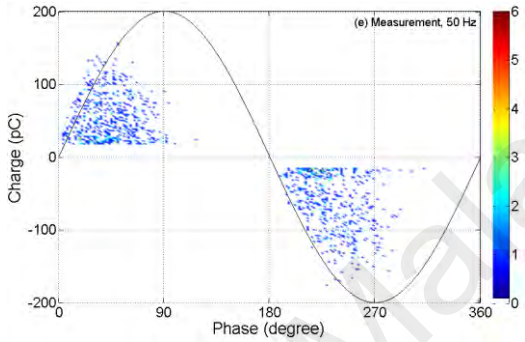

(e) 50 Hz

Figure 4.4: PRPD patterns from the measurement under various frequencies of 8 kV AC applied voltage

Table 4.4: Measured PD data for various applied frequencies

Frequency (Hz)	5	10	20	35	50
Total PDs per cycle	1.1	1.4	1.8	2.5	3.5
Total charge per cycle (pC)	30	55	108	110	204
Mean charge (pC)	29	39	60	44	58
Maximum charge (pC)	73	109	138	152	166
Minimum charge (pC)	17	17	17	17	17

The total number PDs per cycle decreases as the frequency of the applied voltage is decreased from 50 Hz to 5 Hz. This is due to the void surface charge decay between sequential discharges is less important (Forssen, et al., 2008a). At higher frequency magnitude, more charges on the surface of the void are accessible in local shallow traps when the next PD event is probably to happen. Thus, the generation rate of electron is higher and PD happens almost immediately once the level of inception voltage is exceeded, resulting in the higher repetition rate of PD for higher applied frequencies.

The total charge magnitude per cycle and maximum charge magnitude are decreasing as the frequency of the applied voltage is decreased from 50 Hz to 5 Hz. The magnitude of the maximum charge reduces from about 166 pC at 50 Hz to 73 pC at 5 Hz. The change in the maximum charge magnitude is due to the statistical effect, which increases as the frequency of applied voltage is increased. The magnitude of the mean charge is not consistent and the minimum charge magnitude remains unchanged because it is independent of frequency of the applied voltage. The PRPD patterns show almost symmetrical behaviour between positive and negative-half cycles and there is a wide spread in charge magnitude observed at 50 Hz as compared to 5 Hz. These obtained results under different frequencies of applied voltage are in reasonable agreement with past literature (Forssen, et al., 2008a).

The impact of void diameter on PDs within the test object at variable frequency of the applied voltage was also analysed. For this experiment, two test specimens with diameter of 4 mm and 5 mm were prepared in the laboratory and PD measurements were done at 10 kV AC sinusoidal applied voltage. Figure 4.5 shows the PRPD comparison at variable frequency of the applied voltage for the test specimen with the void diameter of 4 and 5 mm and the corresponding PD data is given in Table 4.5 and Table 4.6. There was no PD in the void with diameter of 4 mm and 5 mm below 8 kV

and 7 kV respectively. The lower inception voltage is observed for 5 mm void size as compared to 4 mm due to the variation in the electric field enrichment. As the frequency of the applied voltage is decreased from 50 Hz to 5 Hz, each PD data decreases due to the same reason discussed above.

Referring to Table 4.5 and Table 4.6, the PD event in the void clearly varies with frequency of the applied voltage. The total number of PDs per cycle, total charge magnitude and maximum charge magnitude decrease with decreasing frequency of the applied voltage. There is a wide spread in charge magnitude at all applied frequencies for 5 mm void diameter. The higher number of PDs per cycle for 5 mm void diameter than 4 mm is obtained and this could be due to high generation rate of electron in the larger void. Both total charge magnitude and magnitude of maximum charge are higher for 5 mm void diameter because of larger development of avalanche head with the void compared to smaller void diameter (4 mm). Again, the magnitude of minimum charge remains unchanged for both void diameters.

Table 4.5: Measured PD data for 4mm void diameter under variable frequency at 10 kV

Frequency (Hz)	5	20	30	40	50
Total PDs per cycle	2.0	2.5	3.2	3.5	3.8
Total charge per cycle (pC)	179	208	301	357	388
Mean charge (pC)	89.5	83.2	94.0	102.0	102.1
Maximum charge (pC)	187	206	235	318	407
Minimum charge (pC)	50	50	50	50	50

Table 4.6: Measured PD data for 5mm void diameter under variable frequency at 10 kV

Frequency (Hz)	5	20	30	40	50
Total PDs per cycle	4.0	4.8	5.3	6.0	6.8
Total charge per cycle (pC)	442	707	753	1152	1354
Mean charge (pC)	110.5	147.2	142.0	192	199.1
Maximum charge (pC)	269	544	563	1039	1090
Minimum charge (pC)	50	50	50	50	50

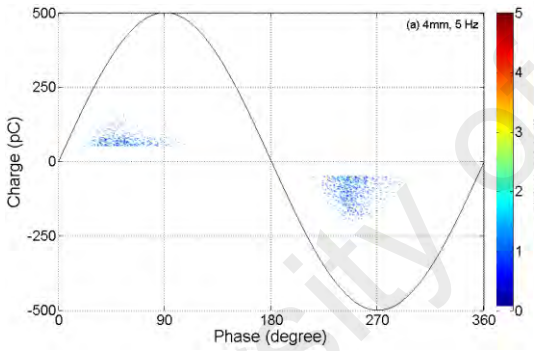

(a) 4 mm, 5 Hz

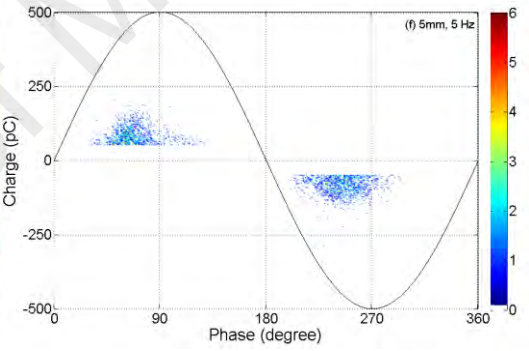

(f) 5 mm, 5 Hz

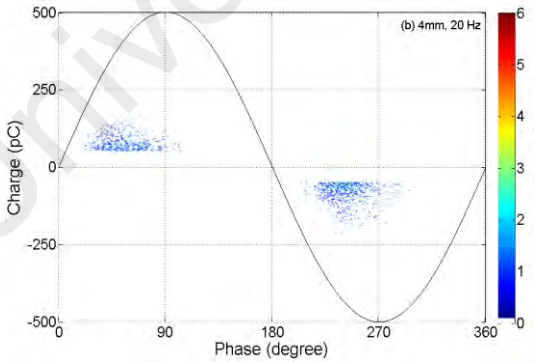

(b) 4 mm, 20 Hz

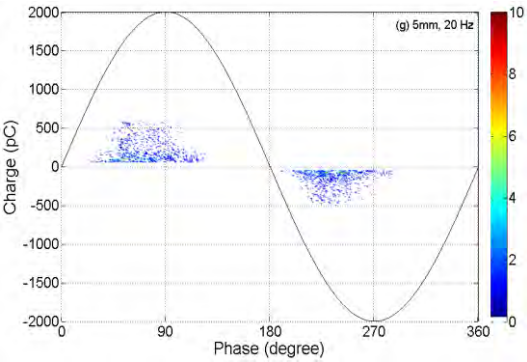

(g) 5 mm, 20 Hz

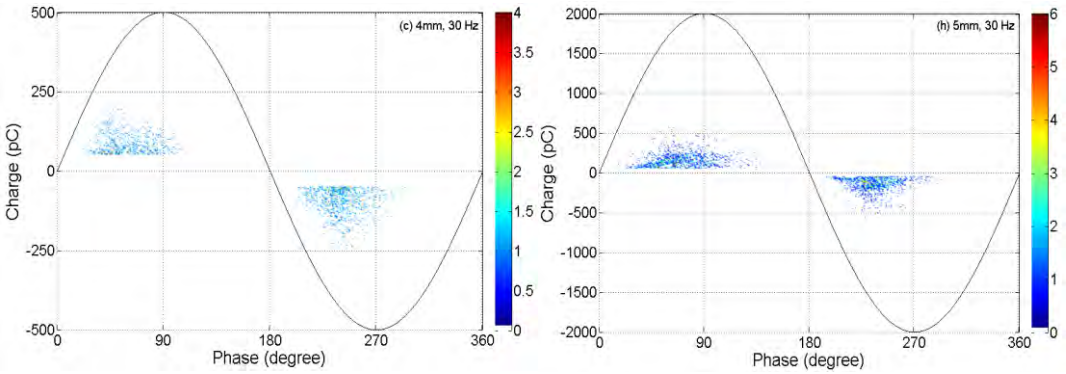

(c) 4 mm, 30 Hz (h) 5 mm, 30 Hz

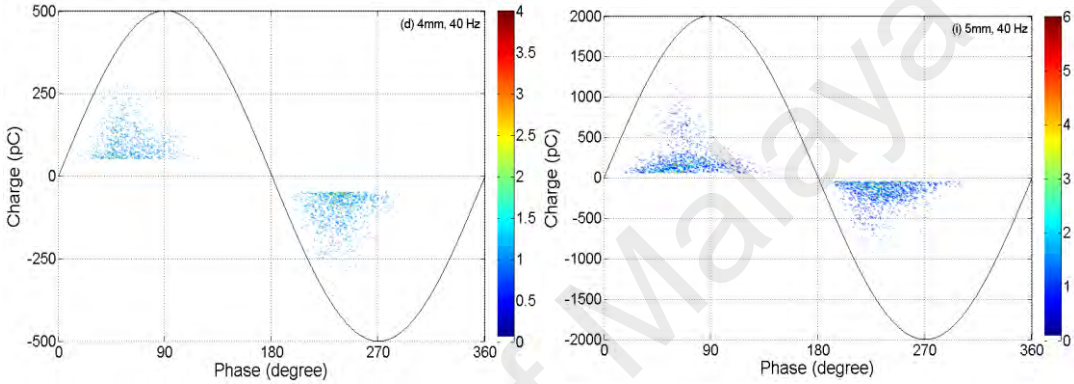

(d) 4 mm, 40 Hz (i) 5 mm, 40 Hz

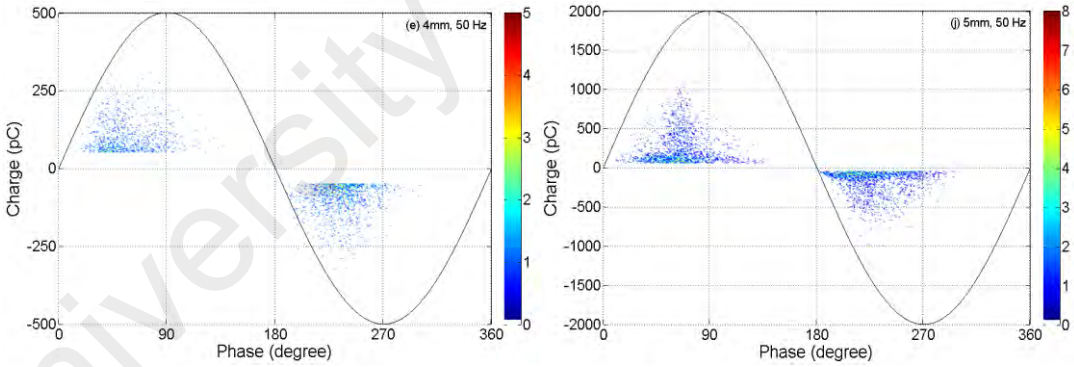

(e) 4 mm, 50 Hz (j) 5 mm, 50 Hz

Figure 4.5: Measured PRPD patterns for (a-e) 4mm void and (f-j) 5mm void diameter at 10 kV

4.5 PD under different applied voltage waveshape

The measured PD charge magnitude vs. time from cylindrical void data under peak magnitude of the applied impulse voltage is shown in Figure 4.6. The measured PD data is shown in Table 4.7. The front/tail time was fixed at 1.2/50 us. The test specimen used

for this experiment consists of an artificial void of 4 mm diameter in cylindrical insulation-shaped geometry. PD events within an artificial void were measured in cylindrical insulation-shaped geometry at 18-25 kV under peak magnitude of the applied impulse voltage. Referring to the experimental results as shown in Figure 4.6, positive discharge magnitude is higher than successive discharges happened during voltage rise time. Throughout the fall time of the applied voltage, negative discharges with lower magnitude happened.

Referring to Table 4.7, the total PD per ms, total charge magnitude per ms and maximum charge magnitude are higher as the peak magnitude of the applied impulse voltage increases. The magnitude of mean charge reduces when peak magnitude of the applied impulse voltage is increased. The number of discharges per ms increases as the peak magnitude of the applied impulse voltage is higher and this is due to due to the slope during the voltage rise time is higher. The magnitude of the maximum charge increases when the peak magnitude of the applied impulse voltage is higher since larger impulse voltage peak assurances a higher voltage drop in the void when a discharge happens. The magnitude of total charge increases as the magnitude of impulse voltage peak is higher and this is because of the number of discharges per ms and the magnitude of maximum charge are higher.

Table 4.7: Measurement results under different peak magnitude of the applied impulse voltage (front/tail time of 1.2/50 us) for cylindrical void

Peak magnitude (kV)	Number of discharges per ms	Total charge magnitude per ms (pC)	Maximum charge magnitude (pC)	Minimum charge magnitude (pC)
18	14	11506.43	1113.49	601.29
19	15	12284.15	1195.87	585.72
20	16	13396.07	1263.70	603.20
21	17	15032.75	1353.82	629.57

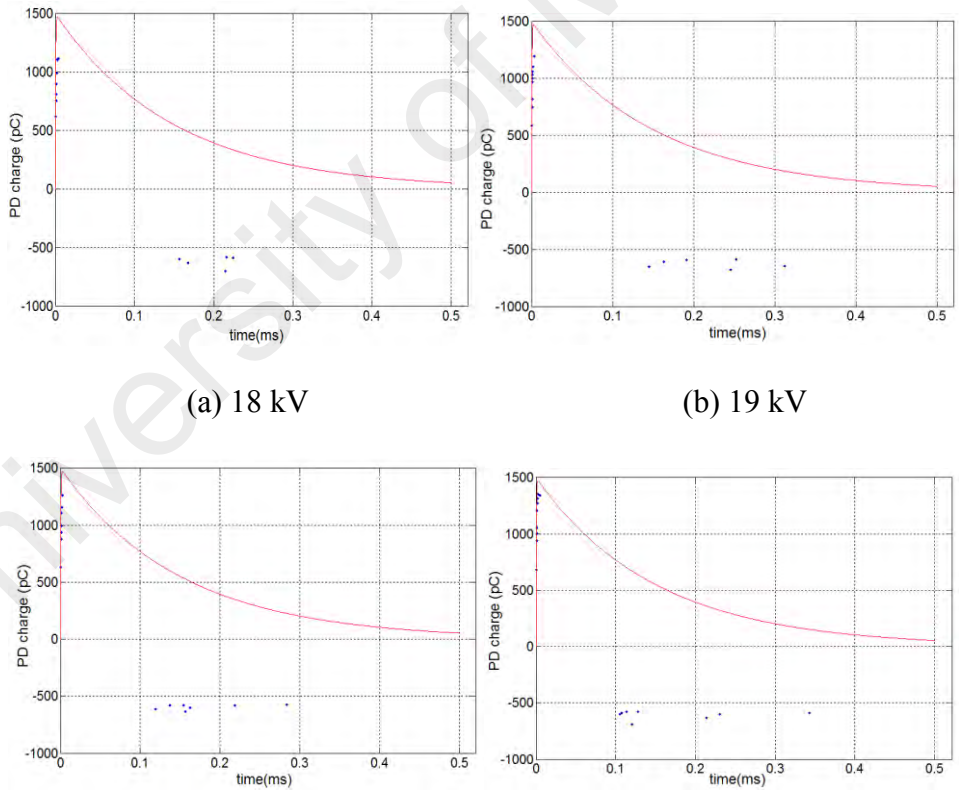

(a) 18 kV (b) 19 kV

(c) 20 kV (d) 21 kV

Figure 4.6: Measurement of charge magnitude vs. time under different applied impulse voltage (front/tail time of 1.2/50 us) for cylindrical void

Figure 4.7 shows PD measurement results under different peak magnitude of the triangle applied voltage while the summarized PD data is given in Table 4.8. The main aim of this test is to investigate the impact of the applied voltage waveform type on PDs within an artificial void in cylindrical insulation-shaped geometry. PD measurements within an artificial void of 4 mm diameter in cylindrical insulation-shaped geometry with 50 Hz, 7.5 kV to 8.25 kV voltages were done as a function of voltage shape.

Referring to Figure 4.7, the electric field in the void follows the triangle voltage waveform curve. The magnitude of the maximum charge increases as the voltage is increased from 7.50 kV to 8.25 kV, due to higher maximum electric field in the cylindrical void. The behavior of PD at both half cycles of the applied voltage is nearly symmetrical because the void is located in the middle of cylindrical insulation-shaped geometry.

Table 4.8: Summarized PD data under triangular wave shape

Peak magnitude (kV)	Total No of PD per cycle	Total charge magnitude per (pC)	Mean charge magnitude (pC)	Maximum charge magnitude (pC)	Minimum charge magnitude (pC)
7.50	0.1410	29.1982	207.0798	457	110
7.75	0.7355	163.4459	222.2242	573	110
8.0	1.4055	334.6293	238.0856	642	110
8.25	3.1005	672.7514	216.9816	841	110

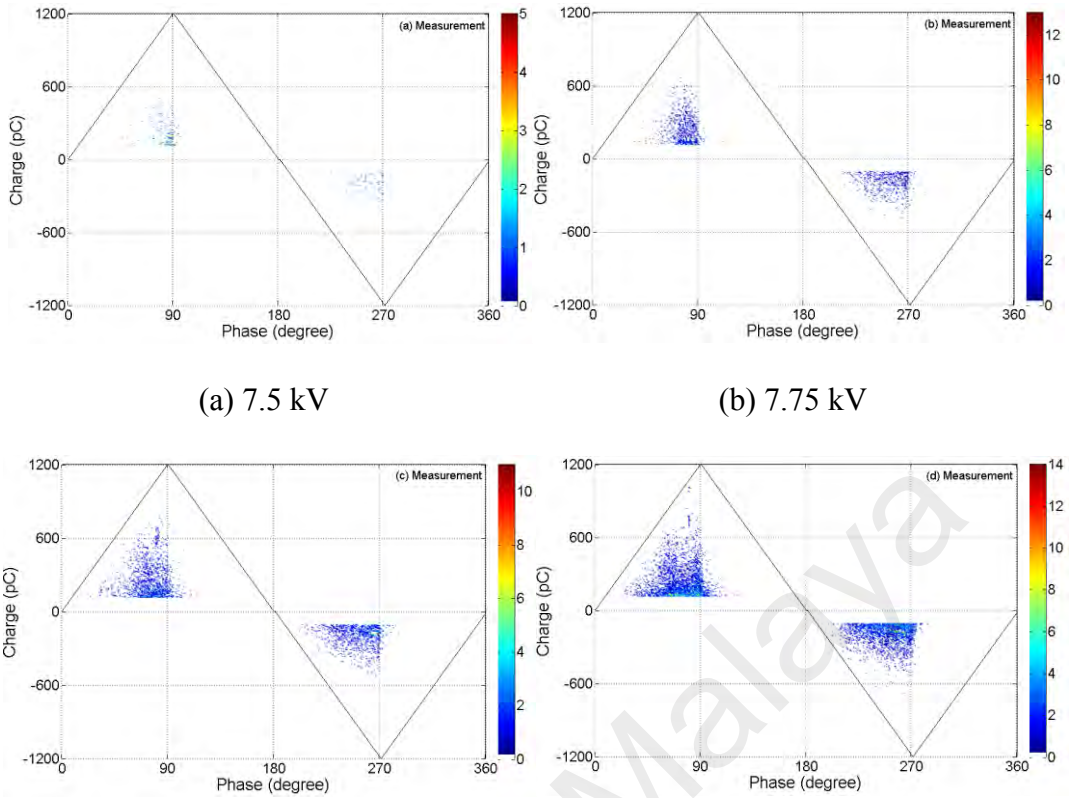

(a) 7.5 kV (b) 7.75 kV

(c) 8.0 kV (d) 8.25 kV

Figure 4.7: Measured PD patterns under triangular wave shape voltage at different peak magnitudes

4.6 PD under different temperature of the material

PD measurements within an artificial void of 5mm diameter in the cylindrical insulation-shaped geometry with a 50 Hz, 10 kV AC sinusoidal voltage were done under different temperature of the dielectric material. All measurement results are shown in Figure 4.8 while the measured PD data is given in Table 4.9. Referring to the PD measurement results, as the material temperature is increased, the total PD per cycle, total charge magnitude and magnitude of mean charge increase except the value of the maximum charge. The higher repetition rate of PD at higher temperature of the material could be due to an enriched electron generation rate in the void. The value of the maximum charge decreases with increasing material temperature because of higher electron generation rate, decreasing the statistical time lag and subsequently PDs are

expected to happen at lower field in the void. The value of the minimum charge remains constant with increasing material temperature.

Table 4.9: Measured PD data at various temperatures

Temperature (°C)	30	40	50	60
Total PDs per cycle	5.3	5.5	5.8	6.1
Total charge per cycle (pC)	976	1016	1334	1470
Mean charge (pC)	184	188	230	241
Maximum charge (pC)	746	708	698	680
Minimum charge (pC)	90	90	90	90

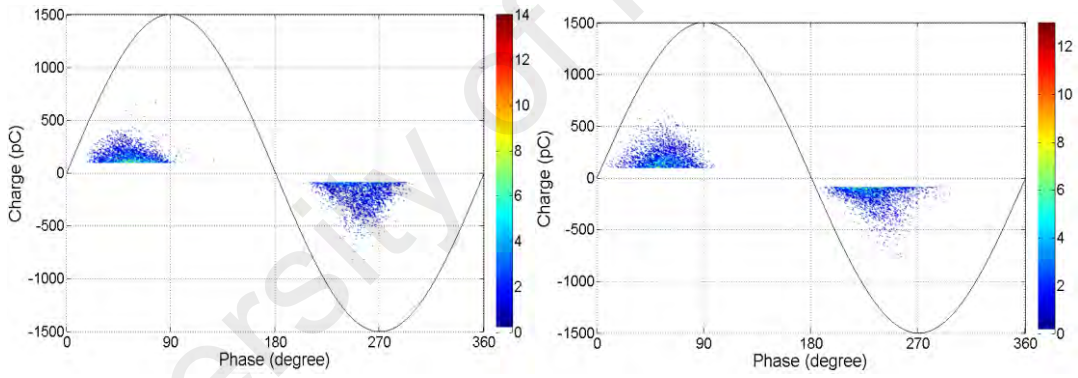

(a) 30°C (b) 40°C

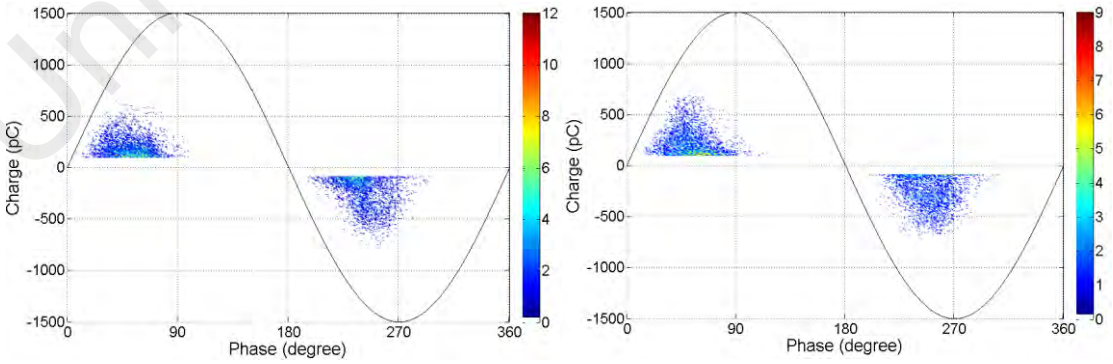

(c) 50°C (d) 60°C

Figure 4.8: PRPD patterns from measurement under different material temperature at 10 kV

4.7 PD under different rectangular void

Figure 4.9 shows measurement results of charge magnitude vs. time from void discharges under different peak magnitude of the applied impulse voltage while Table 4.10 shows discharge data of measurement results. The front/tail time was fixed at 1.2/50 us. From the measurement patterns, discharges with positive charge magnitude and significantly higher than subsequent discharges occurred during the rise time of the applied voltage. During the fall time, negative discharges of lower charge magnitude occurred.

Referring to the measurement data in Table 4.10, the number of discharges per ms, total charge per ms and maximum charge magnitude are larger at higher impulse voltage peak. The number of discharges per ms increases with the impulse voltage peak due to the slope during the voltage rise time is higher. This causes the time when the void field reaches the inception field is shorter compared to lower impulse voltage peak. Hence, more discharges can happen during the rise time of higher applied voltage peak. Higher applied impulse voltage peak also causes the duration of the void field remains higher than the inception field during the voltage fall time. Hence, more discharges can occur during the fall time. As a result, the overall number of discharges per ms becomes higher with higher impulse voltage peak.

Table 4.10 : Measurement results of rectangular void shape under different peak magnitude of the applied impulse voltage (front/tail time of 1.2/50 us)

Peak magnitude (kV)	Number of discharges per ms	Total charge magnitude per ms (pC)	Maximum charge magnitude (pC)	Minimum charge magnitude (pC)
60	37	13467.17	896.28	166.14
70	42	16065.5	1038.29	158.72
80	47	19838.68	1222.27	159.49
90	54	23369.12	1388.67	159.86

The maximum charge magnitude is larger at higher impulse voltage peak due to the maximum void field can achieve higher value. When a discharge happens, the void field reduction is also larger, resulting in larger charge magnitude. The total charge magnitude per ms increases with the impulse voltage peak. This is due to the number of discharges per ms and the maximum charge magnitude are higher. The measured inception voltage does not change with the impulse voltage peak. The reason is the inception voltage is strongly dependent on the size and shape of the void, the material thickness and material type. This finding is also tally with the mathematical equation of inception voltage as reported in previous literature (Gutfleisch, et al., 1995; Niemeyer, 1995), where the inception voltage does not depend on the peak of the applied voltage.

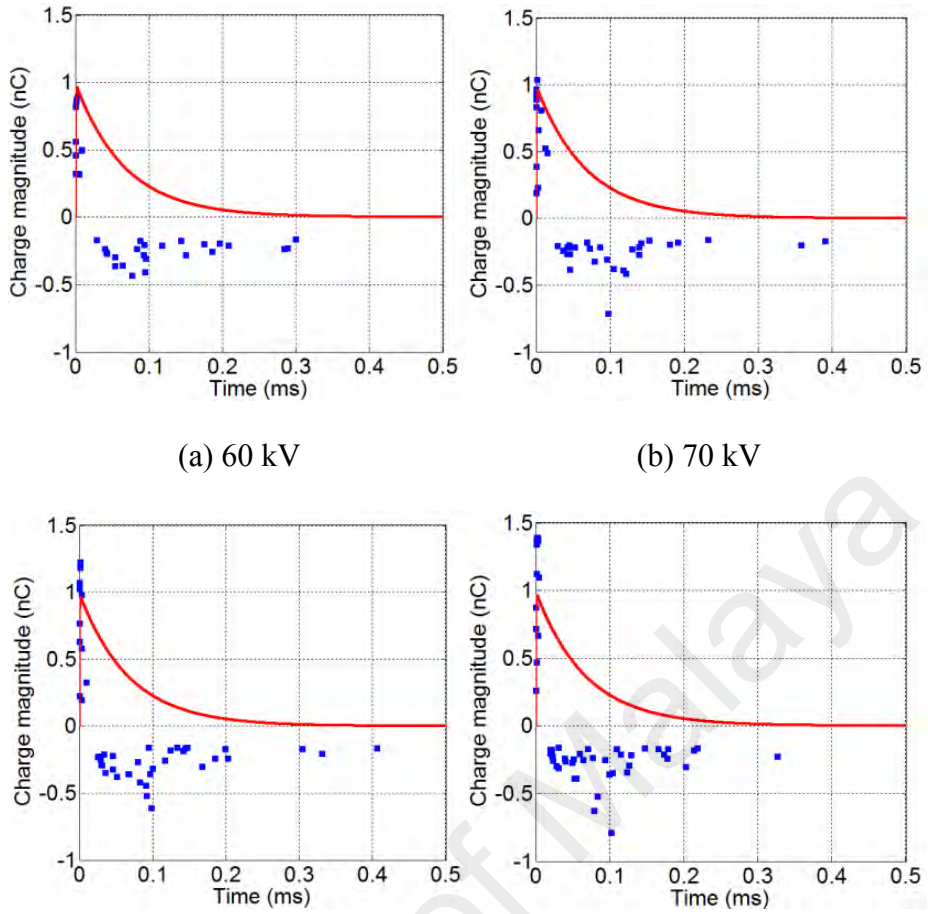

(a) 60 kV (b) 70 kV

(c) 80 kV (d) 90 kV

Figure 4.9: Measurement of charge magnitude vs. time (rectangular void) under different applied impulse voltage (front/tail time of 1.2/50 us)

4.8 Summary

Measurement results on the test specimens of cylindrical insulation-shaped geometry model shows clear PRPD patterns. As the voltage amplitude was increased, the magnitude of maximum charge increases and PRPD pattern becomes wider. Referring to the PD data, the total number of PD per cycle total number of charges and the magnitude of maximum charge increase as the amplitude, waveshape of the applied voltage and diameter of the void were increased. There is a more dispersed PRPD pattern observed for the larger size of a void as compared to the smaller void size. When the frequency of the applied voltage was decreased, the total number of PDs per cycle, total charge magnitude per cycle and maximum charge magnitude reduce due to the statistical effect As the material temperature was increased, the total PD per cycle,

total charge magnitude and the magnitude of mean charge increase except the value of the maximum charge. This may be due to higher electron generation rate at higher temperature of the dielectric material.

CHAPTER 5: SIMULATION RESULTS OF PD ACTIVITY

5.1 Introduction

This chapter deals with the measurement and simulation results. The simulation results of the electric field distribution generated in a cylindrical insulation-shaped model that has been developed using FEA method are presented. The simulation results under different amplitude frequency and waveshape of the applied voltage, void sizes and temperature of the insulation material are compared with the measurement results to study the PD behaviour under these conditions. The comparison between measurement and simulation results has been made to identify the control parameters affecting PD behaviour under different conditions. The parameters of the simulation model were obtained using a well-known optimisation method. The comparison between measurement and simulation results were made through PRPD patterns, total number of PDs per cycle, total charge magnitude, mean and maximum charge magnitude.

5.2 Simulation results

5.2.1 Electric field (EF) distribution in cylindrical insulation-shaped geometry

The electric field (EF) magnitude along the line from points A and B before and after a PD happens is shown in Figure 5.1 while the corresponding field distribution within the model is displayed in Figure 5.2. The parameter values used in the simulation while yield these results are given in Table 5.1. From Figure 5.2, PD charges propagate up to the first section on both high voltage and ground surface from points A and B respectively. This is due to the extinction field was reached by the average field in the void, E_{ave}, which causes PD charges to stop propagating along the void surface. Hence, charge density is higher on these sections than the other sections where PD charges do not propagate. In Figures 5.1 and 5.2, the magnitude of EF in the void is higher than the

surrounding material before a discharge happens because the relative permittivity of the void is not higher than the material. The non-uniformity of the EF magnitude in the void can be clearly seen from Figure 5.1.

Once the first PD event has occurred, the charge density on the high voltage and ground void surfaces increases, resulting in the EF in the void to decrease, as shown in Figures 5.1 and 5.2. However, the magnitude of EF on the void surface closer to the conductor and nearest to the ground increases significantly after a PD happens because of the accumulation of charges along the void surface. The EF distribution in the void remains non-uniform after a PD happens. Therefore, this will affect the time and magnitude of subsequent PDs. Table 5.2 shows the difference in PD characteristics in the case of field non-uniformity (developed model) in comparison with existing cases of uniform field.

Table 5.1: Simulation parameter for Figures 5.1 and 5.2

Definition	Symbol	Value	Unit
Applied voltage	U_{app}	21	kV
Inception field	E_{inc}	2.8	$kVmm^{-1}$
Extinction field	E_{ext}	1.0	$kVmm^{-1}$
EGR from volume ionization	N_{ev}	20	s^{-1}
EGR from surface emission (lower)	N_{es0L}	70	s^{-1}
EGR from surface emission (higher)	N_{es0H}	200	s^{-1}
Void surface conductivity	σ_{vs}	$3x10^{-9}$	Sm^{-1}
Surface charge density	ρ_s	$1x10^{-4}$	Cm^{-2}

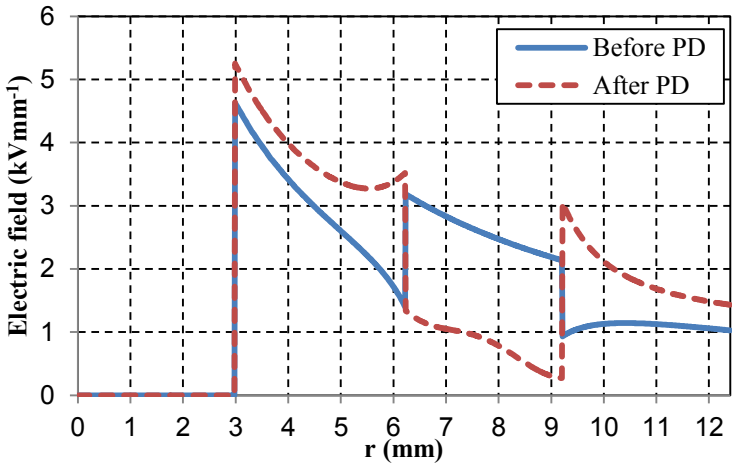

Figure 5.1: Electric field magnitude across the line from points A to B in the model, before and after a discharge happens

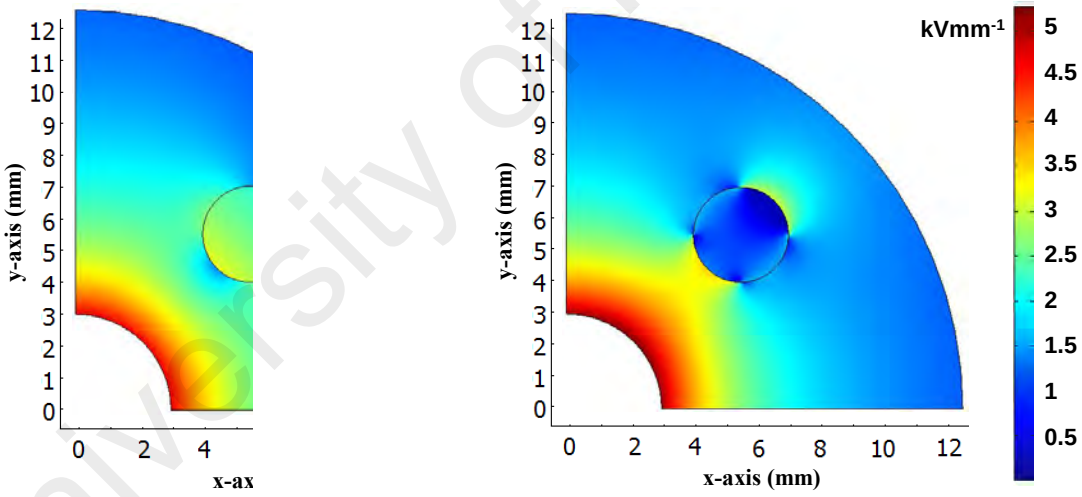

(a) (b)

Figure 5.2: Distribution of the field from the model: (a) before and (b) after a discharge activity

Table 5.2 : Comparison of PD characteristics between developed model and previous model

PD characteristics	Previous PD model	Developed PD model of cylindrical shaped insulation
Electric field distribution within the model is determined using	$\sigma\nabla V + \varepsilon\nabla(\partial V/\partial t) = 0$ where V is the electric potential, σ the conductivity and ε is the permittivity (Illias, et al., 2012).	$\vec{\nabla} \bullet \varepsilon_0\varepsilon_r\vec{E} = 0$ where ε_0 and ε_r is the vacuum and relative permittivity.
Electric field distribution before PD activity	Uniform	Non Uniform
Electric field distribution after PD activity	Uniform	Non Uniform
Distribution of charges on void wall	Uniform and identical (Illias H. A, et al., 2011b)	Not symmetrical

5.2.2 Electric field magnitude vs. time

Figure 5.3 shows the simulation results of the EF vs. time of two voltage cycles. The simulation parameters are given in Table 5.1. Referring to Figure 5.3, E_0 is the applied field, E_{ave} represents the average field in the void, E_s shows the opposing field due to the charges on the surface and E_{inc} is the inception field. Initially, both fields of E_0 and E_{ave} are equal until the first PD occurs. Once the first discharge event has happened at 2ms, the EF in the void centre decreases since the charge accumulation along the void wall that generates opposing field, E_{sc}. The reduction in E_{ave} is dependent on the amount of charges and its distribution along the void wall. It has been seen that E_{sc} becomes higher when the next PD occurs at 2.2ms, 3.3ms and 4.9ms, due to more charge accumulation on the surface of the void.

When both E_{ave} and E_s have the same polarity (e.g. at 7.3 to 12.5ms), the magnitude of E_{ave} is enhanced by E_{sc}. If the discharge event occurs at this stage, then E_{ave} has a significant magnitude change because of higher existing field across the void. During this interval of time, the surface charge tends to move far from points A and B on the void surface through surface conduction. The value of E_{sc} decreases due to the charge redistribution along the void wall. Charge recombination occurs when the charges move towards each other, resulting in reduction of total surface charge. When the polarity of E_{ave} and E_s is not the same (e.g. 12.5 to 18ms), the value of E_s increases and charges move along the void wall towards points A and B, resulting in increase in the density of charge near to points A and B and E_s becomes higher.

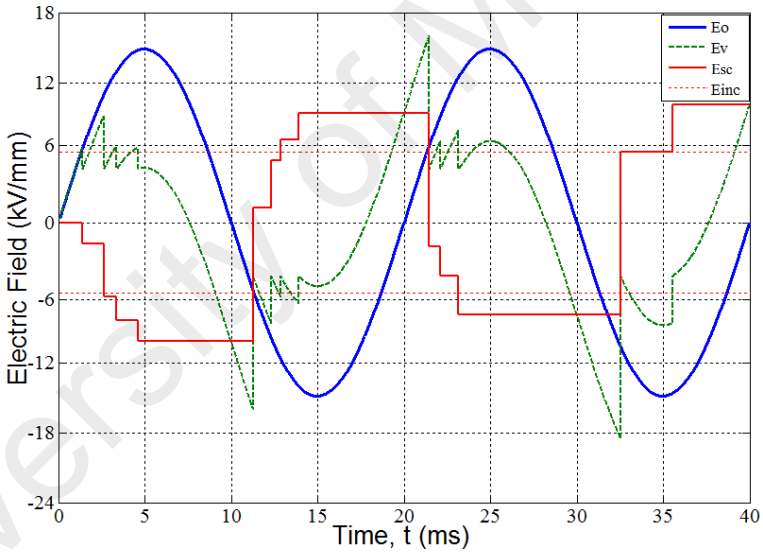

Figure 5.3: Electric field simulation vs. time

5.2.3 Effect of inception field

The inception field, E_{inc} in the void is the minimum field that is required for the occurrence of PD in a void. One of the main conditions for the PD occurrence in a void is that the electric field in the void must be higher than the inception field, E_{inc}. The inception field, E_{inc} can be determined through comparison between the simulation and

measurement data and is subjected to the geometry of the void and the pressure in the void (Gutfleisch, et al., 1995; Illias H. A, et al., 2011b; Niemeyer, 1995).

The PD events within an artificial void of 3 mm diameter in cylindrical insulation-shaped model have been simulated at 22 kV AC sinusoidal voltage to observe the impact of the inception field in the developed model. Figure 5.4 shows the simulated PRPD patterns while the summarized PD data is given in Table 5.3. At higher inception field, the total number of PD per cycle and the magnitude of total charge decreases but the magnitude of mean and minimum charge increase while the magnitude of maximum charge remains constant.

The value of extinction field is derived from the magnitude of minimum charge and is not dependent on the applied field. Higher extinction field is found for smaller void in order to reproduce the magnitude of measured minimum charge. This follows that higher inception field, E_{inc} causes the extinction field, E_{ext} to be higher (Illias H. A., et al., 2011).

Table 5.3: Simulated PD data under different inception field, E_{inc}

Inception field, E_{inc} ($kVmm^{-1}$)	2.8	2.85	2.90	2.95	3.0
Total PDs per cycle	3.45	3.29	3.12	2.97	2.86
Total charge per cycle (pC)	1360	1340	1324	1299	1274
Mean charge (pC)	394	407	424	437	445
Maximum charge (pC)	861	861	861	861	861
Minimum charge (pC)	110	120	130	140	150

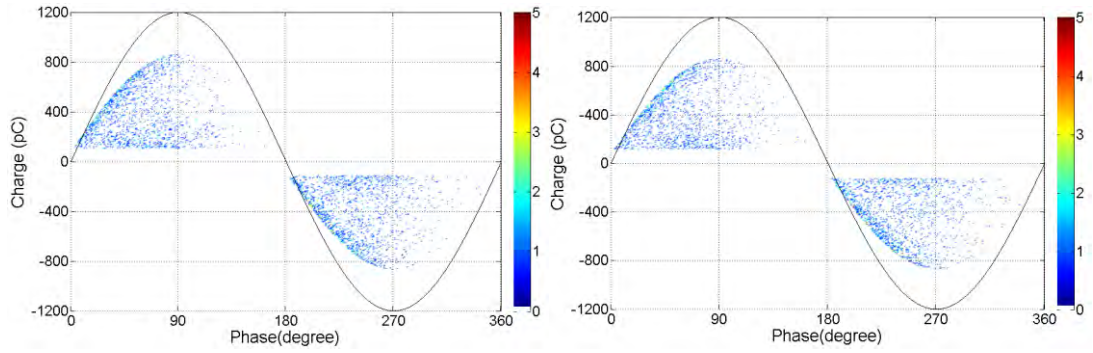

(a) E_{inc} = 2.8 kVmm^{-1} (b) E_{inc} = 2.85 kVmm^{-1}

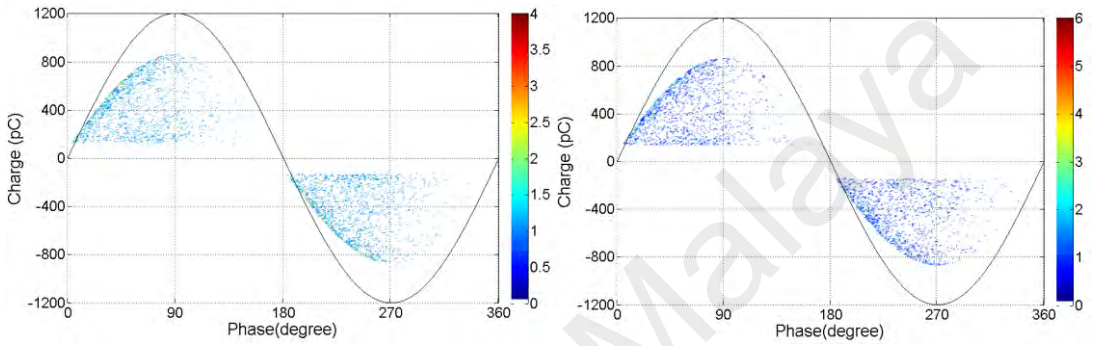

(c) E_{inc} = 2.9 kVmm^{-1} (d) E_{inc} = 2.95 kVmm^{-1}

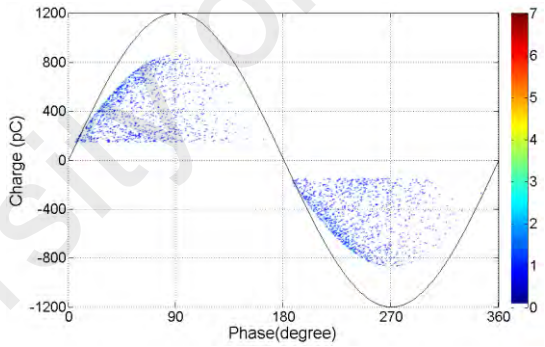

(e) E_{inc} = 3.0 kVmm^{-1}

Figure 5.4: Simulated PRPD patterns under different inception field, E_{inc} at 22 kV applied voltage

5.2.4 Effect of electron generation rate parameters

The PD events for 50 Hz, 21 kV AC sinusoidal applied voltage have been simulated within an artificial void of 3 mm diameter in cylindrical insulation-shaped model. This simulation was done to investigate the impact of electron generation rate (EGR) parameters such as N_{es0L}, N_{es0H} and N_{ev} on PDs in the developed model. The simulated PRPD patterns under different values of N_{es0L}, N_{es0H} and N_{ev} are shown in Figures 5.5,

5.6 and 5.7 respectively, while corresponding results are shown in Tables 5.4, 5.5 and 5.6. Referring to the results, the total PDs per cycle and total charge per cycle are increasing with all EGR parameters. The magnitude of maximum charge decreases when N_{es0L} is increased from 80 to 300 but remain unchanged with N_{es0H} and N_{ev} variation. PRPD patterns close to the magnitude of minimum charge are seen to be determined by N_{es0H}. At higher value of N_{es0H}, the total numbers of PD per cycle increases but with lower magnitude of charge.

Table 5.4: Simulated PD data under different N_{es0L} at 21kV

N_{es0L} (s^{-1})	80	150	200	250	300
Total PDs per cycle	3.13	4.14	4.73	5.19	5.64
Total charge per cycle (pC)	1211	1325	1358	1371	1388
Mean charge (pC)	387	320	287	264	246
Maximum charge (pC)	792	791	760	752	741
Minimum charge (pC)	110	110	110	110	110

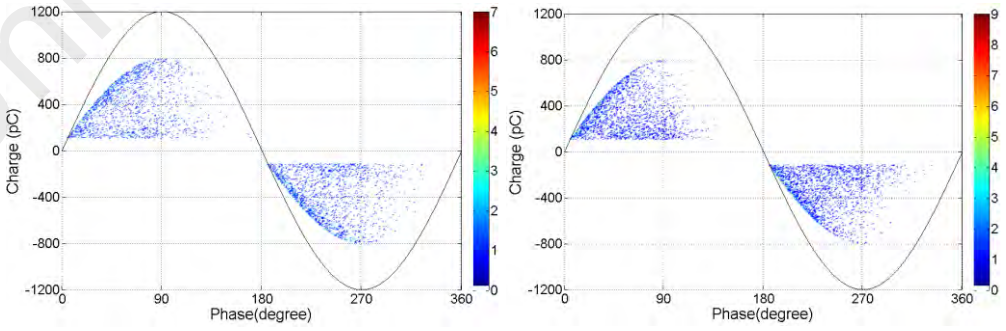

(a) N_{es0L} = 80 (b) N_{es0L} = 150

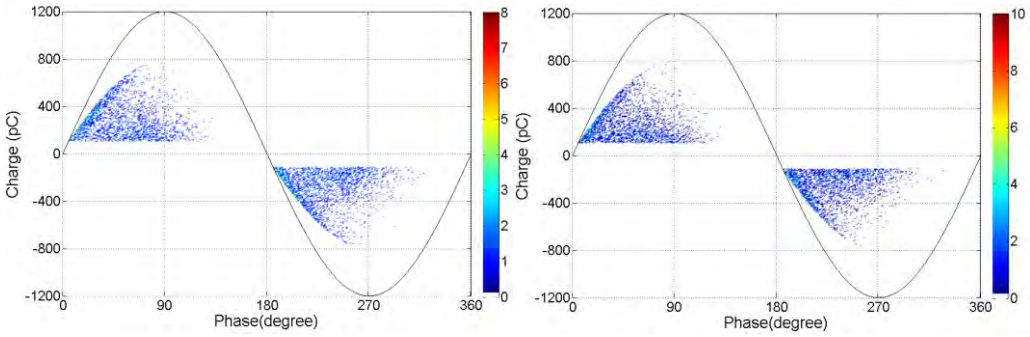

(c) N_{es0L} = 200 (d) N_{es0L} = 250

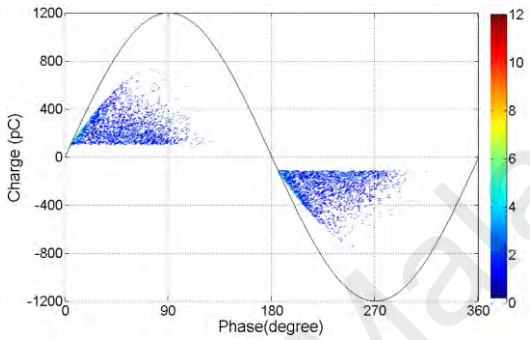

(e) N_{es0L} = 300

Figure 5.5: Simulated PRPD patterns under different N_{es0L} at 21kV (N_{es0H} = 200, N_{ev} = 70)

Table 5.5: Simulated PD data under different N_{es0H} at 21 kV

N_{es0H} (s^{-1})	250	450	650	850	1050
Total PDs per cycle	3.27	3.65	4.0	4.23	4.43
Total charge per cycle (pC)	1233	1278	1320	1337	1356
Mean charge (pC)	377	350	330	316	306
Maximum charge (pC)	792	792	792	792	792
Minimum charge (pC)	110	110	110	110	110

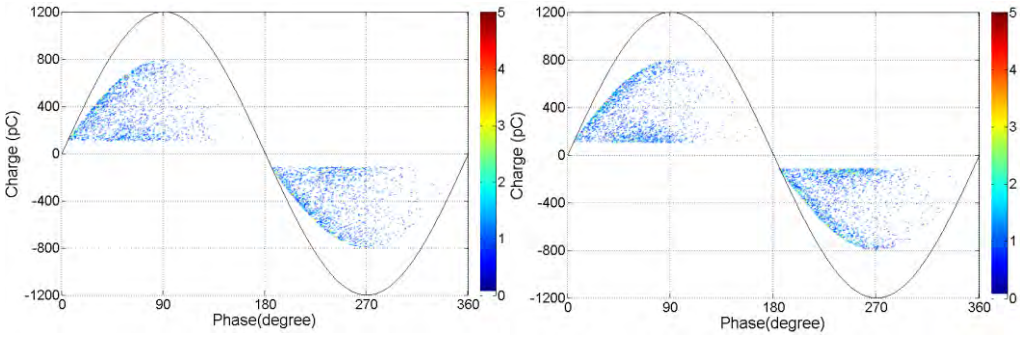

(a) N_{es0H} = 250 (b) N_{es0H} = 450

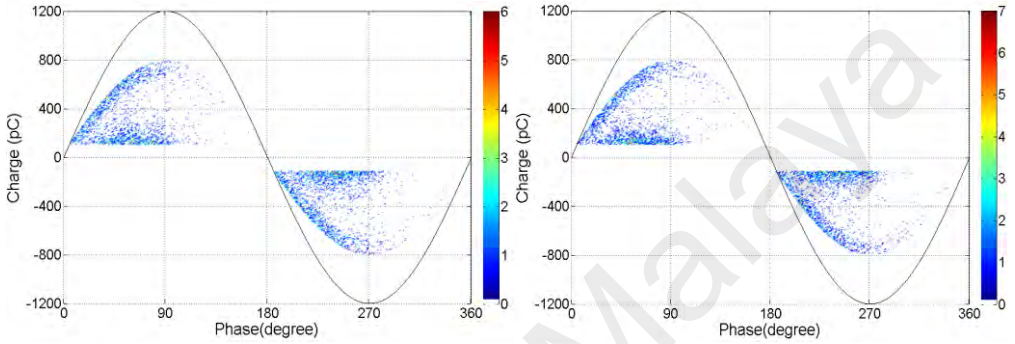

(c) N_{es0H} = 650 (d) N_{es0H} = 850

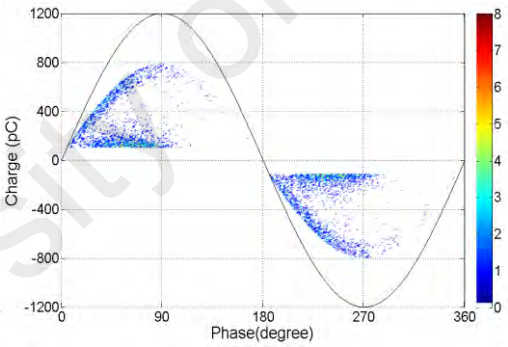

(e) N_{es0H} = 1050

Figure 5.6: Simulated PRPD patterns under different N_{es0H} at 21kV (N_{es0L} =80, N_{ev} =70)

Table 5.6: Simulated PD data under different N_{ev} at 21kV

N_{ev} (s^{-1})	100	120	140	160	180
Total PDs per cycle	3.15	3.16	3.18	3.20	3.21
Total charge per cycle (pC)	1210	1214	1216	1219	1226
Mean charge (pC)	384	384	382	381	382
Maximum charge (pC)	792	792	792	792	792
Minimum charge (pC)	110	110	110	110	110

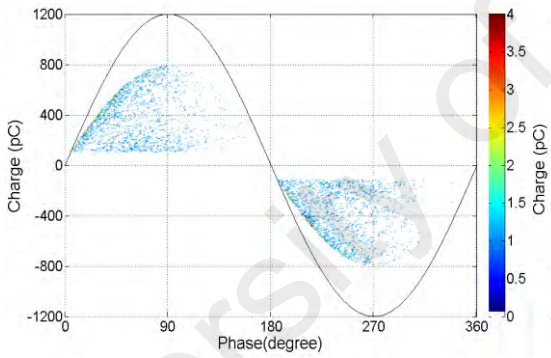

(a) N_{ev} = 100

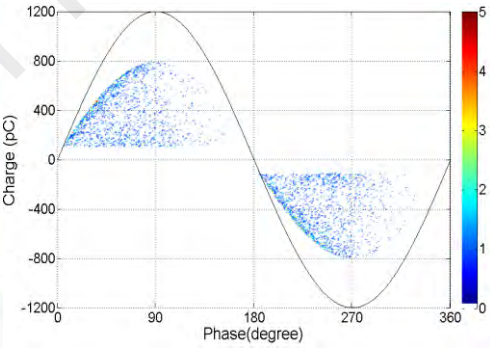

(b) N_{ev} = 120

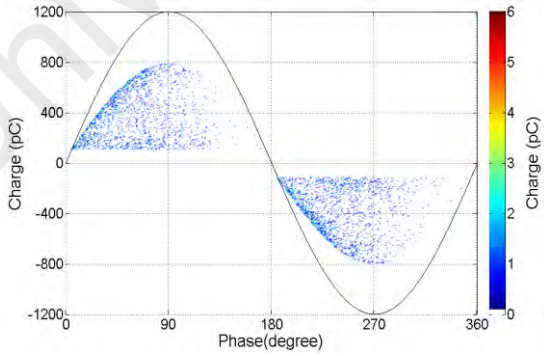

(c) N_{ev} = 140

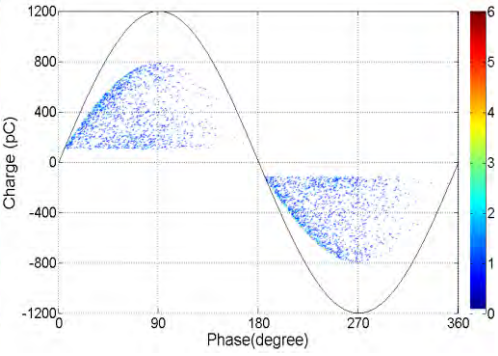

(d) N_{ev} = 160

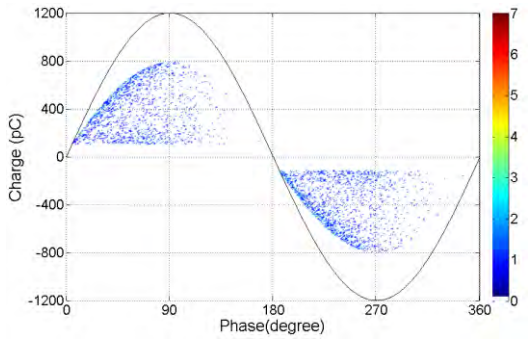

(e) $N_{ev} = 200$

Figure 5.7: Simulated PRPD patterns under different N_{ev} at 21kV ($N_{es0L} = 80$, $N_{es0H} = 200$)

5.3 Comparison between measurement and simulation results

The comparison of PD measurement and simulation results has been made under different amplitudes, frequency and waveshape of the applied voltage, void sizes and material temperatures. The comparison of PD measurement and simulation results was made to identify the key parameters that control the PD occurrences within a void having non-uniform distribution of the electric field in cylindrical insulation geometry. The particle swarm optimisation (PSO) method was used in all simulations to determine the PD model parameter values related to the electron generation rate.

5.3.1 Various applied voltage amplitudes

The PD behaviour from the measurement was reproduced by the simulation model, where the phase resolved partial discharge (PRPD) patterns are shown in Figure 5.8 and the corresponding results are shown in Table 5.7. Referring to Table 5.7, simulation results show reasonable agreement with the experimental results at all applied voltage.

All parameters that were pre-fixed in the simulation are shown in Table 3.3 while parameters that were not pre-fixed are determined from comparison between simulation and measurement data. For the simulation, the inception field, E_{inc}, chosen is independent of the voltage amplitude on the basis of measured data. The value for the

extinction field, E_{ext} is found not to depend on the voltage because the measured minimum charge is constant.

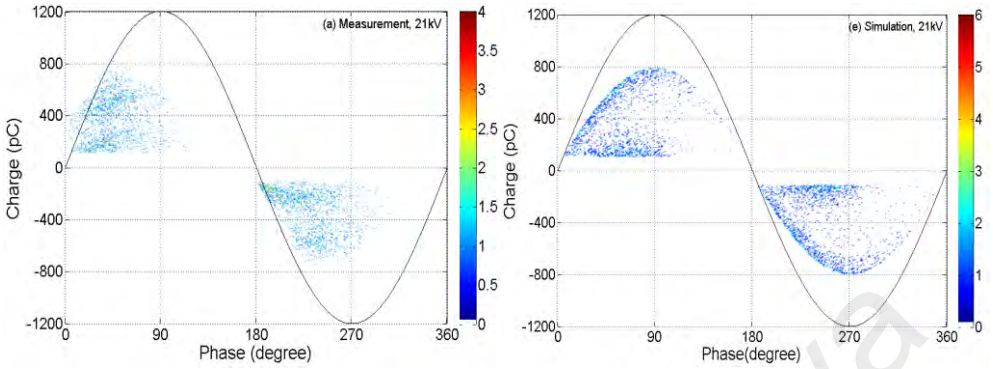

(a) Measurement, 21 kV (e) Simulation, 21 Kv

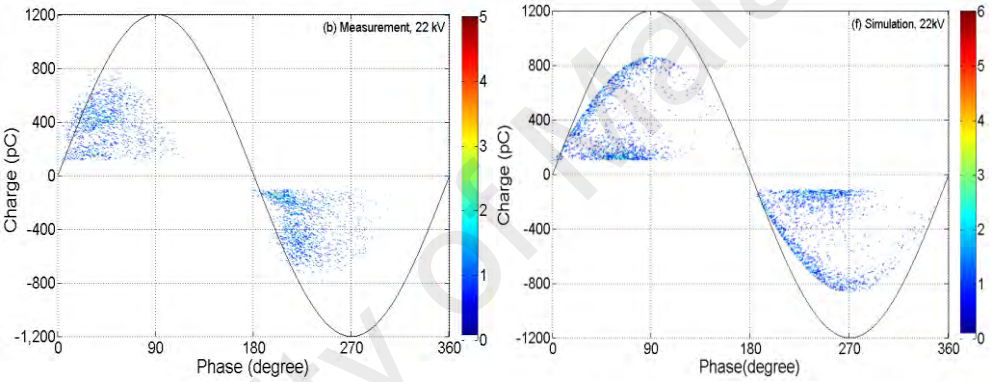

(b) Measurement, 22 kV (f) Simulation, 22 kV

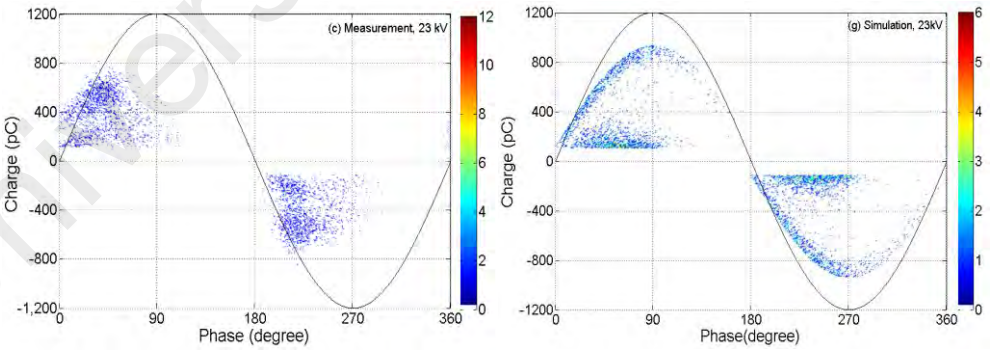

(c) Measurement, 23 kV (g) Simulation, 23 kV

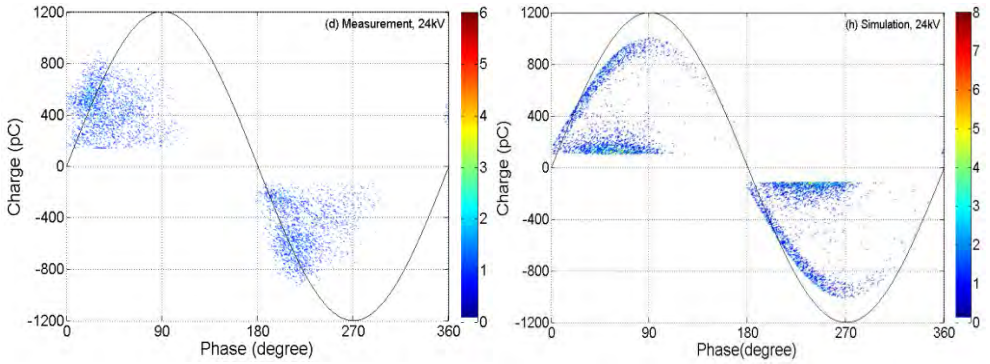

(d) Measurement, 24 kV (h) Simulation, 24 kV

Figure 5.8: PRPD patterns of measurement and simulation results for various applied voltage

Table 5.7: Measurement (M) and simulation (S) results for various applied voltages

Applied Voltage (kV)	21		22		23		24	
	M	S	M	S	M	S	M	S
Total PDs per cycle	3.2	3.15	3.6	3.51	4.2	4.19	4.6	4.67
Total charge per cycle (pC)	1194	1210	1335	1376	1498	1559	1596	1723
Mean charge (pC)	373	384	370	392	356	372	347	369
Maximum charge (pC)	779	791	780	861	823	933	835	1003
Minimum charge (pC)	110	110	110	110	110	110	110	110

The PD model parameters related to electron generation rate due to surface emission and volume ionisation were determined through optimisation method, which is particle swarm optimisation (PSO), as given in Table 5.8. The electron generation rate due to

surface emission is divided into N_{es0L} and N_{es0H}. The value of N_{es0L} is used when the polarity of electric field in the void, E_v alters between successive discharges and N_{es0H} when no change in the polarity. Surface emission from the wall of the void is the key source of free electrons in the void with continuing PD event (Niemeyer, 1995). The effect of electron generation rate due to volume ionisation, N_{ev} is small but initially when there is no PD in the void, the total electron generation rate depends on N_{ev}. After first PD event, the total electron generation depends on the surface emission and volume ionisation, N_{ev}. Referring to Table 5.8, the surface emission N_{es0H} and volume ionisation, N_{ev} increase when the voltage was increased from 21 kV to 24 kV. This is due to the surface emission and volume ionisation are enhanced by the applied voltage. The value of N_{es0L} decreases as the voltage was increased but the combination of these parameters (N_{es0L}, N_{es0H} and N_{ev}) as given in Table 5.8 is producing the same number of PDs per cycle between measurement and simulation results within a tolerance of ±0.1 as mentioned in Table 5.7.

The model parameters, N_{es0L}, N_{es0H} and N_{ev} do not represent the actual value of physical properties of the LDPE dielectric material used in the experiment. Since these values are subjected to each other; unsuitable values will yield a big error between measurement and simulation results. Therefore, PSO method is used to select their values as shown in Table 5.8. Figure 5.9 shows the relationship of N_{es0L}, N_{es0H} and N_{ev} with the applied voltage. It can be seen that N_{es0H} and N_{ev} increase but N_{es0L} decrease with the applied voltage.

The mathematical equations that can best fit the curves in Figure 5.9 as a function of applied voltage, V are

$$N_{es0L} = aV^b + c \tag{5.1}$$

where $a = 3.638\text{x}10^{15}$, $b = -10.98$ and $c = 42.73$,

$$N_{es0H} = aV^b + c \tag{5.2}$$

where $a = 4.565\text{x}10^{-10}$, $b = 8.817$ and $c = 329.5$ and

$$N_{eV} = aV^b + c \tag{5.3}$$

where $a = 0.000707$, $b = 3.561$ and $c = 42.02$.

Table 5.8: Parameters related to EGR for various applied voltages

Applied Voltage (kV)	21	22	23	24
N_{es0L}	53.9160	49.0115	47.3000	45.0898
N_{es0H}	542.6382	628.9799	803.3222	1000.0000
N_{ev}	78.1747	84.7101	92.0000	100.0000

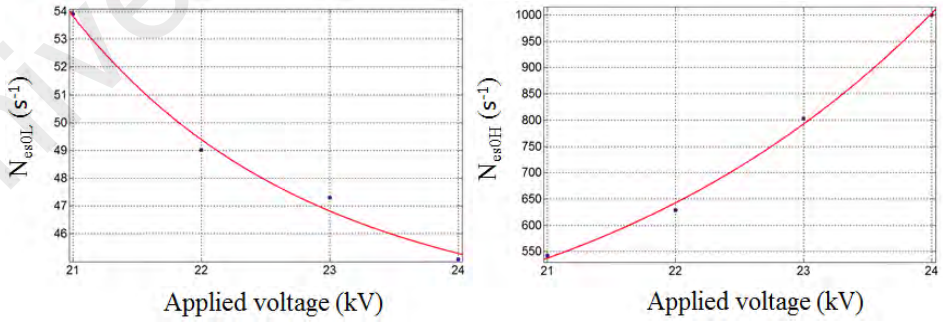

(a) (b)

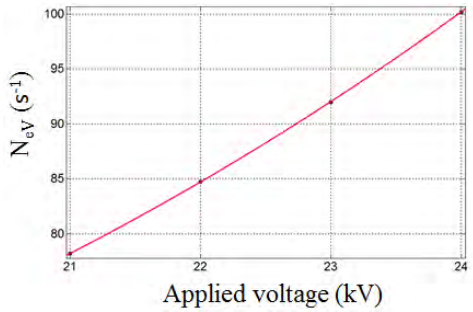

(c)

Figure 5.9: The relationship of N_{es0L}, N_{es0H} and N_{ev} with applied voltage

The simulation parameters are given in Table 5.9. The surface conductivity, σ_{vs} increases with the voltage amplitude. When the applied voltage amplitude is increased, the movement of charges is faster along the void surface, causing faster charge reduction with time. This result is tally with what has been reported in previous literature (Weedy, 1985).

Table 5.9: Parameters used in the simulation for various applied voltages

Definition	Symbol	Value	Unit
Applied voltage	U_{app}	21, 22, 23, 24	kV
Inception field	E_{inc}	2.8	$kVmm^{-1}$
Extinction field	E_{ext}	1.0	$kVmm^{-1}$
Void surface conductivity	σ_{vs}	3.0, 3.1, 3.2, 3.3	nSm^{-1}

5.3.2 Variable void sizes

Comparison between the measured and simulated PRPD patterns, as shown in Figure 5.10 shows general agreement although there is slight difference, especially in the range

of phase of PD occurrences. Table 5.10 shows the details of the PD data from the simulation.

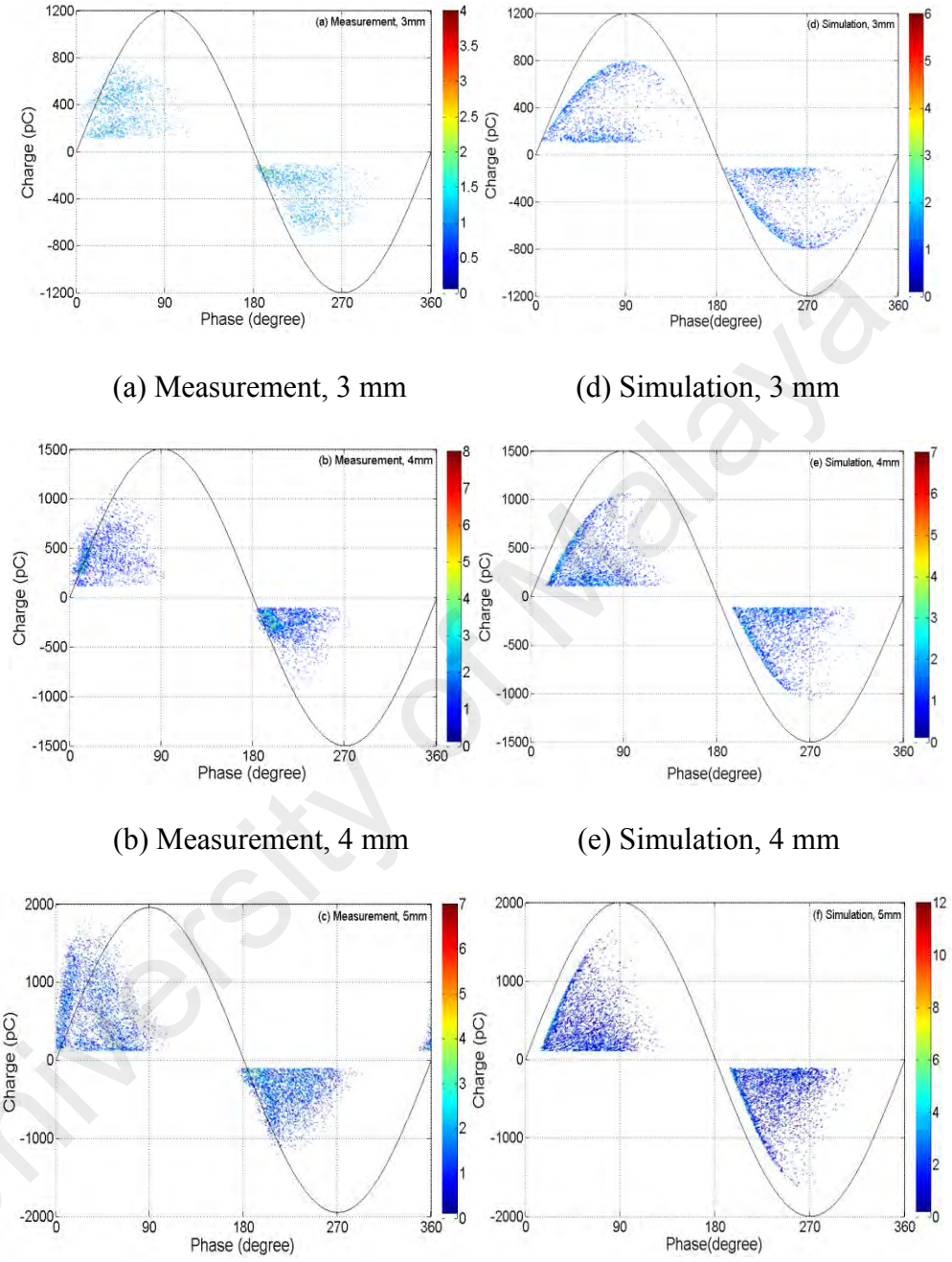

(a) Measurement, 3 mm (d) Simulation, 3 mm

(b) Measurement, 4 mm (e) Simulation, 4 mm

(c) Measurement, 5 mm (f) Simulation, 5 mm

Figure 5.10: PRPD patterns of measurement and simulation results for various void diameters

Table 5.10: Measurement (M) and simulation (S) data for various void diameters

Void diameter (mm)	3		4		5	
	M	S	M	S	M	S
Total PDs per cycle	3.2	3.15	4.8	4.78	6.8	6.7460
Total charge per cycle (pC)	1194	1210	1665	1788	3516	3000
Mean charge (pC)	373	384	347	374	513	445
Maximum charge (pC)	779	791	1037	1058	1522	1655
Minimum charge (pC)	110	110	110	110	110	110

All parameters in this simulation were obtained with the same method as for different applied voltage. From the simulation, the inception field, E_{inc} for smaller void is found to be higher, which is in agreement with literatures (Crichton, et al., 1989; Gutfleisch, et al., 1995; Niemeyer, 1995; Pedersen et al., 1994). Although the minimum charge magnitude of different void size is the same, the extinction field, E_{ext} becomes lower for the smaller size.

The model parameters N_{es0L}, N_{es0H} and N_{ev} are determined through PSO as given in Table 5.11 and it was found that all model parameters related to electron generation rate increases with the size of the void. Larger void size has larger surface area that is perpendicular to the applied field. Hence, the likelihood of free electron to be available from EGR through surface emission, N_{es0L} and N_{es0H} is higher in larger void size. However, EGR through volume ionization, N_{ev} is larger for bigger void because of its bigger volume, where more ionisation through radiation and photo-ionisation can occur. The same number of PDs per cycle within a tolerance of ±0.1 between the measurement

and simulation results is obtained by applying these constraints in the simulation. Figure 5.11 shows the relationship of N_{es0L}, N_{es0H} and N_{ev} with the void size.

Table 5.11: Parameters related to EGR for various void sizes

Void diameter (mm)	3	4	5
N_{es0L}	53.9160	100.0000	110.0000
N_{es0H}	542.6382	807.9465	944.9711
N_{ev}	78.1747	87.5094	107.9592

The parameters used in the simulation model for different void sizes are shown in Table 5.12. The void surface conductivity, σ_{vs} is set higher for larger void surface. This implies that the charge movement per unit time on larger void surface is faster than the smaller void. The reason might be because of the density of charges on larger void surface is higher as a result of larger avalanche head during PD event. Hence, the movement of charges on the void surface is faster since more charges of the same polarity have stronger effect of repelling each other.

The mathematical equations that can best fit the curves in Figure 5.11 as a function of void diameter, d are

$$N_{es0L} = ad^{b} + c \tag{5.4}$$

where a = -1.188 x10^4, b = -4.789 and c = 115.5,

$$N_{es0H} = ad^{b} + c \tag{5.5}$$

where a = -4118, b = -1.579 and c = 1269 and

$$N_{eV} = ad^{b} + c \tag{5.6}$$

where $a = 0.0421$, $b = 4.156$ and $c = 74.13$.

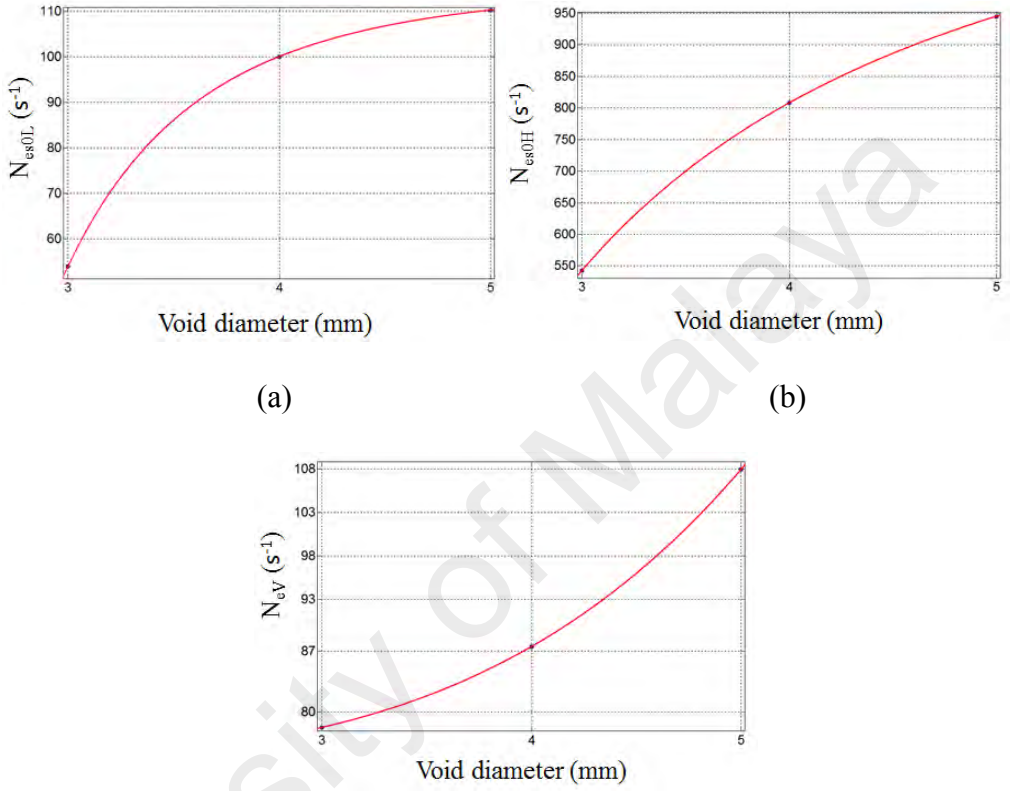

(a) (b)

(c)

Figure 5.11: The relationship of N_{es0L}, N_{es0H} and N_{ev} with void size

Table 5.12: Parameters used in the simulation for different void sizes

Definition	Symbol	Values			Unit
Void diameter	d_v	3	4	5	mm
Inception field	E_{inc}	2.80	2.68	2.59	$kVmm^{-1}$
Extinction field	E_{ext}	1.00	1.09	1.17	$kVmm^{-1}$
Void surface conductivity	σ_{vs}	$2x10^{-9}$	$2.8x10^{-9}$	$3.5x10^{-9}$	Sm^{-1}

5.3.3 Various applied frequency

The comparison between measurement and simulation as a function of frequency of the 8 kV applied voltage is shown in Figure 5.12. Table 5.13 details the comparison between measured and simulated PD results for different frequencies of applied voltage. Referring to Table 5.13, there is reasonable agreement between simulation and measurement data, except the total charge magnitude per cycle.

In the developed model, the parameters related to electron generation rate are determined using an optimization method, the PSO as given in Table 5.14. It was found that at higher frequency of the applied voltage, higher values of N_{es0L}, N_{es0H} and N_{ev} are obtained. This could be due to more charges on the void surface are available in local shallow traps for the next PD event at 50Hz as compared to 5Hz. The same number of PDs per cycle within a tolerance of ±0.1 between the measurement and simulation results is obtained by applying these constraints in the simulation. Figure 5.13 shows the relationship of N_{es0L}, N_{es0H} and N_{ev} with frequency of the applied voltage.

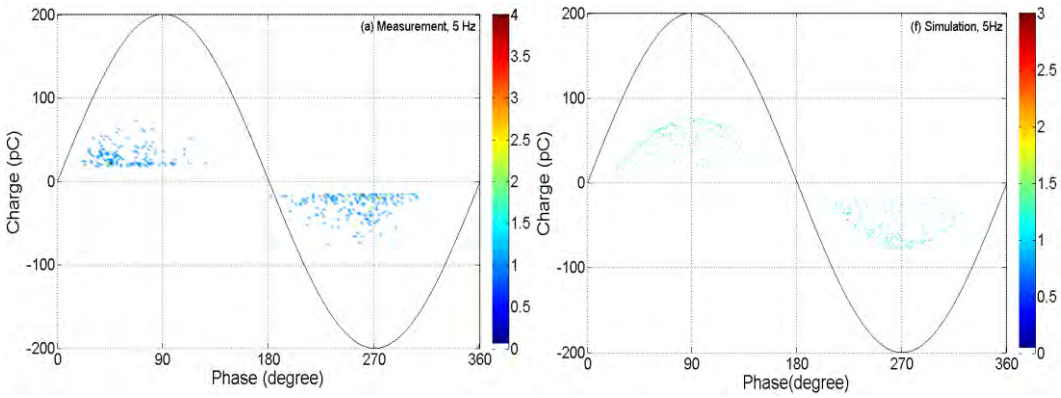

(a) Measurement, 5 Hz (f) Simulation, 5 Hz

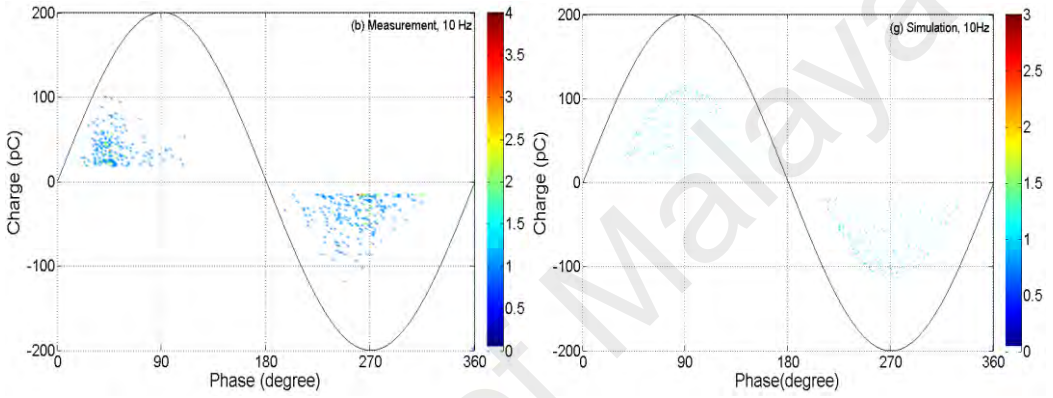

(b) Measurement, 10 Hz (g) Simulation, 10 Hz

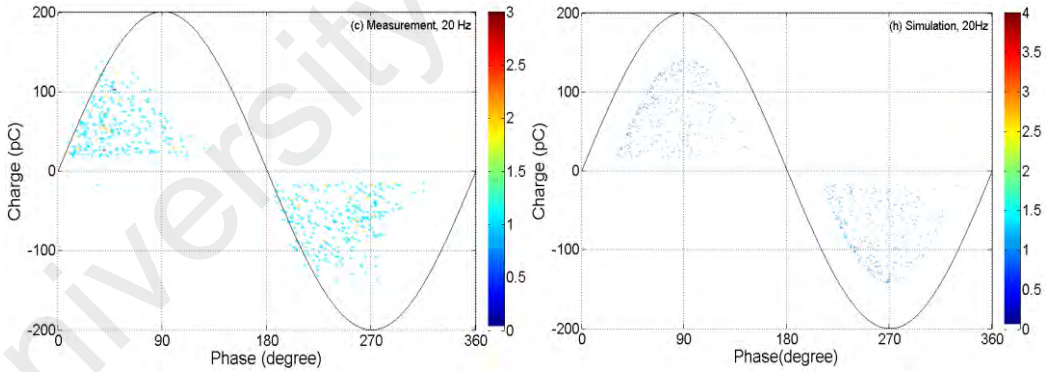

(c) Measurement, 20 Hz (h) Simulation, 20 Hz

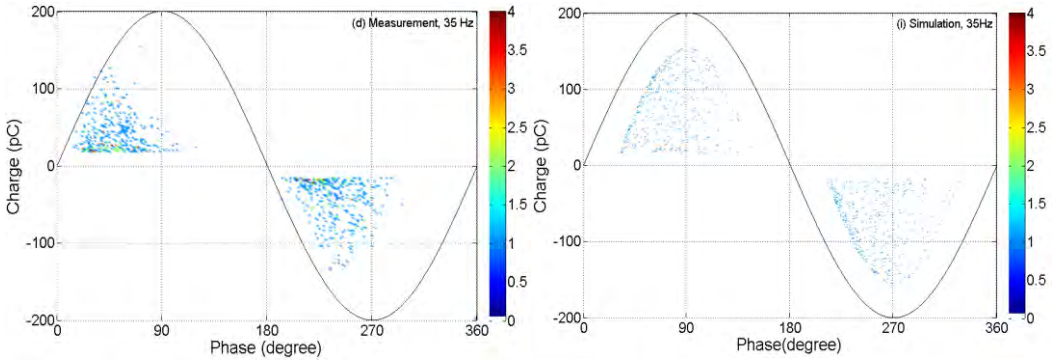

(d) Measurement, 35 Hz (i) Simulation, 35 Hz

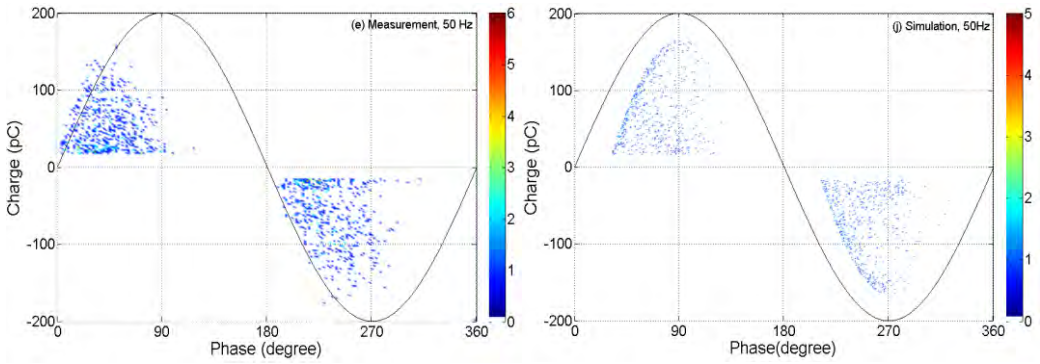

(e) Measurement, 50 Hz (j) Simulation, 50 Hz

Figure 5.12: PRPD patterns of measurement and simulation results for different frequencies of applied voltage

Table 5.13: Measurement (M) and simulation (S) for various applied frequency

Frequency (Hz)	5		10		20		35		50	
	M	S	M	S	M	S	M	S	M	S
Total PDs per cycle	1.1	1.14	1.4	1.44	1.8	1.76	2.5	2.51	3.5	3.55
Total charge per cycle (pC)	30	49	55	91	108	132	110	196	204	245
Mean charge (pC)	29	43	39	63	60	75	44	78	58	69
Maximum charge (pC)	73	76	109	112	138	140	152	153	166	164
Minimum charge (pC)	17	17	17	17	17	17	17	17	17	17

Table 5.14: Parameters related to EGR for various frequencies of the applied voltage

Frequency (Hz)	5	10	20	35	50
N_{es0L}	4.2702	11.5184	29.2190	80.6510	189.1729
N_{es0H}	29.2358	57.8884	78.5531	96.2489	193.4292
N_{ev}	4.4731	9.7228	16.6275	23.3769	32.7015

The parameters used to reproduce the measurement results are given in Table 5.15. It is assumed in the model that the inception field is not dependent on the frequency of the applied voltage, therefore the same value of inception field was used for all applied frequencies in the simulation (Miller et al., 1977). In past literature, PD inception voltage for insulated cavity in polyethylene under different range of frequencies was found not to be frequency dependent (Cavallini, Ciani, et al., 2005). The value of E_{ext} is assigned constant in the simulation because it is subjected to the measured minimum charge, which is independent of the frequency of the applied voltage. The void surface conductivity, σ_{vs} increases as the frequency of applied voltage is higher because a shorter period causes E_v to change faster, resulting in faster movement of free charge along the wall of the void.

The mathematical equations that can best fit the curves in Figure 5.13 as a function of frequency, f are

$$N_{es0L} = af^b + c \tag{5.7}$$

where $a = 0.01318$, $b = 2.437$ and $c = 6.523$,

$$N_{es0H} = af^b + c \tag{5.8}$$

where a = 0.01825, b = 2.296 and c = 44.83 and

$$N_{eV} = af^b + c \tag{5.9}$$

where a = 2.273, b = 0.6924 and c = -2.016.

Table 5.15: Parameters used in the simulation for various frequencies of the applied voltage

Item	Symbol	Value	Unit
Applied Frequency	f	50, 40, 35, 20, 10, 5	Hz
Applied voltage	U_{app}	8	kV
Void inception field	E_{inc}	2.68	$kVmm^{-1}$
Void extinction field	E_{ext}	1.09	$kVmm^{-1}$
Conductivity of the void surface	σ_{vs}	1.5 to 1.1	nSm^{-1}

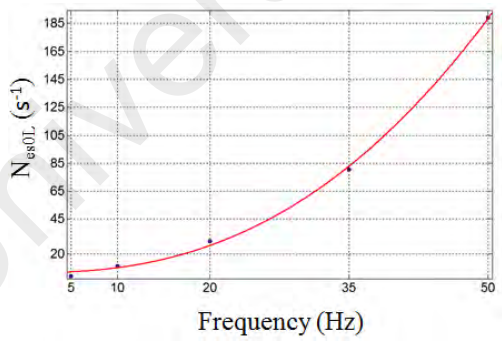

(a)

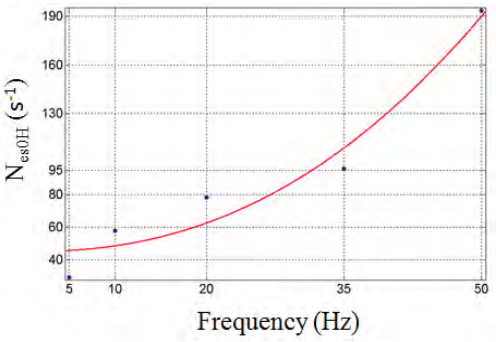

(b)

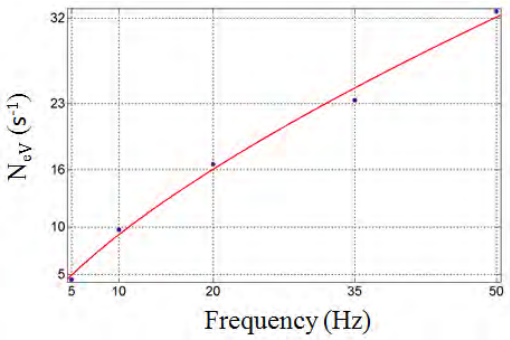

(c)

Figure 5.13: The relationship of N_{es0L}, N_{es0H} and N_{ev} with frequency of applied voltage

5.3.4 Various temperature of the material

The comparison between the measurement and simulation for various temperatures of the dielectric material are shown in Figure 5.14. Table 5.16 details the comparison between measured and simulated PD results for different temperature of the material. Referring to Table 5.16, all PD data increase with temperature of the dielectric material and simulation results are in reasonable agreement with measurement data, except the total charge magnitude per cycle.

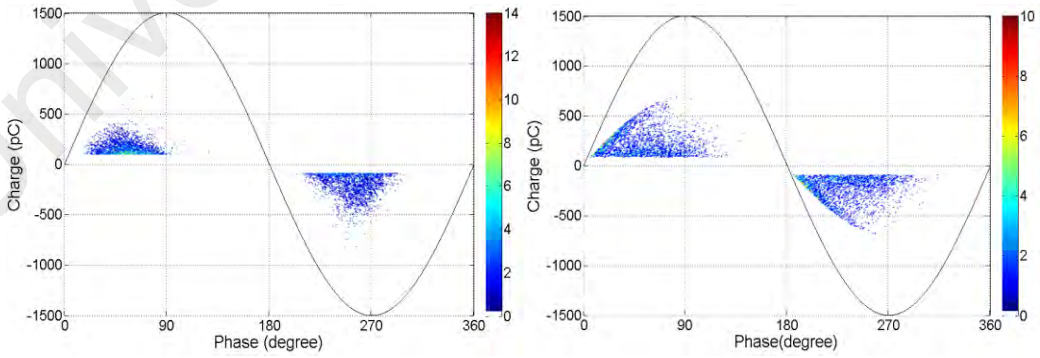

(a) Measurement, 30°C (e) Simulation, 30°C

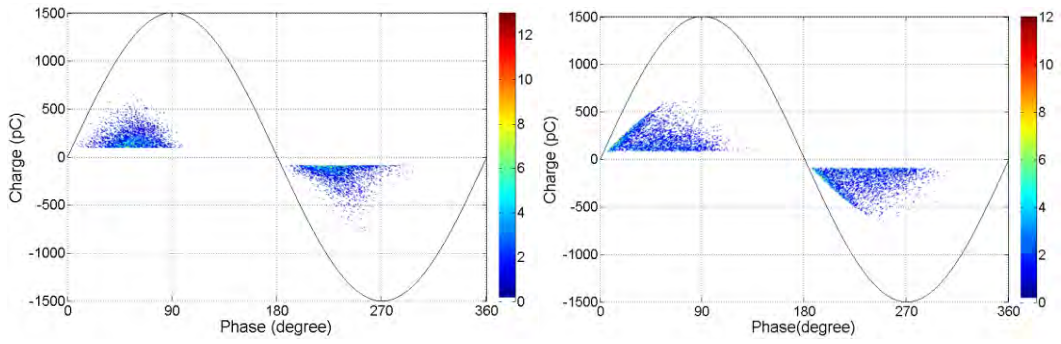

(b) Measurement, 40°C (f) Simulation, 40°C

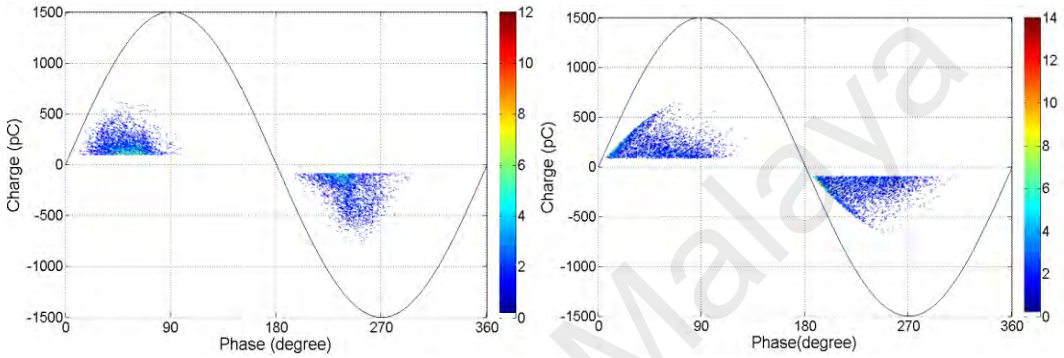

(c) Measurement, 50°C (g) Simulation, 50°C

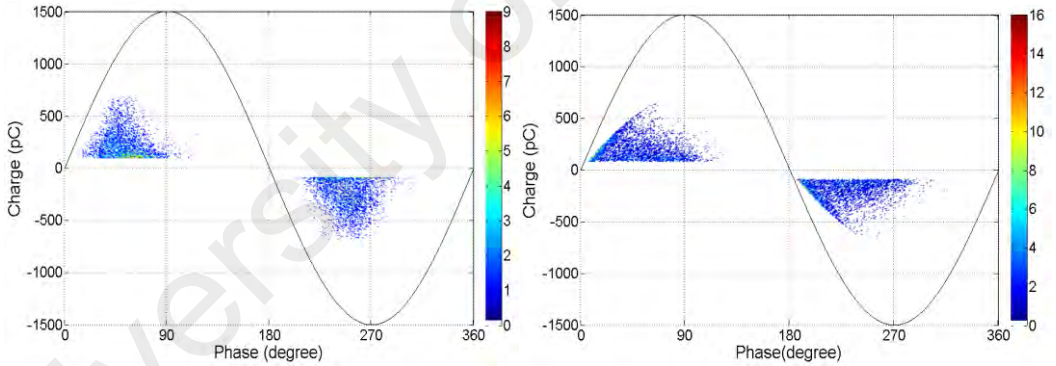

(d) Measurement, 60°C (h) Simulation, 60°C

Figure 5.14: PRPD patterns of measurement and simulation under various material temperatures at 10 kV

Table 5.16: Measurement (M) and simulation (S) for various material temperatures

Temperature (°C)	30		40		50		60	
	M	S	M	S	M	S	M	S
Total PDs per cycle	5.3	5.29	5.5	5.64	5.8	5.88	6.1	6.26
Total charge per cycle (pC)	976	1212	1016	1236	1334	1264	1470	1290
Mean charge (pC)	184	229	188	219	230	215	241	206
Maximum charge (pC)	746	684	708	674	698	648	680	641
Minimum charge (pC)	90	90	90	90	90	90	90	90

The parameters related to electron generation rate were determined using an optimization method, the PSO as shown in Table 5.17 and it was found that electron generation rate due to surface emission N_{es0L} and N_{ev} increase with temperature of the dielectric material. The value of N_{es0L} increases with the temperature, which could be due to a larger amount of charge detrapping from the surface of the void. The volume ionisation, N_{ev} increases with temperature and may be due to higher pressure in the void which may increase the initial free electrons. The same number of PDs per cycle within a tolerance between measurement and simulation results of ±0.1 is obtained by applying constraint in the simulation. The parameters used to reproduce the measurement results are given in Table 5.18. The void surface conductivity, σ_{vs} increases with material temperature and this could be due to charge movement along the wall of the void is enhanced at higher temperature. Figure 5.15 shows the relationship of N_{es0L}, N_{es0H} and N_{ev} with the temperature of the dielectric material.

The mathematical equations that can best fit the curves in Figure 5.15 as a function of temperature of the dielectric material, T are

$$N_{es0L} = aT^{b} + c \tag{5.10}$$

where a = -1979, b = -0.4491 and c = 655.7,

$$N_{es0H} = aT^{b} + c \tag{5.11}$$

where $a = 2.374 \times 10^{6}$, b = -2.594 and c = 29.77 and

$$N_{eV} = aT^{b} + c \tag{5.12}$$

where a = 4.109, b = 0.5968 and c = 7.112.

Table 5.17: Parameters related to EGR for various material temperatures

Temperature (°C)	30	40	50	60
N_{es0L}	225.1250	281.3797	309.4781	342.8017
N_{es0H}	378.6667	202.7474	109.7901	94.7239
N_{ev}	38.4931	43.9283	49.9304	54.2872

Table 5.18: Parameters used in the simulation for various material temperatures

Item	Symbol	Value	Unit
Material Temperature	T	30, 40, 50, 60	℃
Applied Frequency	f	50	Hz
Applied voltage	U_{app}	10	kV
Void inception field	E_{inc}	2.59	$kVmm^{-1}$
Void extinction field	E_{ext}	1.17	$kVmm^{-1}$
Conductivity of the void surface	σ_{vs}	2.5, 2.6, 2.7, 2.8	nSm^{-1}

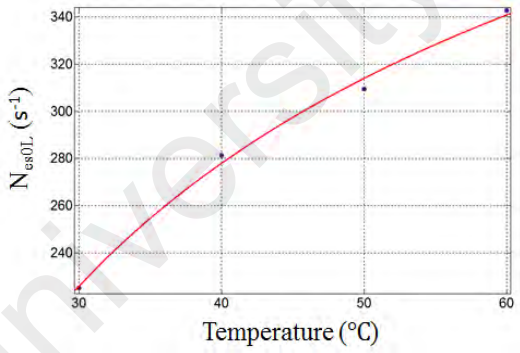

(a)

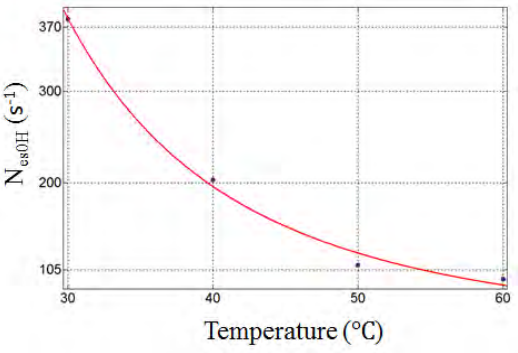

(b)

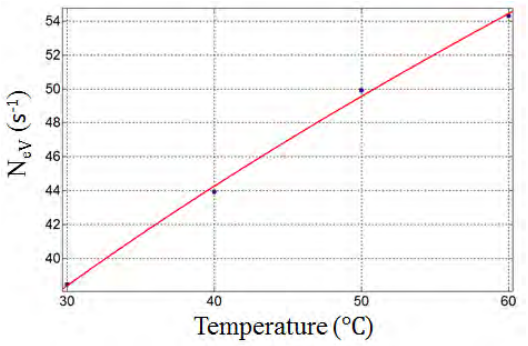

(c)

Figure 5.15: The relationship of N_{es0L}, N_{es0H} and N_{ev} with the temperature of the dielectric material

5.3.5 Various waveforms of applied voltage

Figure 5.16 shows the comparison between measurement and simulation as a function of different peak magnitudes of the triangle applied voltage. Table 5.19 details the comparison between measured and simulated PD results for different peak triangle magnitudes of the applied voltage. Referring to Table 5.19, there is reasonable agreement between simulation and measurement data, except the total charge magnitude per cycle.

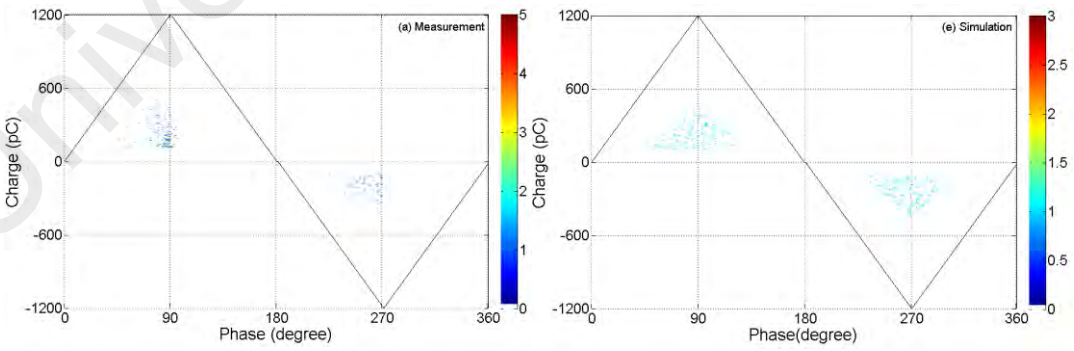

(a) Measurement, 7.5 kV (e) Simulation, 7.5 kV

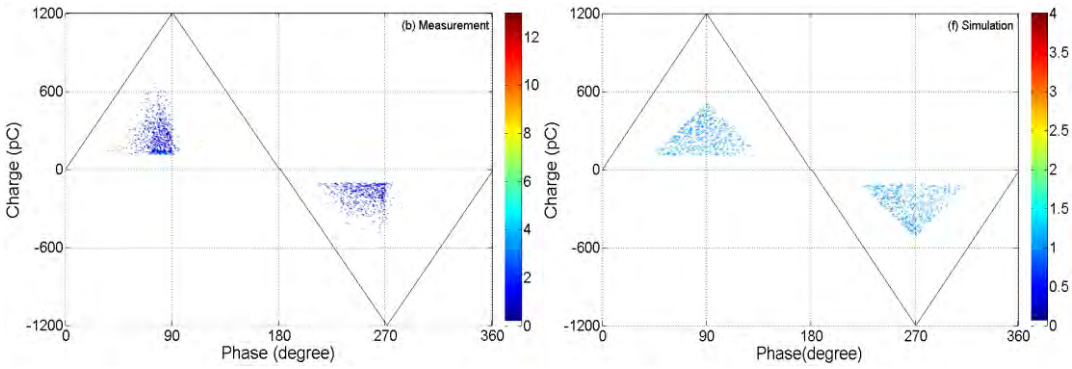

(b) Measurement, 7.75 kV (f) Simulation, 7.75 kV

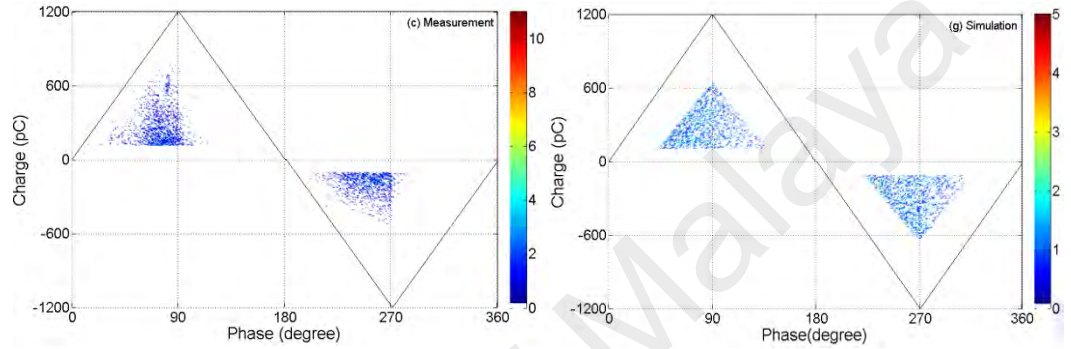

(c) Measurement, 8.0 kV (g) Simulation, 8.0 kV

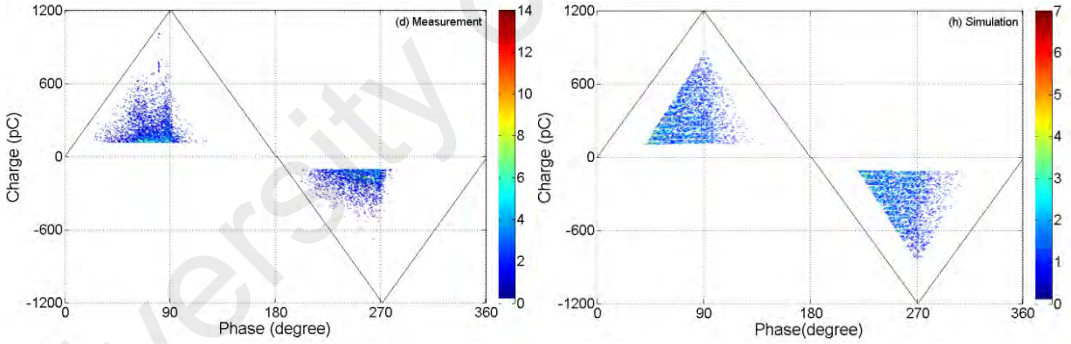

(d) Measurement, 8.25 kV (h) Simulation, 8.25 kV

Figure 5.16: PRPD patterns of measurement and simulation under peak magnitude of the triangle applied voltage

Table 5.19: Measurement (M) and simulation (S) for various under peak magnitude of the triangle applied voltage

Peak magnitude (kV)	7.50		7.75		8.0		8.25	
	M	S	M	S	M	S	M	S
Total PDs per cycle	0.141	0.242	0.735	0.742	1.405	1.399	3.100	3.132
Total charge per cycle (pC)	29.19	69.00	163.44	188.76	334.62	410.86	672.75	1004
Mean charge (pC)	207.0	285.1	222.22	254.39	238.0	293.6	216.9	320.5
Maximum charge (pC)	457	422	573	509	642	633	841	836
Minimum charge (pC)	110	110	110	110	110	110	110	110

In the developed model, the parameters related to electron generation rate were determined through an optimization method, the PSO as given in Table 5.20. It was found that at higher peak triangle magnitude of the applied voltage, higher values of N_{es0L}, $N_{es0H\ and}$ N_{ev} is obtained. Referring to Table 5.19, the surface emission N_{es0L} and N_{es0H} and volume ionisation, N_{ev} increase as the peak triangle magnitude of the applied voltage was increased from 7.5 kV to 8.25 kV. This is due to the surface emission (N_{es0L} and N_{es0H}) and volume ionisation, N_{ev} are enriched by the peak magnitude of the triangle applied voltage. The combination of these parameters (N_{es0L}, N_{es0H} and N_{ev}) as given in Table 5.20 is generating the same number of PDs per cycle between measurement and simulation results within a tolerance of ±0.1 as shown in Table 5.19. The relationship of surface emission (N_{es0L} and N_{es0H}) and volume ionisation, N_{ev} with the peak triangle magnitude of the applied voltage is shown in Figure 5.17. The parameters used in the

simulation are given in Table 5.21. The conductivity of the void surface, σ_{vs} increases with peak triangle magnitude of the applied voltage. This is due to the same reason discussed in various applied voltage amplitude. Table 5.22 shows the comparison of parameters in case of uniform and non-uniform electric field distribution in a void.

The mathematical equations that can best fit the curves in Figure 5.16 as a function of different peak magnitude of the triangle applied voltage, V_{peak} are

$$N_{es0L} = aV_{peak}{}^{b} + c \tag{5.13}$$

where a = 3.107e x10^{-20}, b = 23.86 and c = 0,

$$N_{es0H} = aV_{peak}{}^{b} + c \tag{5.14}$$

where a = 3.208e x10^{-14}, b = 17.34 and c = 0 and

$$N_{eV} = aV_{peak}{}^{b} + c \tag{5.15}$$

where a = 8.053 x10^{-14}, b = 16.3 and c = 18.68.

Table 5.20: Parameters related to EGR for various peak triangle magnitude of the applied voltage

Peak magnitude (kV)	7.50	7.75	8.0	8.25
N_{es0L}	31.1205	57.5742	98.6494	231.4780
N_{es0H}	54.2832	103.0799	117.1040	258.0899
N_{ev}	33.2229	47.1365	56.6625	90.0000

Table 5.21: Parameters used in the simulation for various peak triangle magnitude of the applied voltage

Definition	Symbol	Value	Unit
Applied peak voltage magnitude	U_{app}	7.5, 7.75, 8.0, 8.25	kV
Inception field	E_{inc}	2.68	$kVmm^{-1}$
Extinction field	E_{ext}	1.09	$kVmm^{-1}$
Void surface conductivity	σ_{vs}	1.7, 1.8, 1.9, 2.0	nSm^{-1}

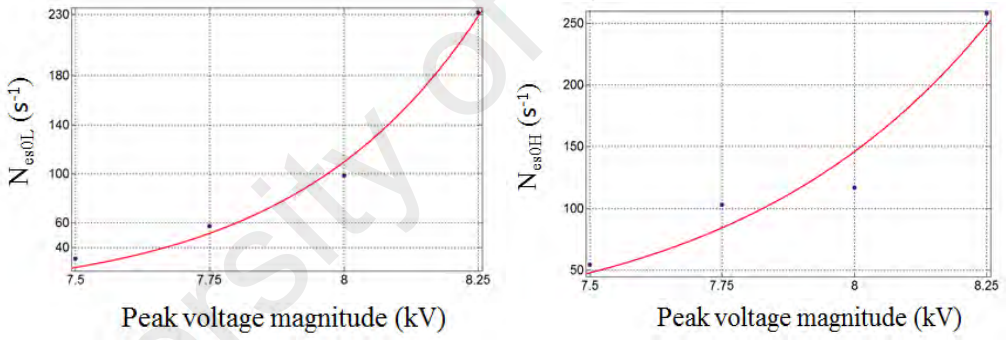

(a) (b)

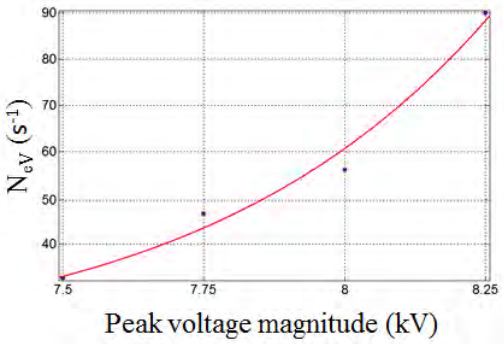

(c)

Figure 5.17: The relationship of N_{es0L}, N_{es0H} and N_{ev} with peak triangle magnitude of the applied voltage

Table 5.22 : Comparison of parameters in case of uniform and non-uniform electric field distribution within a void

Parameter	Uniform Electric Field	Non Uniform Electric Field	Uniform Electric Field	Non Uniform Electric Field	Uniform Electric Field	Non Uniform Electric Field	Uniform Electric Field	Non Uniform Electric Field
	Inception field		Extension field		EGR due to surface emission		EGR due to volume ionization	
Higher applied voltage	No change	No change	No change	No change	No change	Higher	Higher	Higher
Higher frequency of applied voltage	No change	No change	Higher	No change	No change	Higher	Higher	Higher
Larger void diameter	Higher	lower	Higher	higher	Lower	Higher	Higher	Higher
Higher temperature of dielectric material	Higher	No change	Higher	No change	Higher	Higher	Higher	Higher

5.4 Summary

From the developed model using FEA method, before a PD occurrence, the electric field in the void is higher compared to the surrounded dielectric material due to its lower permittivity. Once a PD occurs, the electric field in a void decreases and becomes lower than dielectric material due to the charge accumulation on the void surface. The charge accumulation on the void surface may decay with the time via surface conduction along the wall of a void, causing recombination, resulting in the reduction of the electric field due to the amount of surface charge. All simulation results are in reasonable agreement with the measurement results. Key parameters that control the PD occurrences within a void having non-uniform distribution of the electric field in cylindrical insulation geometry are the distribution of charges on the void wall, decay rate of charges by surface conduction, inception field, extinction field and electron generate rate through surface emission and volume ionisation.

CHAPTER 6: CONCLUSIONS AND FUTURE WORK

6.1 Conclusions

A physical model of PD activities within an artificial void in cylindrical insulation-shaped geometry has been successfully created using Finite Element Analysis method. A two-dimensional model developed was used to simulate PD event for various amplitude, frequency and waveshape of the applied voltage, void sizes and temperature of the insulation material. The model managed to simulate discharge occurrences within the void in the presence of non-uniform electric field distribution. The impact of non-uniform charge distribution is affecting the distribution of the electric field within the void, resulting in subsequent discharge occurrences to be affected. Charge distribution was determined through charge propagation on the sectioned void surfaces and stops when the void average field reduces below the extinction field. Decay of charges through surface conduction was also successfully modelled using increment of surface conductivity from a smaller to a larger value. Higher surface conductivity represents faster movement of charges on the void surface.

PD measurements on test specimens containing an artificial void within cylindrical insulation-shaped geometry for various amplitude, frequency and waveshape of the applied voltage, void sizes and temperature of the insulation material have been successfully performed. For PD experiment, different test samples of cylindrical insulation-shaped geometry containing an artificial cylindrical void were successfully prepared in the laboratory. From PD measurements, it was found that under non-uniform distribution of the electric field within the void and insulation, the PD occurrences per cycle and total magnitude of charge per cycle are higher under higher applied voltage. This is due to higher electron generation rate in the void. The

magnitude of maximum charge also increases with the applied voltage because larger voltage amplitude guarantees a higher voltage decrement in the void when a discharge happens. The minimum discharge magnitude does not depend on the voltage amplitude.

The impact of various frequencies of applied voltage on PD events through PD measurements with the test specimen of cylindrical insulation-shaped geometry was also successfully analysed. It was found that when the frequency of applied voltage is increased, the total number of PDs, total charge magnitudes and maximum charge magnitude increase. Higher number of PD per cycle might be due to more charges on the surface of a void are accessible for next PD event at higher frequency. The total charge magnitude per cycle and maximum charge magnitude reduce as the frequency of applied voltage was decreased and this might be due to the statistical effect. The minimum charge magnitude remains unchanged because it is independent of frequency of applied voltage.

PD events within an artificial void in cylindrical insulation-shaped geometry under different peak magnitude of the applied impulse voltage were also successfully measured. It was concluded that discharges with positive charge magnitude and significantly higher than subsequent discharges occurred during the rise time of the applied voltage. During the fall time, negative discharges of lower charge magnitude occur. The overall number of discharges per second becomes higher with higher impulse voltage peak. The magnitude of maximum charge increases with impulse voltage peak due to the maximum field in the void at higher value of impulse voltage peak. PD measurements within an artificial void in cylindrical insulation-shaped geometry under different peak magnitude of the triangle applied voltage were also successfully performed. From the measurement results, it was found that the electric field in the void follows the triangle voltage waveform curve. From the summarized PD data, it was found that the total number of PDs, total charge

magnitudes and maximum charge magnitude increases with peak triangle magnitude of the applied voltage.

PD measurements within an artificial void in cylindrical insulation-shaped geometry under different void sizes and material temperatures were also successfully performed. From PD measurements under different void sizes, it was found that the PD occurrences per cycle and total magnitude of charge per cycle are higher under larger void size. The PD occurrence per cycle increases with larger size of the void because of higher generation rate of electrons in the void. The magnitude of total charge and maximum charge increase as the void diameter was increased, which might be due to larger development of the avalanche head within large size of the void. The minimum discharge magnitude does not depend on the void size. It was concluded from the PD measurements under different material temperatures that when the material temperature was increased, the total PD per cycle, total charge magnitude and the magnitude of mean charge increase except the value of maximum charge. This may be due to higher electron generation rate at higher temperature of the dielectric material.

The values of the parameters in the PD model were chosen based on the comparison between the measurement and simulation results. The parameters were successfully selected using an optimisation method, the particle swarm optimisation (PSO). PSO was successfully applied for the simulation under different amplitudes, frequencies and waveshape of the applied voltage, void sizes and material temperatures. The PD model parameters related to electron generation rate, which are $N_{es0\mathrm{L}}$, N_{es0H} and N_{ev} have been successfully determined using PSO.

Finally, comparison between measurement and simulation results was made and the key parameters that control the PD occurrences within a void having non-uniform distribution of the electric field in cylindrical insulation geometry have been

successfully identified. These parameters are the distribution of charges on the void wall, decay rate of charges by surface conduction, inception field, extinction field and electron generate rate through surface emission and volume ionisation.

In past more than half of the breakdowns in the cable network are due to internal defect in the insulation. One of the main reasons declared behind these sudden failures is partial discharge (PD), which degrades the insulation and may cause unexpected breakdown. Therefore, it is important to monitor insulation used in high voltage system to schedule maintenance actions timely. Through PD measurement professional engineer determines the type of the discharge. Although, this research work is not directly contributing to the industry but this research work will help engineers to have better understanding of PD characteristics within a cylindrical void while conducting PD diagnostic test during commissioning process of underground cables.

6.2 Future work

Future works that can be performed are:

1. PD measurement within test sample which consists of a cylindrical void in a cylindrical insulation-shaped polyethylene material under various stress conditions can be performed using cross-linked polyethylene (XLPE) dielectric material.
2. PD measurements can be performed on test specimens containing an artificial spherical void in cylindrical insulation-shaped geometry under various stress conditions.

REFERENCES

Ahmed, N. H., Morel, O., & Srinivas, N. N. (1999). Partial discharge measurement in transmission-class cable terminations. *Paper presented at the IEEE Transmission and Distribution Conference.*

Ahmed, N. H., & Srinivas, N. N. (1997). On-Line Partial Discharge Detection in Cables. *IEEE Annual Report - Conference on Electrical Insulation and Dielectric Phenomena, Minneapolis*.

Ahmed, N. H., & Srinivas, N. N. (1998). On-line Partial Discharge Detection in Cables. *IEEE Transactions on Dielectrics and Electric Insulation, 5*, 181-188.

Alapati, S., & Thomas, M. J. (2012). Electrical treeing and the associated PD characteristics in LDPE nanocomposites. *IEEE Transactions on Dielectrics and Electrical Insulation, 19*(2), 697-704.

Argaut, P., Auclair, H., & Favrie, E. (1993). Development of 500 kV low density polyethylene insulated cable. *Third International Conference on Power Cables and Accessories 10kV - 500kV*, 77-81.

Ashtiani, M. B., & Shahrtash, S. M. (2013). On-line decision tree-based insulation assessment employing mathematical morphology filters for HV cables. *IEEE Transactions on Dielectrics and Electrical Insulation, 20*, 1347-1355.

Auckland, D. W., McGrail, A. J., Smith, C. D., Varlow, B. R., Zhao, J., & Zhu, D. (1995). The Application of Ultrasound to the Inspection of Insulation. *IEEE 5th International Conference on Conduction and Breakdown in Solid Dielectrics.*, 590-594.

Bang-Wook, L., Won, C., Young-Min, C., Yong-Han, K., & Ja-Yoon, K. (2013). Comparison Between PD Inception Voltage and BD Voltage of PPLP in Considering HTS Cable Insulation. *IEEE Transactions on Applied Superconductivity, 23*(3), 5402104-5402104.

Bartnikas, R. (1987). Electrical Properties of Solid Insulating Materials: Measurement Techniques: *American Society for Testing and Materials.*

Bartnikas R. (2002). Partial Discharges. Their Mechanism, Detection and Measurement. *IEEE Transactions on Dielectrics Electrical Insulation, 9*, 763-808.

Bartnikas, R., & McMahon, E. J. (1979). Corona Measurement and Interpretation. *Engineering Dielectrics ASTM Publication STP 669.*

Bodega, R., Morshuis, P. H. F., Lazzaroni, M., & Wester, F. J. (2004). PD recurrence in cavities at different energizing methods. *IEEE Transactions on Instrumentation and Measurement, 53*(2), 251-258.

Boggs, S. A. (1990). Partial discharge. ii. detection sensitivity. *IEEE Electrical Insulation Magazine, 6*, 35-42.

Bojie, S., Chengke, Z., Hepburn, D., Xiang, D., Peers, G., Wenjun, Z., & Zeyang, T. (2014). Partial discharge pulse propagation in power cable and partial discharge monitoring system. *IEEE Transactions on Dielectrics and Electrical Insulation, 21*(3), 948-956.

Bojie, S., Wenjun, Z., Jianhui, Y., Shaoxin, M., Chengke, Z., & Hepburn, D. M. (2014). On-line PD detection and localization in cross-bonded HV cable systems. *IEEE Transactions on Dielectrics and Electrical Insulation, 21*(5), 2217-2224.

Braunsberger, U. (2007). Investigations of the dielectric strength of epoxy resin. *European Electromagnetic Launch Society 18th Topical Meeting*.

Cavallini, A., Ciani, F., Mazzanti, G., & Montanari, G. C. (2005). First electron availability and partial discharge generation in insulation cavities: effect of light irradiation. *IEEE Transactions on Dielectrics and Electrical Insulation, 12*(2), 387-394.

Cavallini, A., Montanari, G. C., Puletti, F., & Contin, A. (2005). A new Methodology for the identification of PD in electrical apparatus: Properties and Applications. *IEEE Transactions on Dielectric EIectrical Insulation, 12*(2), 203 - 215.

Chen, X., Xu, Y., & Cao, X. (2014). Nonlinear time series analysis of partial discharges in electrical trees of XLPE cable insulation samples. *IEEE Transactions on Dielectrics and Electrical Insulation, 21*(4), 1455-1461.

Crichton, G. C., Karlsson, P. W., & Pedersen, A. (1989). Partial Discharges in Ellipsoidal and Spheroidal Voids. *IEEE Transactions on Dielectrics and Electrical Insulation, 24*, 335-342.

Eberhart, & Yuhui, S. (2001). Particle swarm optimization: developments, applications and resources. *Paper presented at the Proceedings of the 2001 Congress on Evolutionary Computation.*

Escorsa, M. O., & Garcia-Colon, V. R. (2008). Underground power cable on site testing experience using resonant high voltage power supplies and partial discharge ultra wide band methods. *Paper presented at the Transmission and Distribution Conference and Exposition: Latin America, 2008 IEEE/PES.*

Florkowska, B., Florkowski, M., Roehrich, J., & Zydron, P. (2011). Partial discharge mechanism in a non-uniform electric field at higher pressure. *IET Science, Measurement &Technolog, 5*(2), 59-66.

Florkowska, B., Roehrich, J., Zydron, P., & Florkowski, M. (2011). Measurement and analysis of surface partial discharges at semi-square voltage waveforms. *IEEE Transactions on Dielectrics and Electrical Insulation, 18*(4), 990-996.

Forssen, C., & Edin, H. (2008a). Partial discharges in a cavity at variable applied frequency part 1: measurements. *IEEE Transactions on Dielectrics and Electrical Insulation, 15*(6), 1601-1609.

Forssen, C., & Edin, H. (2008b). Partial discharges in a cavity at variable applied frequency part 2: measurements and modeling. *IEEE Transactions on Dielectrics and Electrical Insulation, 15*, 1610-1616.

Gargari, S. M., Wouters, P. A. A. F., van der Wielen, P., & Steennis, E. F. (2011). Partial discharge parameters to evaluate the insulation condition of on-line located defects in medium voltage cable networks. *IEEE Transactions on Dielectrics and Electrical Insulation, 18*(3), 868-877.

Gulski, E., & Kreuger, F. H. (1992). Computer-aided recognition of discharge sources. *IEEE Transactions on Electrical Insulation, 27*(1), 82-92.

Gulski, E., Smit, J. J., & Wester, F. J. (2005). PD knowledge rules for insulation condition assessment of distribution power cables. *IEEE Transactions on Dielectrics and Electrical Insulation, 12*, 223-239.

Gutfleisch, F., & Niemeyer, L. (1995). Measurement and Simulation of PD in Epoxy Voids. *IEEE Transactions on Dielectrics and Electrical Insulation, 2*, 729-743.

Hao, Z., Blackburn, T. R., Phung, B. T., & Sen, D. (2007). A novel wavelet transform technique for on-line partial discharge measurements. 1. WT de-noising algorithm. *IEEE Transactions on Dielectrics and Electrical Insulation, 14*(1), 3-14.

Huuva, R., Englund, V., Gubanski, S. M., & Hjertberg, T. (2009). A versatile method to study electrical treeing in polymeric materials. *IEEE Transactions on Dielectrics and Electrical Insulation, 16*(1), 171-178.

IEC 60270 3rd Edition. (2000). Partial discharges measurement.

IEC. (1996). High Voltage Testing: Partial Discharge Measurement (Vol. Standard 60270).

Illias, H. A. (2011). Measurement and Simulation of Partial Discharges within a Spherical Cavity in a Solid Dielectric Material. *PhD thesis, University of Southampton UK*.

Illias, H. A., Chen, G., & Lewin, P. L. (2011). The influence of spherical cavity surface charge distribution on the sequence of partial discharge event. *Journal of Physics D: Applied Physics, 44*.

Illias, H. A., Chen, G., & Lewin, P. L. (2011a). Modelling of partial discharge activity in spherical cavities within a dielectric material. *IEEE Electrical Insulation Magazine, 27*, 38-45.

Illias, H. A., Chen, G., & Lewin, P. L. (2011b). Partial Discharge Behavior within a Spherical Cavity in a Solid Dielectric Material as a Function of Frequency and Amplitude of the Applied Voltage. *IEEE Transactions on Dielectrics and Electrical Insulation, 18*, 432-443.

Illias, H. A., Chen, G., & Lewin, P. L. (2012). Partial discharge within a spherical cavity in a dielectric material as a function of cavity size and material temperature. *IET Science, Measurement & Technology, 6*(2), 52-62.

Kai, W., Yasuo Suzuoki, & Dissado, L. A. (2004). The contribution of discharge area variation to partial discharge patterns in disc-voids. *Journal of Physics D: Applied Physics, 37*(13), 1815-23.

Kelen, A. (1976). The Functional Testing of HV Generator Stator Insulation. *CIGRE, 15*(03).

Kennedy, J., & Eberhart, R. (1995, Nov/Dec 1995). Particle swarm optimization. *Paper presented at the IEEE International Conference on Neural Networks.*

Khalil, M. S. (1996). On the use of doped polyethylene as an insulating material for HVDC cables. *Paper presented at the IEEE International Symposium on Electrical Insulation.*

Kreuger, F. H. (1989). Discharge Detection in High Voltage Equipment: *Butterworth-Heinemann.*

Kreuger, F. H. (1992). Industrial High Voltage 4.Co-ordinating 5.Measuring 6.Testing. Delft: *The Netherlands: Delft Univ. Press.*

Kuffel, E., Zaengl, W. S., & Kuffel, J. (2000). High Voltage Engineering: Fundamentals.

Kwang Jin Lim, Kyaw Soe Lwin, Dong Hoon Shin, Noh Joon Park, & Park, D. H. (2008). A Study on the Measurement of Partial Discharges in XLPE Power Cables using Planer Loop Sensors. *2008 International Conference on Condition Monitoring and Diagnosis, Beijing, China*, April 21-24.

Lei, Z., Song, J., Tian, M., Cui, X., Li, C., & Wen, M. (2014). Partial discharges of cavities in ethylene propylene rubber insulation. *IEEE Transactions on Dielectrics and Electrical Insulation, 21*(4), 1647-1659.

Lemke, E. (2013). Analysis of the partial discharge charge transfer in extruded power cables. *IEEE Electrical Insulation Magazine, 29*(1), 24-28.

Lide, D. R. (2008). CRC handbook of chemistry and physics : a ready-reference book of chemical and physical data. *CRC Press 88th ed. Boca Raton, Fla*.

Liu, L., Liu, W., & Cartes, D. A. (2008). Particle swarm optimization-based parameter identification applied to permanent magnet synchronous motors. *Engineering Applications of Artificial Intelligence, 21*(7), 1092-1100.

Mardiana, R., & Su, C. Q. (2010). Partial discharge location in power cables using a phase difference method. *IEEE Transactions on Dielectrics and Electrical Insulation, 17*(6), 1738-1746.

McAllister, I. W. (1997). Partial discharges in spheroidal voids. void orientation. *IEEE Transactions on Dielectrics and Electrical Insulation, 4*, 456-461.

McBride, J. E., Harper V. S, Coffeen, L. T., Stanley, F. T., & Harry W. Ng. (1994). Examination and location of partial discharge sites in severely aged underground distribution cables. *IEEE Transactions on Power Delivery, 9*(2), 629-638.

Miller, R., & Black, I. A. (1977). Partial discharge measurements over the frequency range 0.1 hz to 50 hz. *IEEE Transactions on Electrical Insulation, EI-12*(3), 224-233.

Mohamed, F. P., Siew, W. H., Soraghan, J. J., Strachan, S. M., & McWilliam, J. (2013a). Partial discharge location in power cables using a double ended method based on time triggering with GPS. *IEEE Transactions on Dielectrics and Electrical Insulation, 20*(6), 2212-2221.

Mohamed, F. P., Siew, W. H., Soraghan, J. J., Strachan, S. M., & McWilliam, J. (2013b). The use of power frequency current transformers as partial discharge sensors for underground cables. *IEEE Transactions on Dielectrics and Electrical Insulation, 20*(3), 814-824.

Mohamed, F. P., Siew, W. H., Soraghan, J. J., Strachan, S. M., & McWilliam, J. (2014). Remote monitoring of partial discharge data from insulated power cables. *IET Science, Measurement & Technology, 8*(5), 319-326.

Mori, T., Ishii, R., Banmongkol, C., Mizutani, T., & Ishioka. (1998). Breakdown and space charge of LDPE films prepared using metallocene catalyst. *IEEE Conference on Conduction and Breakdown in Solid Dielectrics*, 489-492.

Mu-kuen, C., Jeng-ming, C., & Chao-Yuan, C. (2014). Partial discharge detection by RF coil in 161 kV power transformer. *IEEE Transactions on Dielectrics and Electrical Insulation, 21*(3), 1405-1414.

Niemeyer, L. (1995). A Gernalized Approach to Partial Discharge Modelling. *IEEE Transactions on Dielectrics and Electrical insuIation, 2*(4), 510-528.

Noske, S., & Rakowska, A. (2014, 8-11 Sept. 2014). Off-line partial discharge measurements as a new data source about the technical condition of MV cables. *Paper presented at the 2014 International Conference on High Voltage Engineering and Application (ICHVE).*

Pedersen, A., Crichton, G. C., & McAllister, I. W. (1991). The theory and measurement of partial discharge transients. *IEEE Transactions on Electrical Insulation, 26* 487-497.

Pedersen, A., Crichton, G. C., & McAllister, I. W. (1994). PD Related Stresses in the Bulk Dielectric for Ellipsoidal Voids. *IEEE Conference on Electrical Insulation and Dielectric Phenomena*, 79-84.

Ruay-Nan, W., & Chien-Kuo, C. (2011). The Use of Partial Discharges as an Online Monitoring System for Underground Cable Joints. *IEEE Transactions on Power Delivery, 26*(3), 1585-1591.

Schifani, R., Candela, R., & Romano, P. (2001). On PD mechanisms at high temperature in voids included in an epoxy resin. *IEEE Transactions on Dielectrics and Electrical Insulation, 8*, 589-597.

Shi, Y., & Eberhart, R. (1998, 4-9 May 1998). A modified particle swarm optimizer. *Paper presented at the The 1998 IEEE International Conference on Evolutionary Computation Proceedings.*

Stone, G. C. (2005). Partial discharge diagnostics and electrical equipment insulation condition assessment. *IEEE Transactions on Dielectrics and Electrical Insulation, 12*, 891-904.

Su, C. Q., & Li, C. R. (2013). Using very-low-frequency and oscillating-wave tests to improve the reliability of distribution cables. *IEEE Electrical Insulation Magazine, 29*, 38-45.

Tenbohlen, S., Denissov, D., Hoek, S., & Markalous, S. M. (2008). Partial discharge measurement in the ultra high frequency (UHF) range. *IEEE Transactions on Dielectrics and Electrical Insulation, 15*(6), 1544-1552.

Tian, Y., Lewin, P. L., & Davies, A. E. (2002). Comparison of on-line partial discharge detection methods for HV cable joints. *IEEE Transactions on Dielectrics and Electrical Insulation, 9*(4), 604-615.

Tian, Y., Lewin, P. L., Pommerenke, D., Wilkinson, J. S., & Sutton, S. J. (2004). Partial discharge on-line monitoring for HV cable systems using electro-optic modulators. *IEEE Transactions on Dielectrics and Electrical Insulation, 11*(5), 861-869.

Tian, Y., Lewin, P. L., Wilkinson, J. S., Schroeder, G., Sutton, S. J., & Swingler, S. G. (2005). An improved optically based PD detection system for continuous on-line monitoring of HV cables. *IEEE Transactions on Dielectrics and Electrical Insulation, 12*(6), 1222-1234.

Vakilian, M., Blackburn, T. R., James, R. E., & Phung, B. T. (2006). Semiconducting layer as an attractive PD detection sensor of XLPE cables. *IEEE Transactions on Dielectrics and Electrical Insulation, 13*(4), 885-891.

Vaughan, A. S., Zhao, Y., Barr, L. L., Sutton, S. J., & Swingler, S. G. (2003). On additives, morphological evolution and dielectric breakdown in low density polyethylene. *European Polymer Journal, 39*, 355-365.

Wang, P., Lewin, P. L., & Sutton, S. J. (2005). Calibration of capacitive couplers for online PD detection in HV cables. *IEEE Electrical Insulation Magazine, 21*(3), 28-39.

Weedy, B. M. (1985). DC conductivity of Voltalit Epoxy Spacers in SF6. *IEE Proceeding A, 132*, 450-454.

Wenjie, L., Jiankang, Z., & Shaoxin, M. (2012, 27-29 March 2012). Partial Discharge Time-Frequency Spectrum Analysis and Extraction for Power Cable. *Paper*

presented at the Power and Energy Engineering Conference (APPEEC), 2012 Asia-Pacific.

Wester, F. J., Gulski, E., & Smit, J. J. (2001). CBM of MV Power Cable Systems on the Base of Advanced PD Diagnosis. *16th International Conference on Electricity Distribution (CIRED) , Amsterdam, The Netherlands*.

Xiaoxing, Z., Song, X., Na, S., Ju, T., & Wei, L. (2014). GIS partial discharge pattern recognition based on the chaos theory. *IEEE Transactions on Dielectrics and Electrical Insulation, 21*(2), 783-790.

Ye, H. f., Qian, Y., Dong, Y., Sheng, G. h., & Jiang, X. c. (2014). Development of multi-band ultra-high-frequency sensor for partial discharge monitoring based on the meandering technique. *IET Science, Measurement & Technology, 8*(5), 327-335.

Zhong, L., Xu, Y., Chen, G., Davies, A. E., Richardson, Z., & Swingler, S. G. (2001). Use of capacitive couplers for partial discharge measurements in power cables and joints. *Paper presented at the Proceedings of the 2001 IEEE 7th International Conference on Solid Dielectrics, 2001. ICSD '01.*

Zhou, C., Song, X., Michel, M., & Hepburn, D. M. (2009). On-line partial discharge monitoring in medium voltage underground cables. *IET Science, Measurement & Technology, 3*(5), 354-363.

LIST OF PUBLICATIONS AND PAPERS PRESENTED

A. Journal Publications

1. H. A. Illias, M. A. Tunio, G. Chen, A. H. A. Bakar, and H. Mokhlis, "Experiment and Modelling of Void Discharges Within Dielectric Insulation Material Under Impulse Voltage," ***IEEE Transactions on Dielectrics and Electrical Insulation*****,** vol. 22, issue 4, pp. 2252-2260, August 2015. (ISI-Cited Publication).

2. H. A. Illias, M. A. Tunio, A. H. A. Bakar, H. Mokhlis, and G. Chen, "Partial Discharge Phenomena within an Artificial Void in Cable Insulation Geometry: Experimental Validation and Simulation", ***IEEE Transactions on Dielectrics and Electrical Insulation***, Accepted in August 2015. (ISI-Cited Publication).

3. H. A. Illias, M. A. Tunio, A. H. A. Bakar, H. Mokhlis, and G. Chen, "Partial Discharges within an Artificial Void in a Cylindrical-Shaped Insulation Material under Various Applied Conditions", in preparation.

B. Conference Publication

1. H. A. Illias, M. A. Tunio, A. H. A. Bakar, and H. Mokhlis, "Distribution of electric field in capacitor and surge arrester bushings," ***IEEE International Conference on Power and Energy***, pp. 973-978, 2-5 Dec. 2012, Kota Kinabalu, Malaysia.